Fabrication of Microfluidic Devices with Application to Membraneless Fuel Cells

by

Jon McKechnie
B.Eng. McMaster University, 2004

A Thesis Submitted in Partial Fulfillment of the
Requirements for the Degree of

MASTER OF APPLIED SCIENCE

in the Department of Mechanical Engineering

Fabrication of Microfluidic Devices with Application to Membraneless Fuel Cells

by

Jon McKechnie
B.Eng. McMaster University, 2004

A Thesis Submitted in Partial Fulfillment of the
Requirements for the Degree of

MASTER OF APPLIED SCIENCE

in the Department of Mechanical Engineering

Supervisory Committee:

Dr. David Sinton (Mechanical Engineering)
Supervisor

Dr. Ned Djilali (Mechanical Engineering)
Departmental Member

Dr. David Levin (Biology)
Outside Member

Supervisory Committee:

Dr. David Sinton (Mechanical Engineering) _____
Supervisor

Dr. Ned Djilali (Mechanical Engineering) _____
Departmental Member

Dr. David Levin (Biology) _____
Outside Member

ABSTRACT

This thesis is part of an ongoing collaborative research project focused on the development of microstructured enzymatic fuel cells. Both enzymatic fuel cells and co-laminar fuel cells are, more generally, varieties of microfluidic membraneless fuel cells. A primary goal of this particular work is the establishment of microfabrication capabilities to develop these technologies. Rapid prototyping soft lithography capabilities are established in-house and protocols specific to the lab equipment are developed. These prototyping methods are then adapted for the fabrication of microfluidic membraneless fuel cells. Fabrication techniques using polymeric stencils and photoresist-based channel structures are developed to enable electrode patterning and current collection in the enzymatic and co-laminar fuel cells of interest. A variety of electrode patterning methods are developed. Gold electrode patterning by etching and lift-off techniques are investigated for the patterning of base electrode layers. An in-situ gold electrode patterning methodology is designed and tested, eliminating the need for precision alignment during device assembly. Carbon electrode patterning methods are

developed for use in a vanadium-based colaminar fuel cell. Thin-film carbon electrodes are fabricated using a mixture of carbon microparticles and a polymeric binder. Alternatively, graphite rods are investigated for use as electrodes due to their high conductivity and chemical stability. The integration of channel structure and electrode fabrication methods is investigated to establish compatibilities and facilitate the assembly of functional devices. In addition to the development of these methods, the application of co-laminar streaming to microfabrication is explored through the development of a dynamic microfluidic photomasking device.

TABLE OF CONTENTS

Chapter 6 SUMMARY AND FUTURE WORK

LIST OF TABLES

LIST OF FIGURES

ACKNOWLEDGEMENTS

I would like to express my sincerest thanks to Dr. David Sinton for his guidance in this endeavour. I also want to acknowledge all that have helped me along with this work, including but not limited to the members of the Microfluidics Lab past and present, the Bio Fuel Cell research group, and the many electrochemistry graduate students who have provided a wealth of knowledge for my work. Special thanks are extended to my family for their unconditional support in my endeavours.

Finally, I dedicate this work to Bronwen, who has shared this experience with me on a daily basis and whose loving support and encouragement held things together even when epoxy couldn't.

Chapter 1

INTRODUCTION

1.1 Aims and Motivations of the Thesis

This thesis is part of an ongoing collaborative research project focused on the development of microstructured enzymatic fuel cells. A primary goal of this thesis is to establish microfabrication capabilities to develop this technology. Throughout the course of this work, a variety of microfabrication processes have been developed for the fabrication of channel structures and electrodes for microfluidic membraneless fuel cells as well as a dynamic microfluidic photomasking device.

The amount of research performed in the field of microfluidics has grown tremendously over the past 10 years, largely due to interest in the "lab on a chip" concept of miniaturized medical testing [Kamholz (2004)]. Microfluidic devices offer different functionality compared to traditional macroscale processes. The most significant benefit derives from the dramatic reduction in the length scales. The result is an increase in surface area to volume ratio, making surface phenomena increasingly influential. This characteristic facilitates reduced sample requirements, improved heat transfer to and from the fluid, and faster processing time [Reyes et al. (2002)]. The mechanics of fluid flow is affected by this reduction in length scale, as viscous forces become dominant over inertial forces [Stone et al. (2004)]. This relationship is quantified by the Reynolds number, a non-dimensional measure of the relative importance of advective and diffusive momentum transport, or in other words inertial and viscous effects, given by:

$$\mathrm{Re} = \frac{LU}{\upsilon} \qquad (1.1)$$

where L is the characteristic length of the flow channel [m] (used often is the hydraulic diameter, D_h), U is the average velocity [m s^{-1}], and υ is the kinematic viscosity [m^2 s^{-1}].

As a comparison, consider a macroscale channel of 1 cm diameter with a flow of water at a typical speed of 10 cm/s. This results in a Reynolds number of 1000, indicating the large influence of inertial forces. In contrast, water flow in a 100 μm diameter channel with a typical flow rate of 1 mm/s has a Reynolds number of 1. It quickly becomes evident that flows on the microscale are strongly dominated by viscous forces and that flow will be predominantly laminar and free of turbulence. In microfluidic devices, the laminar nature of the flow can be exploited since the manipulation of fluid flows becomes predictable and easily controlled. This approach has been employed in analytical devices to perform, for example, on-chip capillary electrophoretic separations [McDonald et al. (2000); Lagally et al. (2000)] and miniaturized nucleic acid analysis [Auroux et al. (2004)].

Miniature fuel cell devices have recently attracted a great deal of attention as an improved power supply for portable electronics [Bazylak et al. (2005); Choban et al. (2004); Moore et al. (2004)]. As energy storage demands increase with the next generation of portable electronic devices, current lithium ion battery technology is considered unlikely to keep pace [Dyer (2002)]. Within similar performance constraints, lithium ion battery technology can provide 94 Wh/L, while a miniature fuel cell system could provide significantly more energy storage of 550 Wh/L [Dyer (2002)]. Fuel cells have the potential to fill this increasing need, due primarily to their potential for higher

energy density. Fuel cell performance benefits from the unique characteristics of miniaturization. Most evident is the potential for increased power density. Electricity generation in fuel cells occurs as the result of oxidation and reduction reactions at the surface of the anode and cathode, respectively. As this process is a surface-based reaction, the increase of the surface area to volume ratio inherent in miniaturization presents an opportunity to improve fuel cell performance.

Recently, bio fuel cells have emerged as potential solutions for portable power sources. The fundamental concept of these devices is to exploit electrochemical processes occurring naturally in microbes to provide useful electrical energy. Bio fuel cells that utilize whole microbes require complex reaction steps and are quite inefficient [Bennetto (1990)]. Enzymatic fuel cells, on the other hand, utilize only the functional part of the organism. A schematic of enzymatic fuel cell architecture is shown in Figure 1.1a. Enzymes naturally catalyze reactions of specific substances and are largely unaffected by the presence of other substances, allowing the combination of fuel and oxidant streams in a single flow channel [Heller (2004)]. Additionally, enzymes can be produced cheaply through simple fermentation processes, whereas traditional fuel cells require precious metals, typically platinum, to catalyze the reactions [Barton et al. (2004)]. In the context of microfabrication, microstructured enzymatic fuel cells fall into a larger category of membraneless microfluidic fuel cells.

Another type of membraneless microfluidic fuel cell exploits the nature of liquid flow in microchannels, achieving advanced functionality unique to the microscale. Although momentum diffusion is rapid in these flows as evidenced by their viscous nature, characterized by a low Reynolds number, species diffusion is relatively slow. The

Schmidt number quantifies the relative speed of momentum to mass diffusion by:

$$Sc = \frac{\upsilon}{D} \qquad (1.2)$$

where D is the species diffusivity [m^2 s^{-1}]. Typical values for the Schmidt number in liquid flows are on the order of 1000, indicating the greater importance of momentum diffusion. Thus the colaminar flow of multiple, distinct streams is possible, with a mixing region developing at the interface of the two streams that grows gradually by cross-stream diffusion. A schematic of colaminar fuel cell architecture is shown in Figure 1.1b. The mixing region between the fuel and oxidant streams essentially serves as a fluidic membrane.

Eliminating the membrane from fuel cell architecture by exploiting either enzyme specificity or colaminar serves several advantages. The overall size of the fuel cell is reduced, thus increasing power and energy density. Also, performance can be improved through elimination of water management issues and fuel crossover associated with membranes in traditional fuel cells. Challenges associated with the fabrication of these devices were the main focus of this work.

The aims of this thesis work are to:

1.) Establish in-house fabrication capabilities for microfluidic devices.

2.) Identify microfluidic channel geometries for optimal performance of membraneless microscale fuel cells

3.) Expand manufacturing techniques for the fabrication of channel structures for microfluidic membraneless fuel cells

4.) Develop gold and carbon electrode patterning methods for use in microscale redox devices and microfluidic membraneless fuel cells

5.) Develop a dynamic microfluidic photomasking device

1.2 Advantages of Polymeric Microfluidic Devices

When the field of microfluidics was first developing, it borrowed manufacturing techniques that had been developed in the microelectronics industry [Madou (1997)]. Initially, the most common materials used in the fabrication of channels were glass and silicon, patterned by standard photolithography and wet-etching techniques [de Mello (2002); Quake et al. (2000); Duffy et al. (1998)]. For microfluidic chips, however, the use of glass or silicon as a substrate poses several difficulties. While microfluidic devices are quite small, their incorporation into larger devices in the range of 100 cm^2 may be necessary for some applications [de Mello (2002)]. As such, the relatively high cost of these materials becomes significant. The mechanical properties of these materials pose further problems. The fragile nature of glass and silicon reduces their longevity, while their stiffness requires larger part sizes than necessary [Quake et al. (2000)]. The planar orientation of silicon limits the variety of feature orientations that are easily attainable, such as rounded channels and reservoirs [Duffy et al. (1998)]. Also, the processes to micromachine these materials are time-consuming and expensive, requiring clean room facilities. As such, glasses and silicon generally do not lend themselves well to mass manufacturing.

As a result of these difficulties, a great deal of focus has been placed on the use of alternate materials in the fabrication of micro-channels. While polymers and plastics are by no means perfect materials, they possess many advantages over glasses and silicon-based materials for microstructure applications. The cost of polymers is much less than

that of ceramics, with PDMS costing approximately 50 times less than silicon per volume [Quake et al. (2000)]. Further, the fabrication of polymer-based microstructures does not necessarily require the use of a clean room and can be performed by simpler and much faster methods, such as replica molding and hot embossing. These techniques and materials allow for the rapid fabrication of micrometer-scale features with high aspect ratios, equaling or surpassing the geometric qualities of silicon and glass devices [Lorenz et al. (1998)]. Fabrication methods of polymeric microstructures have been applied to nanofabrication, creating fluidic channels on the order of tens of nanometers [Guo et al. (2004); Chen and Pepin (2001)].

One significant characteristic of polymers and plastics is their variability. Plastics are simply polymers that have been functionalized by the presence of additives. The physical and chemical properties of both classes of materials can be manipulated by altering their composition, degree of cross-linking and other processing parameters [de Mello (2002)]. As a result, material selection can be tailored to best fit the necessary or desirable characteristics for a specific application. With a wide variety of polymeric materials available and with many very different materials finding use in specific applications, a large variety of production methods are needed to efficiently fabricate microstructures.

1.3 Polymeric Microfabrication Methods

A variety of fabrication methods exist that are tuned to the demands of both the substrate material and the future application of the structure. These methods can be grouped into two classes: replication methods and direct machining methods [Quake et

al. (2000)]. Replication methods use a negative template to define microstructures on a substrate through imprinting or molding techniques. Direct machining methods, by comparison, structure individual polymer surfaces. In general, the choice of fabrication method depends on the material being properties and consideration of the scale of output, from experimental prototypes to mass produced devices.

Both classes of fabrication methods create one structured surface with grooves that will define the microfluidic channels. In order to create enclosed channels, a planar material is bonded to the structured surface. In traditional glass and silicon based systems, such a bond requires extreme temperatures or very high voltages [de Mello (2002); Quake et al. (2000); Duffy et al. (1998)]. On top of processing issues, such processes can have detrimental consequences for the surface properties of the material. Polymeric systems offer the benefit of low-temperature bonding by a variety of methods, differing by material. These include adhesives, low-temperature thermal annealing [Becker and Locascio (2002)] post-patterning curing of a surface with excess monomer to another with excess curing agent [Ng et al. (2002)], and reversible sealing of flexible polymers by conformal contact to a smooth planar surface [Duffy et al. (1998)].

1.3.1 Direct Machining Methods

Devices created by direct machining methods are individually patterned instead of being formed with a template [Becker and Locascio (2002)]. This offers the benefit of not requiring the manufacture of a precise template, which allows for rapid prototyping. Individual fabrication, however, is not amenable to mass production.

Laser Ablation and Plasma Etching

Laser ablation uses high-power UV laser pulses to break chemical bonds in the polymer chain. Degraded fragments of polymer are ejected from the workpiece by the resulting shockwaves [de Mello (2002)]. The formed geometries can be highly controlled as each pulse cuts a specific depth of material based on pulse power. Laser ablation offers the option of using a mask during the process and flooding the surface with laser impulses, which is beneficial for mass production, while rapid prototyping is possible by direct-writing to the material surface without a mask [de Mello (2002)]. As many polymers have significant absorption of UV light, this method is applicable to a wide range of substrates [de Mello (2002)]. The resulting channel walls are straight, although the surfaces are generally rougher than those created by other methods [Becker and Locascio (2002)]. Plasma etching is a similar method to laser ablation, except it uses gaseous plasmas to degrade and remove the polymer. Plasma etching has been successful in fabricating narrow and deep reservoirs and flow-through holes [de Mello (2002)]. Other variations of this style of fabrication include ion-beam etching and electron beam lithography, which can be used to create channels with widths on the order of nanometers [Quake et al. (2000)], as well as micro electrochemical milling [Kim et al. (2005)].

1.3.2 Replication Methods

Replication methods are used to transfer patterns from a negative master onto a polymeric substrate [Becker and Locascio (2002)]. The major limitation of replication is that the final quality of the fabricated piece is highly dependent on the quality of the template used. As such, care must be taken in the manufacture of the template to avoid defects and ensure specific geometric constraints are met. This can be quite costly.

However, since the application of these types of processes to mass production is typically quite straight-forward, the economy of scale softens the impact of a high template cost. For research and design prototyping, however, a more cost-effective and timely means of creating the template is necessary.

Imprinting and Hot Embossing

Imprinting and hot embossing are both very efficient methods of fabricating microstructures on polymer surfaces. The first successes of this technique used wires with diameters in the range of microns as templates, although machined or wet-etched silicon templates are now also commonly used [Chen and Chen (2000)]. To transfer the pattern from master to the polymer by imprinting, the negative template is placed in contact with the substrate and compressed. The template is then heated to near the material's glass temperature where it becomes very malleable to facilitate the transfer of the pattern and, following cooling, the pieces are separated [Chen and Chen (2000)]. Hot embossing is a very similar process, except that both the template and substrate are heated to near the glass temperature under vacuum before pressing [Juang et al. (2002)]. Feature sizes down to approximately 10 microns can be accomplished by imprinting and hot embossing [de Mello, (2002)]. These methods are used quite frequently as a wide range of polymers and plastics can be structured in this way, varying from hard plastics to soft polymers [Qin et al. (1998)].

Injection Molding

Injection molding is useful for fabricating devices with thermoplastic materials [Becker and Gartner (2000)]. The substrate material is heated to its melting temperature and injected under high pressure into the mold cavity, similar to macroscale mold

processes [Becker and Gartner (2000)]. One significant difference is that micro-molds must be kept at a temperature above the material's melting point until the end of the fill process to ensure a complete fill of the mold, thereby increasing the cooling time until the piece can be released. The quality of pieces manufactured by injection molding is highly dependent on the quality of the template. Polymer relaxation and shrinkage upon cooling must be accounted for in the mold design and manufacture process [Becker and Locascio (2002)]. With these problems accounted for, injection molding offers good dimensional control, short cycle time, and high productivity [de Mello, (2002)].

Soft Lithography

Soft lithography is essentially the curing of polymer on top of a negative template. The process can be divided into 2 steps: negative template fabrication and replica casting. Templates can be made by several different methods and are similar to templates previously described for other replication methods. These methods include the micromachining of silicon [Madou (1997)], LIGA [Hruby, (2001)], solid object printing, photocopying [de Mello, (2002)], and the photolithographic patterning of photoresist [McDonald et al. (1998)]. The template type to be used is decided based on cost and production scale. More durable and better-defined templates are more expensive to make, but can withstand the rigors of large volume production and thus are more useful for industrial applications. Alternatively, inexpensive, quickly produced templates are ideal for most research and prototyping. As polymer curing times are typically on the order of hours, soft lithography allows for very short device production times.

Rapid Prototyping Soft Lithography

Photolithographic patterning of photoresist is of particular interest to research as it

facilitates the rapid and low cost prototyping of new designs [McDonald et al. (2000)]. Photomasks, which selectively transmit light through to the photoresist layer, can be printed onto transparencies at low cost. This allows for quick turnaround from design to photomask, typically not more than one day. Patterning of the photoresist layer to create a channel structure template can be performed in under an hour, depending on the thickness of the photoresist layer.

The rapid prototyping process is depicted in Figure 1.2. The channel design is initially drafted using a CAD program and printed to a transparency by a high-resolution printer capable of drawing the desired pattern with acceptable accuracy. The transparency then serves as a photomask during collimated photolithographic template fabrication as light will only be transmitted through the clear surfaces. A thin layer of photosensitive polymer, referred to in this work as photoresist, is then spin-coated onto a durable substrate, with the rotational speed determining the resultant photoresist height. Spin-coating creates a surface of uniform thickness, which allows for good dimensional control of feature height [MicroChem (2002a)]. Exposure with collimated UV light through the photomask defines the microstructure features. Two classes of photoresist exist. Positive-tone photoresist is degraded by exposure to light and as such only unexposed areas of photoresist remain after development. Crosslinking of negative-tone photoresist is initiated by exposure to light and exposed regions remain following development.

Typically in microfabrication, thin layers of photoresist on the order of 100 nm to 100 μm are desired. However, some applications require taller structures. This is difficult to achieve with available photoresist products that are designed to create a thin

layer. For thicker photoresist layers, multiple spin-coating steps can be used to build up the layer of photoresist before exposure [Gray and Jaffer, (2005); Zhang et al. (2001)]. A simpler method has been developed by Lin et al. (2002) wherein a known volume of SU-8 photoresist is spread manually onto a substrate and baked. When heated, SU-8 self-planarizes, creating a thick layer of uniform thickness in one step. By this method, microstructures of height ranging between 0.5 mm and 1.5 mm have been fabricated.

Following the fabrication of the template, a pre-polymer is poured over top of the mold as is typical to soft lithography. The polymer is subsequently cured and removed from the template. Of the polymers available, polydimethylsiloxane (PDMS) in particular has attracted much attention. PDMS is a durable and cheap material that remains chemically stable over a wide range of temperatures and is easily molded [de Mello, (2002)]. With PDMS it is possible to create high-fidelity replications of the template features [Quake et al. (1998)]. Further, it is easily removed from the template without damage to either surface. Its optical transparency down to 280 nm, refractive index of 1.49, and small degree of autofluorescence allows for visual investigation techniques to be used, which makes PDMS useful in experimentation [Becker and Gartner (2000)]. PDMS is also an ideal material for cellular studies as it is non-toxic as well as being gas permeable, facilitating cell respiration [Ng et al. (2002)]. Surface characteristics can also be tailored to fit specific applications by the attachment of functional groups, thus improving its applicability to specific devices [Ng et al. (2002)].

PDMS channels can be sealed either reversibly or irreversibly to a planar polymer or ceramic. Reversible sealing is possible by conformal contact between surfaces. The elastic nature of PDMS allows it to conform to small imperfections in the planar surface

through van der Waals forces [Ng et al. (2002)]. This method of sealing is adequate for low-pressure flows and supports resealing without any damage to the PDMS or substrate. It is especially beneficial to some biological applications as flow arrays can be disassembled and easily cleaned before reuse [Duffy et al. (1998)].

For many applications, especially high-velocity pressure-driven flows, strong, permanent seals are required. Traditional methods of attaining this are limited. Adhesives must be used carefully, as excess quantities can block flow channels and alter the channel geometry. Similarly, thermal annealing of thermoplastic devices can cause a slight deformation in the channel, thus changing the geometry. For PDMS, improved irreversible sealing is made possible by altering its surface chemistry. In its native form, PDMS is composed of repeating – O Si $[CH_3]_2$ O_2 – groups. It has been proposed by a number of sources [Becker and Locascio (2002); Duffy et al. (1998)] that oxidizing the surface with oxygen plasma for a short time destroys the Si – CH_3 methyl groups, which are replaced by Si – OH silanol groups. In this form, PDMS can be irreversibly bonded to oxidized glass, PDMS, and some other polymers simply by bringing the two oxidized surfaces into contact. Oxidized surfaces that are compatible with irreversible bonding to PDMS contain – OH – groups. When brought into contact with silanol groups on the PDMS surface, a condensation reaction occurs, creating a permanent siloxane [Si – O – Si] bond between the two surfaces [Duffy et al. (1998)]. Attempting to remove one of the surfaces results in a failure in the bulk material. This method of sealing, developed by Duffy et al. greatly simplifies and improves upon other sealing practices.

Besides the capability for irreversible seals, the oxidized PDMS surface allows for a much different functionality than native PDMS. The oxidized surface is hydrophilic,

whereas the native surface is hydrophobic. This allows for easier filling of micro-channels, eliminating both the need for a sieving matrix to facilitate channel filling and unwanted bubbles that can result from filling a hydrophobic channel [Duffy et al. (1998)]. The silanol groups formed by oxidation create a net negative charge at the surface. As such, oxidized PDMS is able to support electro-osmotic flow toward the cathode [Duffy et al. (1998)]. Microscale flow driven by electrical potential is in many ways simpler than pressure driven flow. Potentials that drive the flow are applied at electrodes placed in the inlet and outlet reservoirs, as opposed to connecting tubing that must withstand considerable pressures.

One major obstacle for oxidized PDMS systems is that the silanol surfaces are unstable. Uncross-linked chains migrate to the surface quite readily if exposed to air, thus causing the surface to revert toward its native hydrophobic form [Lee et al. (2003)]. However, techniques exist for extending the lifetime of the oxidized surface. The simplest method is submersing the piece in water or another polar organic solvent, which prevents the migration of hydrophobic chains from the bulk to the surface [Duffy et al. (1998)]. Surface modifications can also extend the lifetime of the charged layer. The surface is reactive to a wide range of silanes [$Si - x$] that are terminated with functional groups. This allows for the tailoring of surface chemistries, including the attachment of layers that maintain the hydrophilic nature of the surface for days instead of hours [Ng et al. (2002)].

1.3.3 Expansions of the Rapid Prototyping Soft Lithographic Method

Since the publication of "Rapid Prototyping of Microfluidic Systems in Poly(dimethylsiloxane)" [Duffy et al. (1998)], use of the rapid prototyping has become

widespread in microfluidics research due to its inexpensive and time-efficient manner of prototyping microstructures. The initial paper has been cited 546 times according to ISI Web of Science, evidence of the popularity of this fabrication method. Many aspects of the method have been investigated for improvement and attempts have been made to overcome its limitations.

One drawback of soft lithography is the difficulty involved in fabricating three-dimensional structures. The exposure of photoresist by UV light is conventionally an "all-or-nothing" phenomenon, thus limiting the design to two dimensions. Adaptations to overcome this limitation have been developed. Cabral et al. [2004] created multilevel fluidic devices with controlled height through frontal photopolymerization, wherein the photoresist is exposed through a transparent substrate and the 'front' of polymerized resist grows out from the substrate with increasing exposure dose. By controlling the exposure dose, the resulting structure height can be manipulated through selective, multiple exposures. Other methods worked toward creating grayscale photomasks to allow for three-dimensional patterning in a single exposure. O'Shea et al. [1995] used ultra high resolution halftone chrome masks, where different densities of the opaque chrome create varying exposure levels. Wu et al. [2002] employed reduction lithography through an array of microlenses to pattern low resolution gray scale masks on a transparency. These methods, however, are limited with respect to depth resolution (sometimes only one intermediary exposure level), expense, or exposure complexity. Other attempts at creating three-dimensional structures focus on creating multi-level channel geometries [Jo et al. (2000); Anderson et al. (2000)]. These methods use two templates, both of which define geometries of the different levels. Connections between

the two levels or the creation of multiple levels between the templates are created by multiple photoresist exposure steps during template fabrication, thus allowing for the creation of three-dimensional designs [Anderson et al. (2000)]. This method has been used to create basket-weave flow patterns, a helical channel surrounding a linear channel, and many other possibilities [Anderson et al. (2000)]. By these and other methods, the applicability of soft lithography is extended to the third dimension.

One method to attain three-dimensional geometries is through the use of a microfluidic photomask [Chen et al. (2003)]. This method uses liquid, UV-absorbing dye filled channels to define the design geometry in the photoresist. By varying the microchannel height and concentration of the dyes, infinite degrees of transmittance, and hence exposure, can be realized [Chen et al. (2003)]. This allows for variation of channel height between channels or within a single channel. The major drawback of this method is its spatial limitations. An adaptation of this method that allows for dynamic, reconfigurable photomasking is presented in Chapter 5.

The minimum feature size attainable by rapid prototyping soft lithography is also limited. The final structures are an exact replica of the template mold, which itself is dependent on the quality of the transparency design. Due to the pixilated nature of some transparency prints, the vertical walls can be quite rough [Duffy et al. (1998)]. Limitations in image setting, a common method of creating transparency photomasks, also prevent the fabrication of designs with features less than 20 μm in size [Duffy et al. (1998)]. By using a technique called photoplotting instead of image setting to create the photomask, well-resolved features as small as 8 μm are possible with much smoother edges [Linder et al. (2003)]. Higher-resolution photomasks are also achievable. Chrome

on glass photomasks can generate patterns with feature size as small as 0.5μm, but require increased cost and time expenditures, which eliminates the fast turnaround desired for rapid prototyping but serves mass production well [McDonald et al. (2000)].

Some researchers have attempted to overcome the limitations of PDMS in particular applications. PDMS is generally incompatible with non-polar solvents [Lee et al. (2003)] as swelling of the bulk PDMS and the release of PDMS oligomers to solution can occur. This can result in channel distortion and the tainting of samples in analysis systems. These and other incompatibilities of PDMS for specific applications, such as gas permeability, low thermal conductivity and high flexibility, have led some researchers to investigate the use of other polymers. Using soft photolithographic fabrication methods, Fiorini et al. examined the usefulness of thermoset polyester as a substrate material [Fiorini et al. (2004)]. Polyester has several advantages over PDMS, namely better thermal conductivity, more stable surface properties, and better solvent compatibility. Other features of polyester make it more or less applicable to certain applications, such as reduced clarity and gas impermeability [Fiorini et al. (2004)]. Other materials have been similarly investigated. While poly(methylmethacrylate) (PMMA) is more amenable to stamping and embossing manufacture, its rigidity and structural strength is necessary for some applications [Becker and Locascio (2002)]. Poly(tetrafluoroethylene) (PTFE) and a number of other polymers have also been investigated for fabrication by soft lithography [Rolland et al. (2004)].

SU-8 photoresist (MicroChem, Newton, MA), typically employed in template fabrication, has also been used as a structural material for the fabrication of microfluidic devices [Sikanen et al. (2005); Zhang et al., (2001); Bilenberg et al. (2004)].

Polymerized SU-8 offers mechanically strong structures of minimal reactivity, as well as chemical stability with many acids and bases and high transparency to near-UV and visible light, allowing direct visualization [Sikanen et al. (2005)]. Microchannels are formed by first patterning a layer of photoresist with the channel structure. This structure is then sealed to a planar substrate using a layer of non-polymerized SU-8. Subsequent polymerization of the adhesive layer creates a strong bond to the channel structure. After assembly, the SU-8 channel structures can be removed from the base substrates to reduce the volume of the device. SU-8 photoresist has also been employed to fabricate fluidic interconnects, allowing for the integration of multiple microfluidic devices and connection to the macro environment [Gray and Jaffer (2005)]. Fabrication of SU-8 components will be discussed in Chapter 2, while the use of SU-8 as a channel structure will be investigated in Chapter 3.

1.4 Microfluidic Membraneless Fuel Cell Fabrication

Recent attention on fuel cells for portable power devices has featured unique attempts at their miniaturization. Traditionally, the incorporation of membranes in fuel cells serves to separate fuel and oxidant streams into anodic and cathodic compartments, respectively. Membranes have, however, introduced a number of technical and performance issues, including membrane dry-out, water management, fuel crossover, and additional ohmic resistance [Choban et al. (2004); Chang et al. (2005)]. Membraneless fuel cells can eliminate most of these problems, and fuel cell miniaturization efforts also benefit from the simplicity of membraneless architectures. The two major initiatives in the design of membraneless fuel cells are enzymatic fuel cells with specific electrodes

and microfluidic membraneless fuel cells with colaminar streaming. Fuel crossover can be minimized in membraneless fuel cells by proper electrode design [Choban et al. (2005b)]. For mixed-reactant fuel cells, proper design requires selective electrodes, either based on metallic or enzymatic catalysts [Priestnall et al. (2002); Moore et al. (2005); Heller, (2004)]. For colaminar fuel cells, proper design simply needs to prevent contact between the electrodes and minimize mixing between the colaminar fuel and oxidant streams.

Channel structures utilized for microscale membraneless fuel cells can differ greatly from methods previously described for microfluidic channel construction. Fabrication of a three-walled channel structure, typical of most fabrication techniques, allows for electrode patterning only on the fourth surface that seals the channel. As such, only one of four walls of the channel is employed in the electrochemical reactions, thus limiting power density and fuel utilization. This method has therefore been mostly limited to proof-of-concept membraneless fuel cells [Ferrigno et al. (2002)]. However, impressive performance was recently achieved using a single-sided electrode design, with the three non-active channel walls facilitating the transport of gaseous fuel and oxidant to the electrodes [Mitrovski et al. (2004)]. This prototype device achieved a maximum power density of 700 $\mu W\ cm^{-2}$.

Alternative approaches have predominately employed a "top-and-bottom" electrode configuration, wherein the anode and cathode face each other from opposite channel walls as depicted in Figure 1.3b. To achieve this, a variety of fabrication and assembly techniques have been utilized. Conductive graphite plates have been used to define the length channel structure by placing two plates with a specific spacing [Choban

et al. (2005a)]. A previous catalyst deposition procedure functionalizes the plates, which act as channel walls, electrode supports, and current collectors. Similar results have been achieved with polymer plates that have been previously patterned with platinum-functionalized gold electrodes [Choban et al. (2004)]. Incorporation of an air breathing gas diffusion electrode as the cathode has been shown to dramatically increase the power density of membraneless fuel cells by improving the transport of oxygen to the cathode, an issue that typically limits the performance of liquid-based fuel cells [Jayashree et al. (2005)].

Due to the electrode configuration of the "top-and-bottom" method, as shown in Figure 1.3b, mixing between the fuel and oxidant streams occurs rapidly and consumes a large portion of the reactants. The diffusion area, defined as the contact area between the colaminar streams, is relatively large, being equal to the anode and cathode areas in a side-by-side configuration. Alternative geometries that exhibit a larger electrode area to diffusion area ratio would be expected to waste less reactants. A computational study of fuel utilization in membraneless microscale fuel cells was recently published, comparing various channel geometries [Bazylak et al. (2005)]. For given operating parameters, a top-and-bottom geometry was found to have fuel utilization of 8% while 19% of the reactants were mixed and therefore unusable. In contrast, a side-by-side geometry, as depicted in Figure 1.3c, achieved identical fuel utilization with only 8% of reactants lost to mixing. Further optimization of inlet flow rates and the incorporation of tapered electrodes attained 52% fuel utilization with this design. The side-by-side design is therefore preferable for optimizing fuel cell performance, although this design introduces additional complexities to the fabrication process.

Enzymatic fuel cells, on the other hand, do not require a side-by-side electrode geometry. As the fuel and oxidant can be flowed in a single stream due to the specificity of the electrodes, mixing between streams is not an issue. A top and bottom electrode geometry is required to increase the active area of the fuel cell. The fabrication of channel structures amenable to this electrode configuration is presented in Chapter 3.

Efficient methods of patterning electrodes are essential to the performance and fabrication of microfluidic fuel cells. Techniques to accomplish this borrow greatly from methods used in the microelectronics industry [Ruska (1987)]. Thin metallic films acting as current collectors or electrodes can be deposited on top of glass *via* thermal deposition [Holland (1963)]. The thin films are typically comprised of a thin adhesion layer of chromium or titanium, typically on the order of 10 nm thick, and a conductive layer of gold or catalytic metal, typically on the order of 100 nm [Moore et al. (2004)]. Electrode geometries may be defined by two methods. Following thin film deposition on a bare substrate, photoresist can be patterned to cover the desired electrode location. The unprotected metal layers are then etched away using the appropriate metal etchant products. Alternatively, a bare substrate can be patterned in photoresist such that the desired electrode areas are not covered in photoresist. After thin film deposition, the removal of photoresist also removes metal deposited on top of it, creating electrodes in a pattern opposite to that of the initially applied photoresist [Mitrovski et al. (2006)].

A variety of additional methods of incorporating electrodes in microfluidic fuel cells have been attempted. Choban et al. (2005), as mentioned previously, employed catalyst-coated graphite plates to act as electrodes, current collectors, and channel structures. Integration of molded electrodes has been successfully attempted, wherein

platinum electrodes were embedded in a polymer [Mitrovski et al. (2004)]. A gas diffusion electrode, carbon paper seeded with palladium black nanoparticles, has been employed as the cathode in a formic acid fuel cell [Jayashree et al., 2005]. Carbon microelectrodes have been fabricated by filling microfluidic channels with a carbon ink solution and hardening [Moore et al. (2005)]. The development of methods for gold and carbon electrode patterning, targeted to microfluidic membraneless fuel cell applications, will be discussed in detail in Chapter 4.

1.5 Overview of This Thesis

The high degree of interest in this field has produced and exponential increase in the number of contributions to the literature over the past 10 years [Kamholz (2004)]. This is further evidenced by the number of contributions referenced in this thesis that were published post-2004, the year this thesis was begun. The microfabrication capabilities developed through this work have provided an enabling technology for the research group, and have resulted in prompt contributions to the literature [McKechnie and Sinton (2006 – submitted), Kjeang et al. (2006 – submitted), Coleman et al. (2005 – in press)] and conference proceedings [McKechnie and Sinton (2005), McKechnie and Sinton (2006)]. The specific contributions of this thesis are summarized below:

In Chapter 1, the aims and motivation of the thesis work were presented. A brief overview of polymeric microfluidic device fabrication was presented, along with improvements on established methods. The application of microfabrication techniques toward microscale fuel cell fabrication was investigated, identifying the two essential

components of membraneless fuel cell fabrication: microfluidic channel structure and electrode fabrication.

In Chapter 2, the development of general in-house fabrication techniques for microfluidic devices is described. Processing parameters of SU-8 photoresist are investigated to determine optimal patterning strategies, including spincoating, baking and exposure steps for desired photoresist thicknesses. Fabrication of ultra-thick photoresist structures is briefly investigated.

In Chapter 3, fabrication techniques are developed for the construction of microfluidic fuel cell channel structures. For optimal fuel utilization, electrode access must be available on top and bottom channel walls. Two approaches are taken: fabrication of two-walled channel structures in PDMS and fabrication of channels in SU-8 photoresist.

In Chapter 4, electrode patterning techniques with applications to microfluidic fuel cells are investigated. A number gold patterning methods are presented, along with the merits of each. Using techniques for fabrication within microfluidic channels, a gold patterning method is presented that negates precision alignment in the assembly of double-sided fuel cells. Multiple carbon electrode fabrication methods are also developed and implemented in vanadium microfluidic colaminar fuel cells..

In Chapter 5, a dynamic microfluidic photomasking device is presented. Laminar microfluidic streaming is exploited to achieve photomasking with dynamic spatial control. Two light absorbing streams hydrodynamically focus a transparent stream to define a line of light transmission. A multiple layer microfluidic device incorporating two such microfluidic layers, aligned orthogonally, enables light transmission only where

the transparent streams overlap. Control of fluid flow in the microfluidic layers enables dynamic spatial control of the exposed region. Application to microarray patterning and microfabrication is investigated.

In Chapter 6, a brief overview of the key contributions of the thesis is given, and a summary of future projects stemming from these findings are proposed.

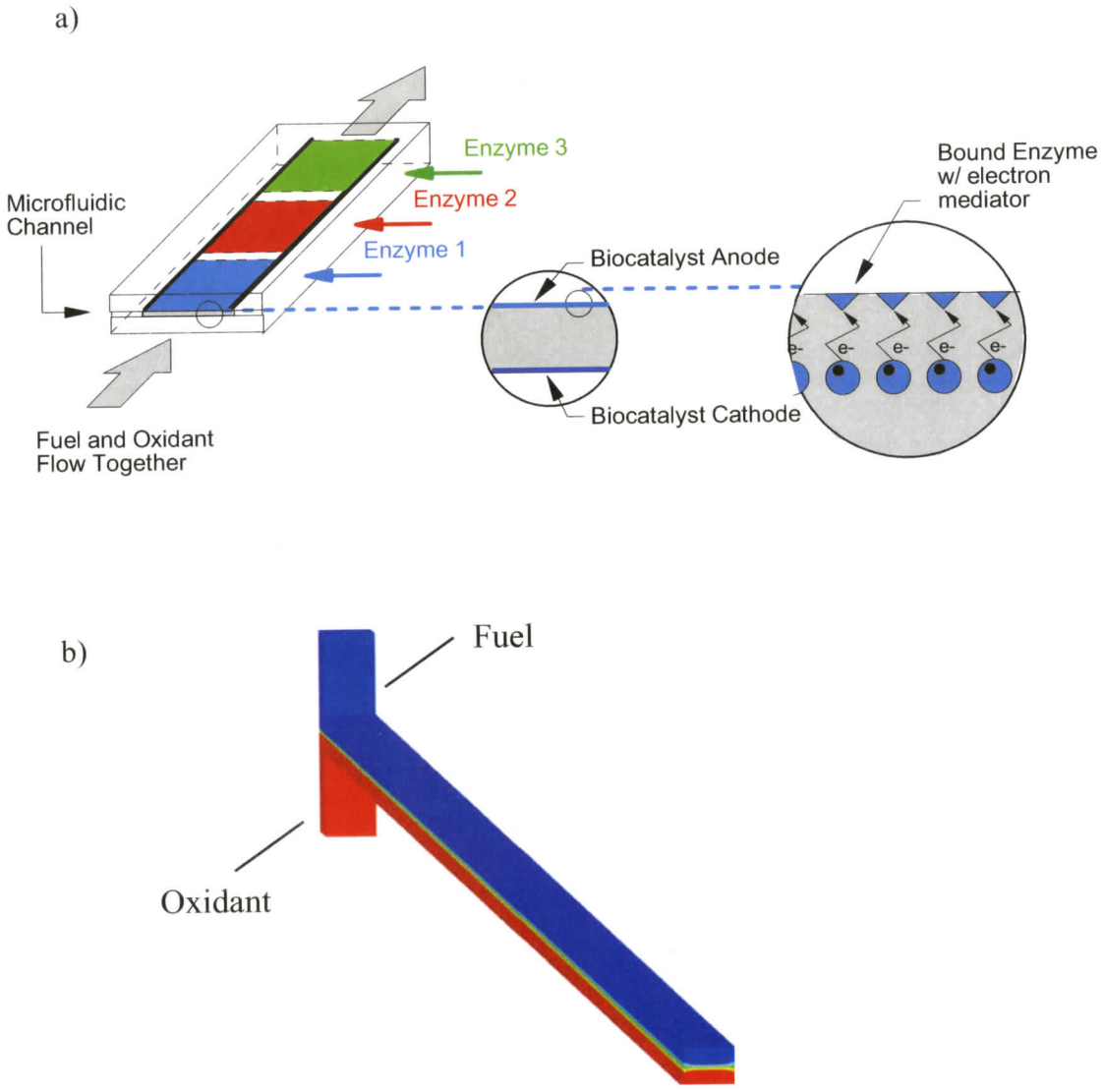

Figure 1.1 Schematic of enzymatic microfluidic membraneless fuel cell architectures: a) enzymatic fuel cell, b) colaminar fuel cell

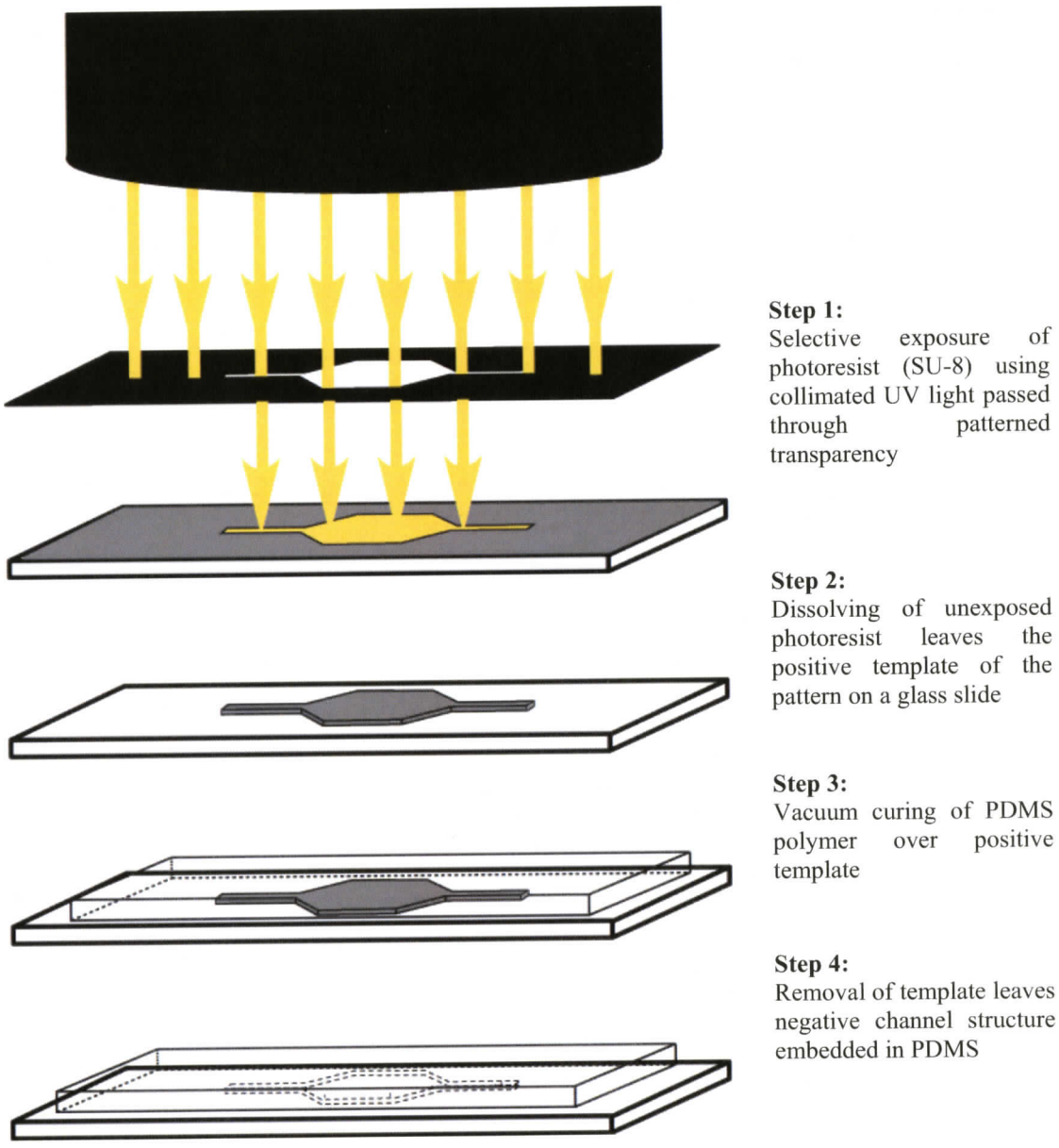

Figure 1.2 Schematic and description of the soft-lithography microfabrication method.

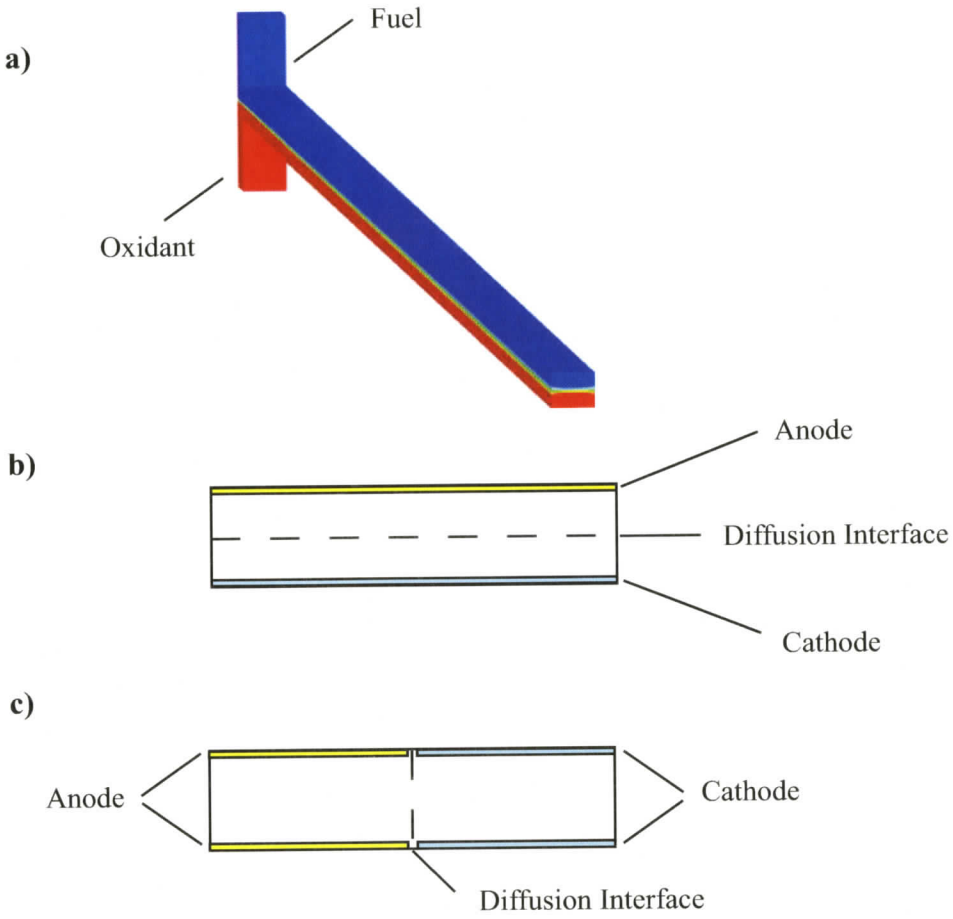

Figure 1.3 Examples of electrode configurations for microfluidic membraneless fuel cell; a) colaminar flow pattern, b) top-and-bottom design, c) side-by-side design. The reduced diffusion interface inherent in the side-by-side design reduces the amount of reactant wasted to the mixing region.

Chapter 2

DEVELOPMENT OF IN-HOUSE FABRICATION PROCESSES TOWARD RAPID PROTOTYPING SOFT LITHOGRAPHY

This chapter details the development of rapid prototyping soft lithography microfabrication techniques in the context of facilities available at the University of Victoria's Microfluidics Laboratory. This method allows a for quick turnaround from design conception to operating device on the order of a single day, enabling rapid design iterations and accelerating the pace of research. The quality of fabricated devices by this method is highly dependent on processing parameters involved in creating the channel template. The processing parameters are, to some extent, equipment-specific. The optimization of processing parameters and the expansion of template fabrication to ultra-thick photoresist structures is detailed in this chapter.

2.1 Rapid Prototyping Soft Lithography Background

The rapid prototyping soft lithography method has been employed by many researchers since its initial publication [Duffy et al. (1998)], as evidenced by the 564 citations listed by ISI Web of Science as of April 30, 2006. This methodology allows for very fast turnaround from design conception to an operating device, allowing for rapid design iterations and an accelerated research and development pace [McDonald et al. (2000)]. High-resolution transparency photomasks can be cheaply and quickly created by

a simple image setting process that is common to commercial print shops, enabling photoresist template patterning with minimum features of ~ 20um [Ng et al. (2002)]. Channel fabrication is achieved by molding poly(dimethylsiloxane) (PDMS) prepolymer on the template and curing. In all, the design and fabrication of a novel microfluidic device can be performed within a single day.

A wide variety of microfluidic devices have been fabricated by this method to perform many functions. These include capillary electrophoresis [Duffy 1998], gateable fraction collection of mass-limited samples [Tulock et al. (2004)], DNA sorting [Chou et al. (1998)], substrate patterning with biological materials [Folch et al. (1999); Takayama et al. (1999)], and microfabrication devices [Chen et al. (2003); Kenis et al. (2000)]. Integrated components of complex devices have also been created using the method, including diffraction grating detectors [Schueller et al. (1999)], switches [Duffy et al. (1999)], pressure monitors [Hosokawa et al. (2002] and large scale flow control valve systems [Thorsen et al. (2002)]. Other applications have replaced PDMS with alternative materials, including thermoset polyester [Fiorini et al. (2004)] and photocurable perfluoropolyethers [Rolland et al. (2004)], extending the method to applications where PDMS is not a suitable material. SU-8 photoresist has been employed as a structural material in the fabrication of a micromixer with on-line optical detection [Jackman et al. (2001)], nozzle dispenser [Bohl et al. (2005)], and as a channel structure for a vanadium species flow battery [Ferrigno (2002)].

This chapter describes the establishment and development of basic rapid prototyping soft lithography fabrication methods. The development of in-house fabrication techniques has proven to be an enabling technology in the University of

Victoria Microfluidics Lab, facilitating the fabrication of a large variety of microfluidic devices. These devices include a sequential injection microfluidic mixer [Coleman et al. (2006)], a microfluidic photomasking system [McKechnie and Sinton (2005); McKechnie and Sinton (2006); McKechnie and Sinton (2006)], a redox-based flow velocimetry device [Kjeang et al. (2006)], and a nanohole array on-chip detection device [De Leebeck et al. (2006)], as well several projects that are currently under development. In this chapter, details of the optimization of fabrication for the existing equipment in the University of Victoria's microfluidics laboratory are presented. Photomask design and production is detailed and analyzed. The various stages of photoresist processing toward the creation of channel templates are investigated and optimized. The fabrication of channel structures in PDMS is detailed, as well as irreversible sealing to enclose the channel. Finally, the expansion of fabrication techniques to ultra-thick photoresist structures is investigated.

2.2 Materials and Methods

Laboratory equipment is shown in Figure 2.1. Equipment includes a spincoater (G3P-8 Desk-Top Precision Spin Coating System, Specialty Coating Systems, Indianapolis, IN), digital hot plates (EchoTherm HP30A, Torrey Pines Scientific, San Marcos, CA), collimated 350 W mercury arc lamp exposure system (PRX 350-9, Tamarack Scientific, Corona, CA), plasma cleaner (PDC-32G, Harrick Scientific, Ossining, NY), vacuum oven (280A, Fisher Scientific, Pittsburgh, PA), and ultrasonic cleaner (FS20H, Fisher Scientific, Pittsburgh, PA).

Photoresist products (SU-8 25 and SU-8 50 photoresists, and SU-8 Developer)

were purchased from MicroChem (Newton, MA). PDMS pre-polymer and curing agent (Sylgard 184, Dow-Corning) were purchased from E.B. Peerless (Vancouver, BC). Methanol of minimum 98% purity was attained from EMD Chemicals (Hawthorne, NY). Millipore water (Millipore, Billerca, MA) was deionized to an ohmic resistance of 18.2 MΩ/cm.

Relevant dimensions of photomasks and photoresist structures were measured with a Leica DMLM microscope equipped with a Retiga 8-bit cooled CCD camera. Samples were illuminated from below using a standard halogen microscope bulb. Height of photoresist structures was measured using a Mitutoyo Digimatic micrometer with 1 μm graduation.

2.3 Rapid Prototyping Soft Lithography Method

The rapid prototyping soft lithography microfabrication method is explained in detail in Chapter 1. Briefly, a negative template is fabricated with photoresist, a photosensitive polymer, on a durable substrate. The spin-coating speed during the application of the photoresist layer determines the structure height, while the selective exposure of the photosensitive layer through a photomask with opaque and transparent designs defines the channel structure width and length. Fabrication quality in the rapid prototyping method is dependent on the photomask resolution and its fidelity to the original design, as well as the photoresist processing methodology. A pre-polymer, typically poly(dimethylsiloxane) (PDMS), is then cast on the template and cured, creating a three-walled PDMS channel structure. Sealing this to a flat substrate encloses the channel structure. PDMS can be reversibly sealed to a flat substrate via conformal

contact, while irreversible sealing of PDMS to a variety of materials, including glass, some polymers, and itself is also possible.

2.4 Template Fabrication

2.4.1 Photomask Design and Production

Photomasks were initially drafted using AutoCAD 2006 LT (Autodesk, San Rafael, CA). As the relation between the software's drawing units (DU) and actual printed units (PU) is user-defined, all drafting can be performed using a convenient scale determined by the user. Structures are drafted by drawing the outline of the design and hatching to fill. Lineweight must be set to zero, or a finite line thickness will be added to the dimensions of the printed design, although this is not visible in the AutoCAD interface. All photomasks were printed by image setter at a local commercial printer (Island Graphics, Victoria, BC). The facility required all photomask designs to be in Encapsulated Post Script format (EPS), requiring a conversion from the standard AutoCAD DWG format. Designs can be plotted directly to an EPS file with a resolution of 5080 dpi, equivalent to a pixel size of 5 μm.

Printing of the photomasks introduced some dimensional inaccuracies to the photomask design process. Feature widths were reproduced with a fairly high degree of accuracy, but were limited by the pixel size of the image setter. Reproductions of features contained a finite number of pixels, so rounding of dimensions occurs to a closest pixel fit. As Figure 2.2 illustrates, feature sizes smaller than 20 μm were not properly reproduced in the photomask. Nominally clear exposure regions were distorted and partially opaque. Resolution varied between the horizontal and vertical directions,

suggesting a non-square pixel shape. While larger features can be reproduced to allow proper exposure, the actual dimensions of these features are subject to significant error. Figure 2.3 shows images of photomasks with feature widths of 20 μm, 25 μm, 40 μm and 50 μm. Slight imperfections due to the printing process are introduced at interfaces between opaque and transparent sections, creating rough feature walls, as seen in Figures 2.2 and 2.3. Measurements of the 20 μm and 25 μm masks revealed that their dimensions were identical, the horizontal feature of both measuring a width of 20.2 μm and the vertical feature of both measuring a width of 17.5 μm. Features with a width of 40 μm were reliably reproduced by the image setting method, varying between 37.0 μm and 40.2 μm, whereas nominally 50 μm features had a printed width of 56.3 μm. This brief analysis illustrates the inaccuracies introduced during the printing process due to pixel rounding. Fidelity of the printed photomask to the original drawing improves as feature size increases, as expected since the influence of discrete pixel size becomes less significant. At lower feature sizes, prior knowledge of the pixel size may be used to minimize pixel rounding error, albeit at a cost of increased design constraints.

2.4.2 Substrate Preparation

To ensure a high quality photoresist coating, the base substrate must be properly cleaned as contaminants readily cause defects in the photoresist layer. A three-step cleaning procedure was developed to accomplish this. Initially, substrates were cleaned with methanol, employing ultrasonication to accelerate the cleaning process. The substrates were then rinsed with Millipore water under ultrasonication. Subsequently, the substrates were bathed in piranha solution, a 3:1 mixture of sulfuric acid and hydrogen

peroxide, to actively oxidize any surface contamination. Before use, substrates were rinsed in Millipore water and dehydrated by baking at 120 °C.

2.4.3 Photoresist Patterning

A variety of photoresists can be employed for template fabrication. SU-8, a common, negative tone photoresist, is used exclusively here. SU-8 photoresists are mixtures based on EPON SU-8 resin [Lorenz et al. (1997)]. The resin is dissolved in gamma-butylorlactone solvent to thin the resin to a desired viscosity, determined by the target photoresist thickness [Zhang et al (2001a)]. Triaryl sulfonium salt is added to act as the photoinitiator, locally generating acids and initiating the cross-linking of SU-8 when exposed to near-UV light [Zhang et al, (2001b)]. A variety of SU-8 photoresists are available, with typical patterned thicknesses ranging from 2 μm to 100 μm due to the variation in photoresist viscosity [MicroChem (2002a); MicroChem (2002b)]. Processing methods are similar for all SU-8 products, as they differ only in solvent concentration.

Spin-Coating

A thin SU-8 photoresist layer is created on a planar substrate by spin-coating. An initial ramping stage from stop to 500 rpm at an acceleration of 100 rpm s^{-1} serves to spread the photoresist and cover the entire slide. Spinning speed is then accelerated at a rate of 300 rpm s^{-1} to the final speed and held for a total of 30 s [MicroChem (2002a)]. The thickness of the photoresist layer is determined by the final rotational speed during spin-coating and the viscosity of the photoresist. Approximate correlations between spin speed and the resulting photoresist thickness for SU-8 photoresist products are provided by the supplier [MicroChem (2002a); MicroChem (2002b)]. However, knowledge of the

exact dimensions of microfluidic channels is vitally important for experimentation where channel height is a critical parameter. The actual thickness is highly dependent on the exact processing parameters and composition of the photoresist. For example, the viscosity of SU-8 photoresist is sensitive to temperature, thus resulting in significantly shorter structures if coated at elevated temperatures [Bogdanov and Peredkov (2000)].

In order to better correlate the resulting structure height with spin speed, direct measurements of SU-8 25 photoresist layers were obtained. The resulting data is depicted in Figure 2.4. Near the edge of the substrate, photoresist thickness increases due to the well-known edge bead effect, an artifact of the spin-coating process [Lin et al. (2002)]. As such, data was not collected close to the substrate edge. A significant trend was found to exist, showing actual photoresist structures to be on average 20% thicker than predicted by the supplier. In order to attain microfluidic devices of accurate dimensions, this must be factored into the processing of the photoresist template.

Small variations of photoresist height over a single substrate were also noted. SU-8 25 layers spin-coated at 1000 to 6000 rpm were investigated. Not including measurements near the edge bead where a non-planar surface was expected, the standard deviation in thickness measurements across a single coated slide typically ranged from 1 μm to 5 μm. Ideally, photoresist layers self-planarize during the spin-coating and baking steps, creating a consistent height across the substrate [Liu et al. (2004)]. Fluctuations in height across a single sample suggest the presence of defects due to improper processing or inconsistent height of the base substrate. The thickness of a microscope slide, employed as the substrate, was found to have a standard deviation of 2.9 μm about the mean value of 0.988 mm, a variation similar to that witnessed in photoresist height

measurements. To determine whether deviations are due to irregularities in the substrate or photoresist surface would require further investigation. While these irregularities introduce random error into thickness measurements, it is not expected that the systematic discrepancy between the average measured and expected photoresist thicknesses would result from this.

Soft Bake

Following the spin coating step, photoresist layers are soft baked to evaporate their solvent content and condense the photoresist film [Liu et al. (2004)]. Soft bake temperatures and times for a two step process were provided by the supplier and proved sufficient for use in the laboratory [MicroChem (2002a)]. Initially, a short bake at 65 °C ramps the temperature of the substrate and photoresist, allowing the solvent to evaporate out of the film at a steady rate. This improves the coating fidelity and adhesion to the substrate, while also reducing the edge bead [MicroChem (2002a)]. A subsequent longer bake at 95 °C continues the evaporation and condensation process. Of note is the necessity of using a level hot plate to attain a planar photoresist surface of consistent height [Bogdanov and Peredkov, (2000); Liu et al. (2004)]. SU-8 is baked above its glass transition temperature, rendering it susceptible to gravity-forced flow on a non-level surface.

During the soft bake step, photoresist layers are highly susceptible to contamination from airborne particulates. Contamination causes the local retreat of the photoresist layer, creating divots in the surface. However, in order to allow for proper baking, solvent evaporation to the local environment must be allowed. To accommodate both needs, simple dust covers were created that blocked particulates from contacting the

photoresist surface while also allowing the exchange of gases. An image of the dust cover is shown in Figure 2.5. A supportive ring was made by cutting out the top surface of a polystyrene petri dish lid. The supportive ring was placed on the hotplate around the photoresist-coated substrate. A Kimwipe tissue (Kimberly-Clark Professional, Roswell, GA) was placed on top of the supportive ring and used as a filter, preventing dust from settling on the photoresist while allowing the transport of evaporated solvent. This design proved effective in preventing the contamination of photoresist surfaces. A visual comparison of protected and unprotected photoresist layers is shown in Figure 2.6.

Exposure

One of the more vital steps of the fabrication process is exposing the photoresist through the photomask. Exposure to near-UV light of wavelengths between 350 nm and 400 nm locally generates acid which initiates photoresist cross-linking [MicroChem (2002a)]. The exposure of photoresist creates a "front" of exposed resist, which grows out from the addressed surface with increasing exposure time [Cabral et al. (2004)]. Insufficient exposure doses are unable to adequately initiate polymerization throughout the thickness of the photoresist and transferred patterns are not strong enough to resist slight dissolution during the development stage. Detachment from the substrate surface can occur in cases of extreme underexposure. An upper limit to the exposure dose also exists. Over-exposing results in the creation of "shadows", finite areas of partially exposed photoresist around the desired features due to a combination of Fresnel diffraction at the edge of opaque sections, refraction at the air-photoresist interface, and reflection from the base substrate [Zhang et al. (2004)]. The effect of over-exposure can be readily seen in Figure 2.7. Improvements on the fidelity of photoresist patterns to the

photomask design can be attained by determining an optimal exposure dose, which is dependent on the resist thickness. Approximate exposure doses for a range of photoresist thicknesses with 365 nm light source are provided by the supplier [MicroChem (2002a)]. Figure 2.8 shows the relation between exposure time and shadow thickness for a number of photoresist thicknesses, labeled by spin-coating speed. Optimal exposure times can be determined for a variety of spin-coating speeds by minimizing the shadow thickness while also ensuring adequate exposure. A selection of exposure times for SU-8 25 spin speeds is presented in Table 2.1.

Post-Exposure Bake

Following the exposure step, the substrates are baked to accelerate the cross-linking reaction in the exposed photoresist. Inadequate post exposure bake times, therefore, will result in poorly cross-linked resist structures, which can cause the deterioration or failure of the transferred design during developing. Besides ensuring adequate cross-linking of the photoresist, care must be taken to minimize stresses that are induced during the post-exposure bake. In extreme cases, stresses in the film can cause photoresist cracking and bowing of flexible substrates [Lorenz et al. (1998a)]. Stress can be minimized by reducing thermal gradients during the heat-up to 95 °C for the post exposure bake and by avoiding rapid cooling after the bake [Lorenz et al. (1998a)]. Performing the post-exposure bake at excessive temperatures has been found to cause flowing of the exposed photoresist structure, causing structural deformations [Liu et al. (2004)]. Bake time is dependent on resist thickness. Approximate post-exposure bake times and temperatures for a two-step bake process are provided by the supplier and were found to be sufficient [MicroChem (2002a)].

Development

The templates are subsequently developed in PM acetate developer. The time required to completely remove unexposed photoresist is dependent on the photoresist thickness, presence of agitation or vibration, feature size of the exposed pattern, and previous use of the developer solution. While it is possible to determine an optimal development time for a given photoresist structure, this would be unique for the combination of the aforementioned parameters and as such is of little benefit to the rapid prototyping process. Developing can be visually inspected to approximate when the process is complete. A subsequent rinse with isopropyl alcohol serves to both arrest the development process by removing developer and indicate if development is complete. Unexposed photoresist remaining on the surface turns into a white, flaky material during the isopropyl rinse [Bogdanov and Peredkov (2000)]. Further development will remove the white material and complete the development process. Any remaining surface contamination can be removed with a short acetone bath, although care must be taken as overexposure to acetone will strip photoresist structures from the substrate surface [Agarwal et al. (2004)].

2.5 Channel Fabrication

Microfluidic channels are created by curing a polymer on the photoresist-patterned template. PDMS is commonly used, due to its many favourable characteristics including chemical stability, high reproduction fidelity, minimal cost, optical transparency down to 280 nm, and ease of sealing. PDMS is made by mixing the base and curing agent at a 10:1 weight ratio. The mixed prepolymer is degassed under

vacuum for approximately 45 minutes or until all air bubbles are removed from the bulk polymer. The polymer is then poured over the templates in a petri dish and cured. Elevated temperatures decrease the curing time; PDMS baked at 95 °C cures in less than two hours.

Following curing, the PDMS design can be removed from the template and sealed to a planar surface, thus enclosing the channels. Sealing of microfluidic structures is generally non-trivial [Duffy et al. (1998)]. Irreversible sealing can be attained by plasma treating the channel structure and base substrate. When brought into contact, a condensation reaction occurs, creating a permanent bond between PDMS and a variety of substrate materials [McDonald et al. (2000)]. This also results in a microchannel structure that is hydrophilic and can support electro-osmotic flow [Duffy et al. (1998)]. Plasma treatment times vary by equipment. For the particular plasma cleaner available, a treatment time of 30 s on high power has been found ideal for the irreversible sealing of PDMS. Care must be taken when exposing the PDMS to oxygen plasma; overexposure can cause surface cracking and does not result in a permanently sealable surface. In order to ensure an adequate supply of oxygen, the bleed valve is opened slightly and adjusted to attain maximum plasma intensity. Under excessive vacuum, an inadequate supply of oxygen limits the amount of oxygen plasma present. While PDMS can irreversibly bond to a variety of materials, the PDMS to PDMS bond is superior. Figure 2.8 shows a 50 μm tall dye-filled PDMS channel structure irreversibly sealed to a glass substrate.

In circumstances when the plasma treating strategy is ineffective, for instance PDMS sealing to a metallic surface, the elastomeric nature of PDMS can be exploited to achieve clamping with a pressure-based seal. This method is discussed further in Chapter

4. Although less elegant than the plasma-based method, clamping seals are robust and reversible.

2.6 Ultra-Thick Photoresist Patterning

While microfluidic devices typically employ channels with height on the order of 10 μm, some applications may require taller channels or photoresist structures. Channel structures taller than 100 μm have been employed in the fabrication of thrust-generating micronozzles and a high-performance micropost microreactor [Lin et al. (2002)], as well as a mass spectrometry device with capillary tube interface [Carlier et al. (2004)]. Components for microelectromechanical systems (MEMS) frequently require thick photoresist structures, which are often employed as device components. Conradie and Moore (2002) employed high aspect ratio SU-8 structures to increase the mass of a silicon cantilever. Lorenz et al. (1998b) used thick SU-8 structures as a mold pattern to facilitate injection molding and as a template to electroplate metallic gears and coils. SU-8 photoresist has also been employed as a material for the fabrication of fluidic interconnects [Gray, (2005)].

Fabrication of thick photoresist layers is problematic, as photoresists are primarily designed to produce thin films. SU-8 photoresist has the advantage of being quite adaptable to thick layers. SU-8 100 can create a resist layer 250 μm thick with a single coat [MicroChem (2002b)]. Taller structures, however, require alternative methods of coating. For instance, spin-coating successive layers of photoresist has been used to build up tall structures [Gray (2005); Lorenz et al. (1998b); Carlier et al. (2004)]. This process, however, is very time consuming as each photoresist layer requires a soft bake

step. Soft bake, exposure, and post-exposure bake steps must be calibrated for the significantly taller photoresist heights.

Ultra-thick SU-8 layers, ranging in structure height from 0.5 mm to 1.5 mm, have been fabricated using a single photoresist dispensing step and modified processing procedure [Lin et al. (2002)]. Employing a precision volumetric dispensing method, an amount of photoresist equivalent to the desired structure thickness is deposited on a substrate. Self-planarization of the photoresist layer occurs during the soft bake step, as thick layers are highly susceptible to gravity-induced flow. The soft bake step is conducted at 120 °C to accelerate the evaporation of solvent. Exposure, post-exposure bake, and development followed a methodology similar to that for thin SU-8 layers, although thermal gradients must be more conscientiously avoided due to the increased risk of stress-induced failure. After development, a second exposure step is employed to further cross-link the SU-8 structure.

Both methods were employed for the fabrication of thick structures using the available laboratory equipment and achieved results similar to that in the original publications. Building up a thick SU-8 layer by coating successive thin layers was found to increase the possibility of contamination by increasing bake times. Divots created in the initial layer were generally reproduced in subsequent layers until a thickness of ~ 400 μm was attained. At this thickness, gravity-forced flow of the liquid photoresist was sufficient to overcome surface contamination. Applying the methodology of Lin et al. (2002) served to streamline the production of thick layers. Results attained within the range of 500 μm to 1.5 mm were consistent with those recorded by the authors. Figure 2.10 shows a 1 mm tall structure fabricated in SU-8 by this method. The expansion of

this process for coating thinner photoresist layers down to 125 μm was attempted. This adaptation successfully created consistent, planar layers of photoresist, allowing for the use of this method to create a wide range of photoresist layer thicknesses unattainable by a single spin coat. Exceeding a thickness of 1.5 mm is not possible by this method, as the photoresist flows over the substrate edges due to gravity.

2.7 Summary

This chapter detailed the establishment and customization of rapid prototyping soft lithography fabrication processes at the University of Victoria's microfluidics laboratory. The design and production of photomasks was described. Processing steps for the fabrication of photoresist-patterned microchannel templates were optimized for the available laboratory equipment to attain high quality templates. Of particular importance are the prevention of contamination during the soft bake step and the calibration of exposure dose to avoid structure deterioration and excessive shadowing. Channel fabrication in PDMS was also investigated, as well as the irreversible sealing of the resultant channels. Finally, two methods of fabricating thick template structures were investigated: the multiple coating method and precise volumetric dispensing method. The precise dispensing method was expanded to pattern photoresist structures as thin as 125 μm, expanding the functionality of this method. Optimization of these processes has allowed for the in-house fabrication of a wide variety of microfluidic device prototypes, and forms the basis for electrode patterning and integrated microfluidic fuel cell fabrication.

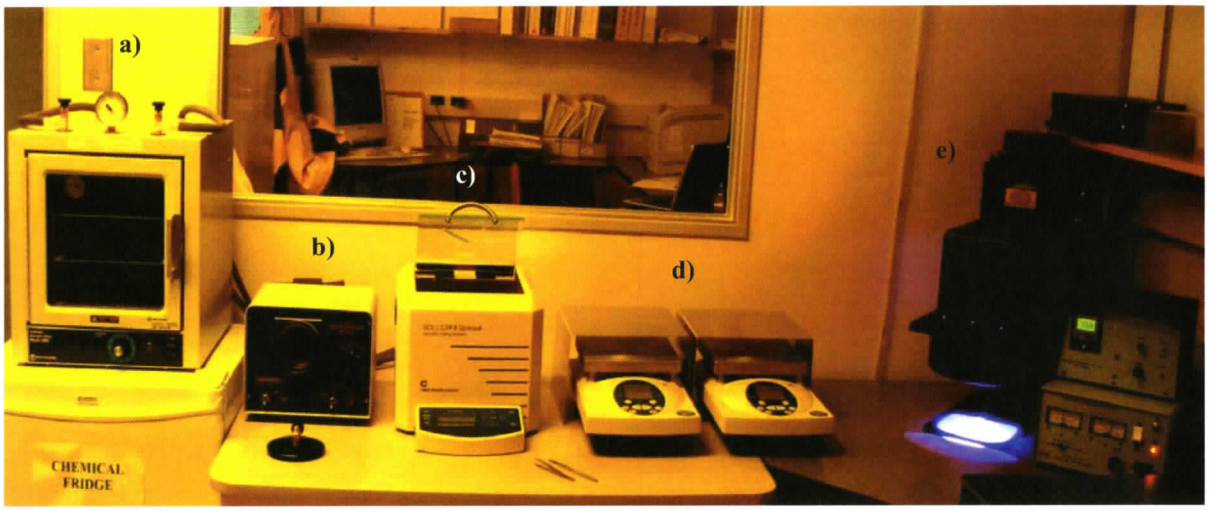

Figure 2.1 Microfabrication equipment in the microfluidics laboratory: a) vacuum oven, b) plasma cleaner, c) spin coater, d) digital hot plates, e) exposure unit, including power supply and timer. Ultrasonic cleaner is not pictured.

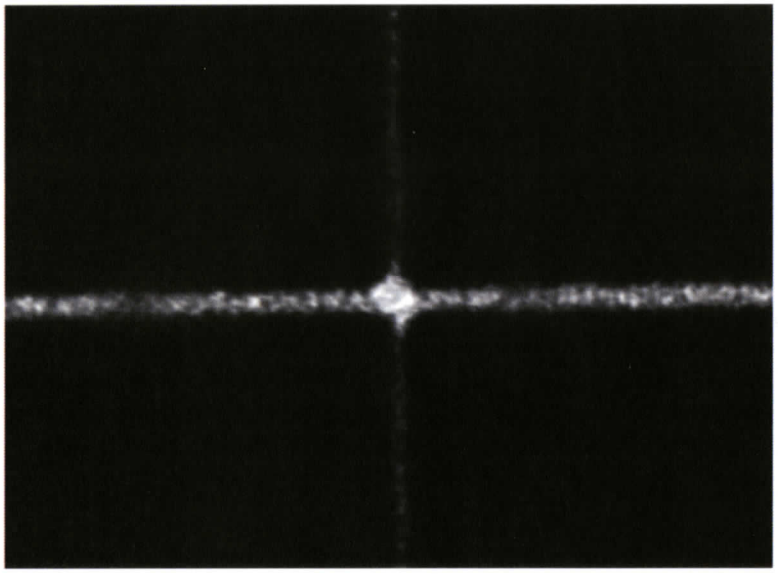

Figure 2.2 Image set photomask containing nominally 15 μm lines in the horizontal and vertical direction. Resolution of lines in either direction is insufficient to adequately reproduce features; however resolution in the vertical direction is especially limited.

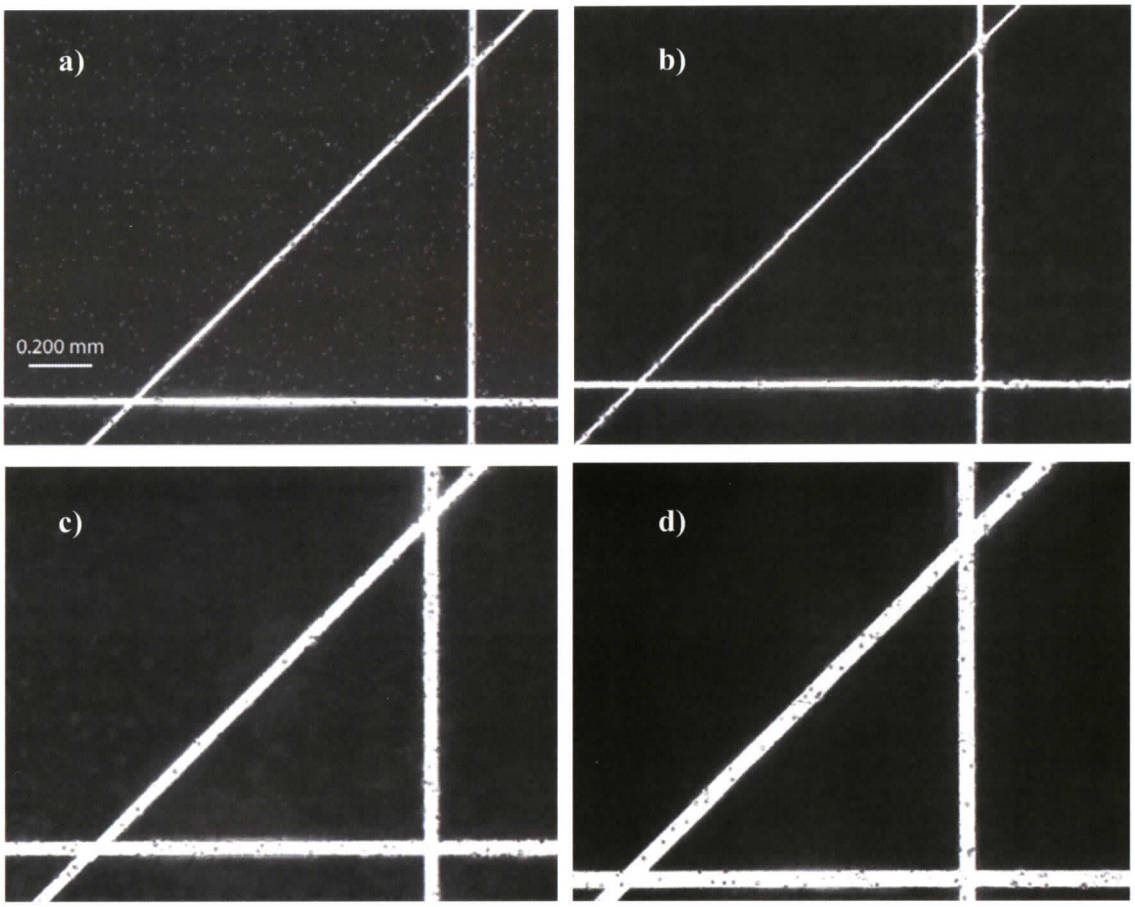

Figure 2.3 Image set photomask reproduction of various line thicknesses: a) 20 μm, b) 25 μm, c) 40 μm, and d) 50 μm. Finite pixel size of the printing process introduced geometrical errors, although images a) and c) were faithfully reproduced with minimal error because of their fit with pixel size. Line thickness of image b) was measured as ~ 20.2 μm in the horizontal direction, a 20% error, while the measured thickness of image d) exceeded the design thickness by 12%.

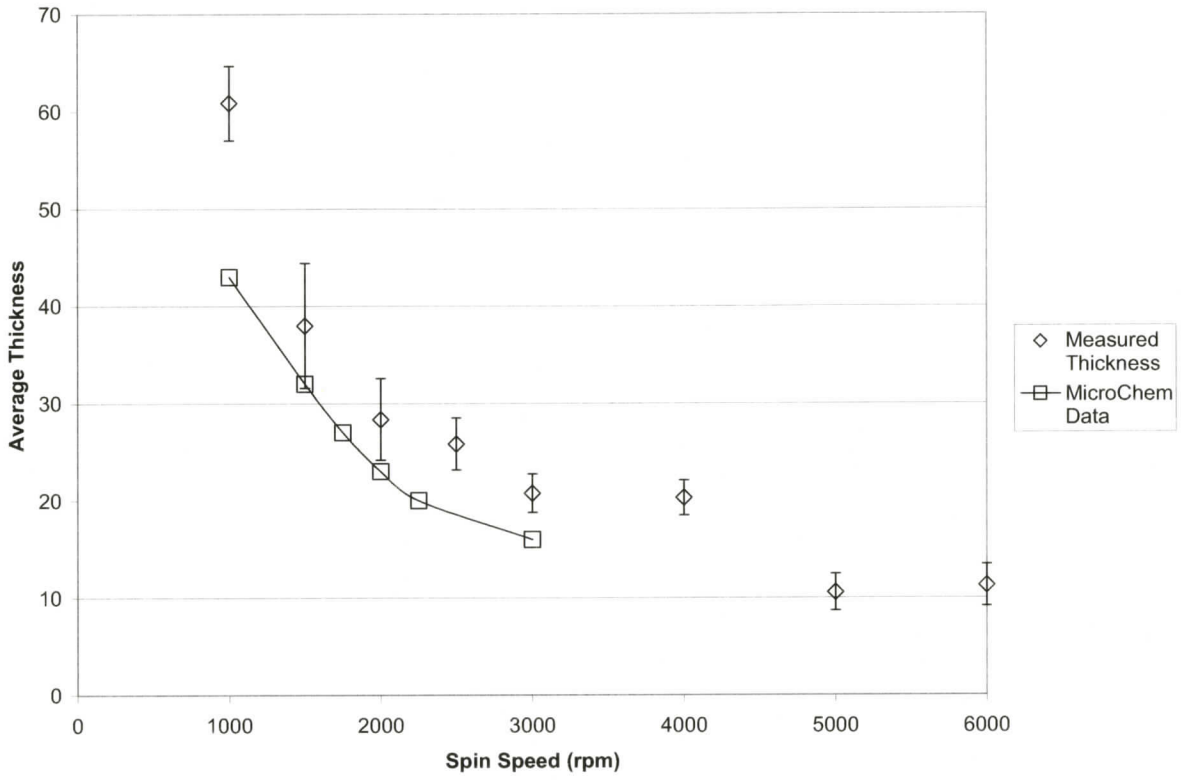

Figure 2.4 SU-8 25 photoresist thicknesses for a variety of spin coating speeds, comparing measured and supplied correlation [MicroChem (2002)]. Measured thicknesses were consistently ~ 20% larger than supplied data. Error bars represent one standard deviation of measurements.

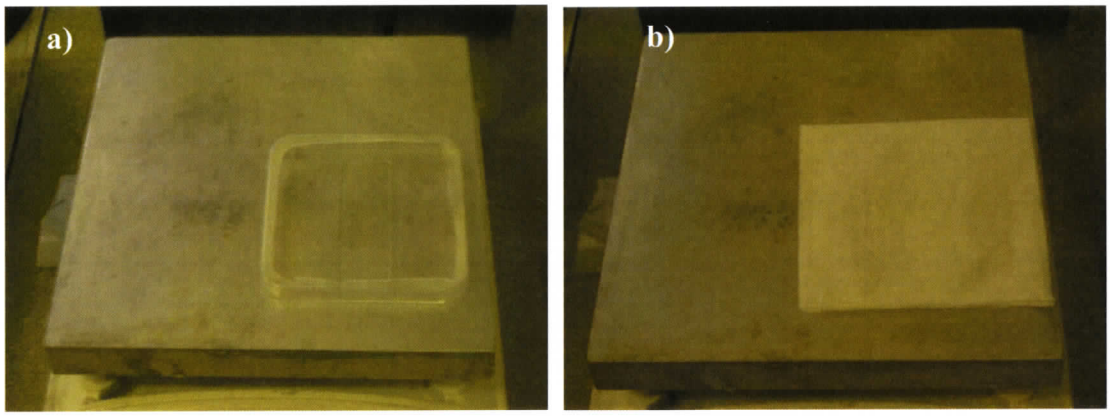

Figure 2.5 Images of dust cover during soft bake. A) Supportive ring is placed over top of photoresist sample and B) covered with Kimwipe to protect from airborne particulates while allowing transport of evaporated solvent.

Figure 2.6 Image of photoresist-coated microscope slides. Sample on the left was protected by dust cover during soft bake, while the layer on the right was unprotected and contains a number of surface imperfections.

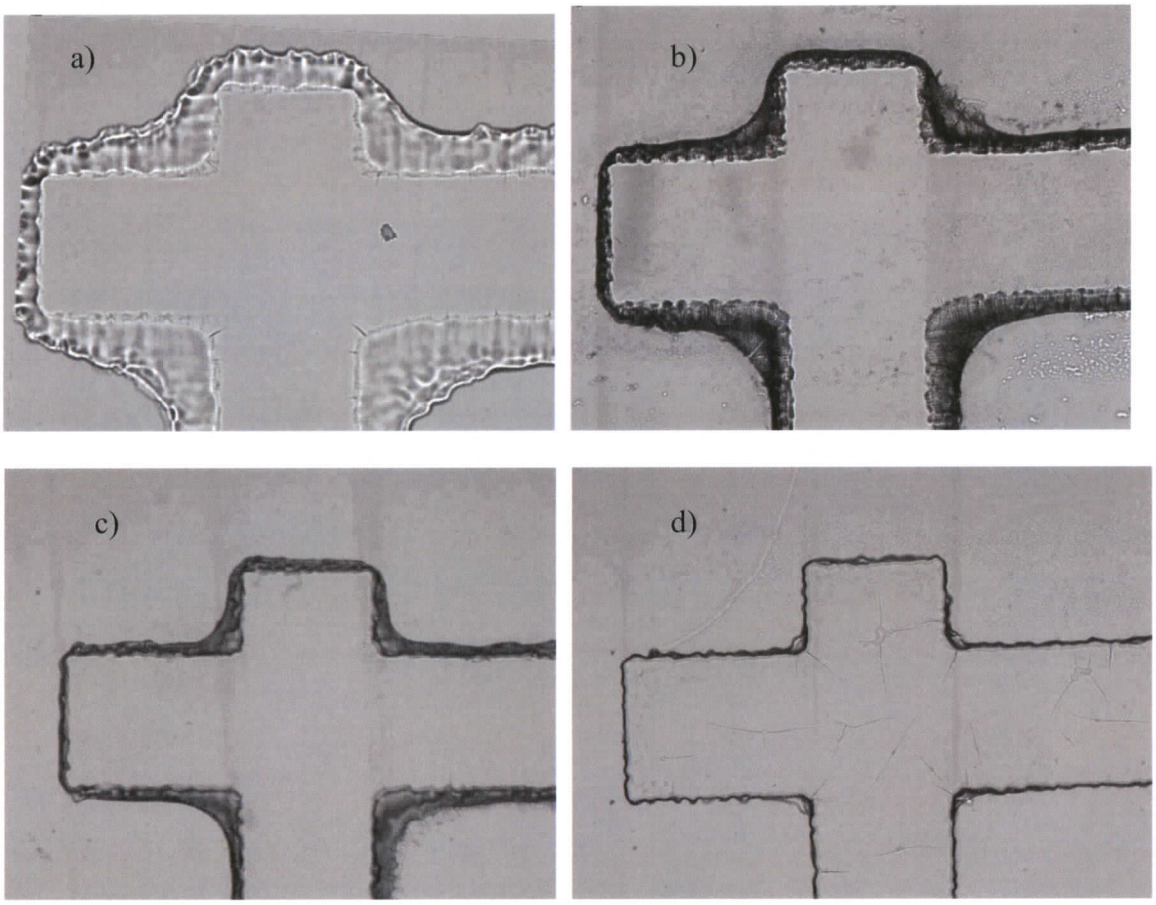

Figure 2.7 Variation of shadow thickness with exposure time. SU-8 25 photoresist layer spin coated at 5000 rpm. Exposure times of a) 50 s, b) 40 s, c) 30 s, and d) 15 s.

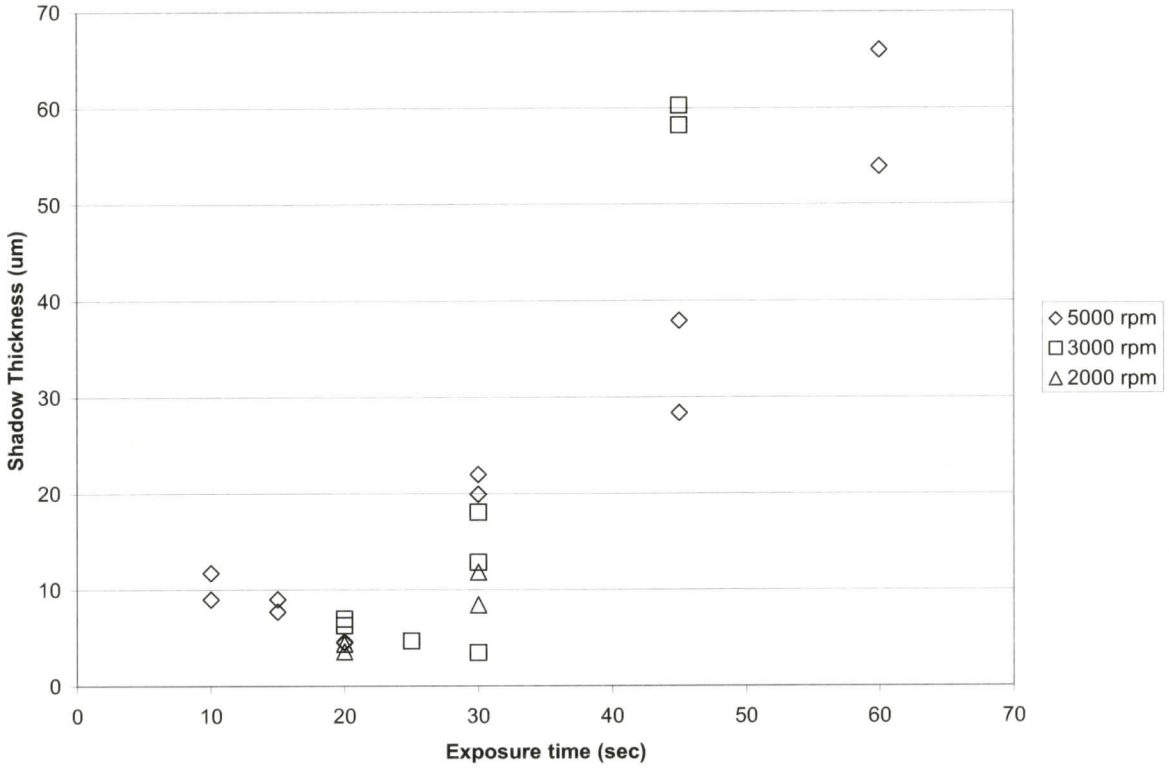

Figure 2.8 Thickness of feature "shadows" for a variety of SU-8 25 thicknesses. Shadow thickness becomes significant at extended exposure times.

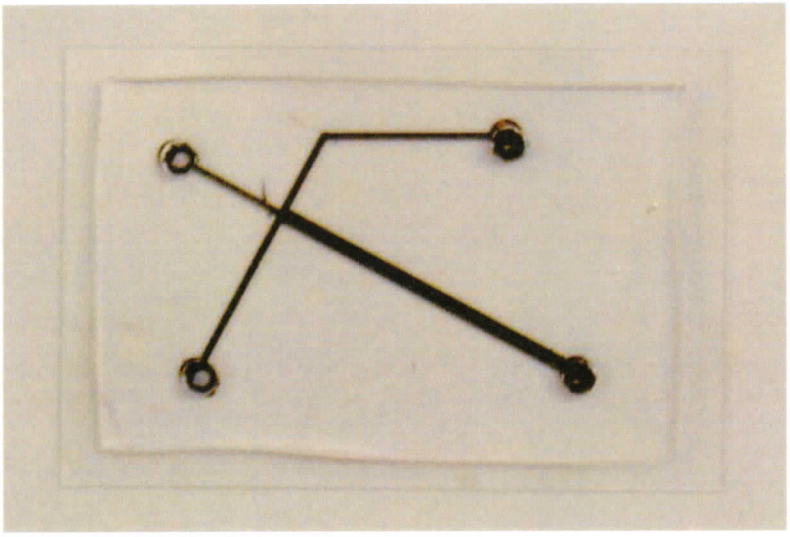

Figure 2.9 Microfluidic channel fabricated in PDMS, sealed irreversibly to microscope slide by plasma treatment. Channel is filled with dye to enable visualization. Channel height (out of plane) was 50 μm.

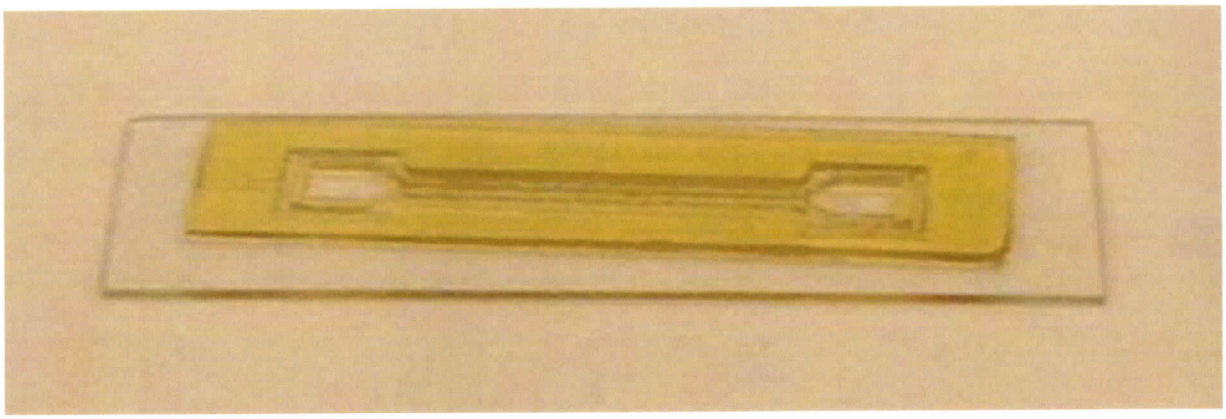

Figure 2.10 Patterned SU-8 layer with a structure height of 1 mm.

Spin-Coating Speed (rpm)	Exposure Time (s)
1000	45
2000	30
3000	25
5000	15

Table 2.1 Optimized SU-8 25 photoresist layer exposure times for various spin-coating speeds. Exposure was performed using a Tamarack 350 W mercury arc lamp collimated light source.

Chapter 3

CHANNEL FABRICATION FOR MICROFLUIDIC MEMBRANELESS FUEL CELLS

In this chapter, channel fabrication techniques for the production of microfluidic membraneless fuel cells are discussed. As described earlier, microfluidic membraneless fuel cells refer here to both colaminar based strategies and biological enzyme-based strategies, the end goal of the microfluidic biological fuel cell initiative. Design parameters for microfluidic membraneless fuel cell architecture are briefly detailed. Fabrication techniques are then developed to facilitate the optimization of channel structure and electrode geometry. First, the fabrication of PDMS stencils with two open surfaces for use with electrode substrates is investigated. A novel adaptation of standard fabrication techniques of microfluidic channels in SU-8 photoresist is then presented, allowing for the use of this method in microfluidic membraneless fuel cell construction. Finally, the extension to three-dimensional fuel cell architectures is discussed.

3.1 Introduction

Miniature fuel cell devices have recently attracted a great deal of attention as an improved power supply for portable electronics [Bazylak et al (2005); Choban et al. (2004)]. Increasing energy density demands associated with the next generation of portable electronics are unlikely to be fulfilled with lithium ion battery technology [Dyer

(2002)]. Fuel cells have the potential to fill this increasing need, due primarily to their potential for higher energy density. Some unique characteristics of miniaturization offer further performance benefits for fuel cells. Of importance is the increase in surface area to volume ratio, offering the potential of increased power density and decreased device size.

Strategies have been employed to preclude the necessity of a separating ion-exchange membrane, offering a number of benefits. The overall size of the fuel cell is reduced, thus increasing power and energy density. Also, performance is improved through the elimination of water management issues and fuel crossover associated with membranes in traditional fuel cells [Yu et al. (2003); Choban et al. (2004); Chang et al. (2005)]. In order to allow for proper functionality without a membrane, the operation of microfluidic membraneless fuel cells must significantly differ from that of standard fuel cells. Enzymatic fuel cells exploit the specificity of enzymes electrically-tethered to and coating the electrodes, eliminating performance losses associated with fuel crossover and allowing for the flowing of fuel and oxidant in a combined, homogenous stream. Colaminar fuel cells take advantage of the laminar nature of low Reynold's number flow in microchannels, which facilitates colaminar streaming of distinct streams. The streams mix slowly by cross-stream diffusion at their interface, with the mixing region essentially serving as a fluidic membrane. Avoiding contact between the mixing region and the electrodes prevents fuel crossover.

The major focus of enzymatic fuel cell research in literature pertains to electrochemical glucose sensors and implantable glucose-based fuel cells to power medical devices [Zhu et al. (2002); Joshi et al. (2005); Heller (2004); Mano et al. (2003)].

The application of enzymatic fuel cells to power portable electronics and lab-on-a-chip devices has also been investigated [Moore et al. (2005)]. Research has largely presented enzyme wiring strategies, including fixation in a polymeric matrix [Ma et al. (2005); Mano et al. (2002); Moore et al. (2005); Gregg and Heller (1990)] and enzyme wiring to an electrode surface layer [Degani and Heller (1988); Katz et al. (1999); Willner and Willner (2001); Xiao et al. (2003); Heller (2003)]. Few investigations have been performed to optimize enzymatic fuel cell architecture. As an exception, Kjeang et al. (2005 – in press) computationally investigated enzyme patterning strategies to optimize fuel utilization for the oxidation of methanol, a three-step reaction requiring three different enzymes.

Literature pertaining to colaminar fuel cells has developed significantly beyond the initial proof-of-concept stage [Ferrigno et al. (2002); Choban et al. (2004)]. The flexibility of membraneless fuel cells to function with different media allowed the successful operation of mixed alkaline and acidic fuel cells [Choban et al. (2005a)]. Incorporation of an air-breathing cathode was found to greatly increase the supply of oxidant to a colaminar fuel cell, greatly improving the power density from previous designs [Jayashree et al. (2005)]. Choban et al. (2005b) investigated the performance-limiting factors of colaminar fuel cells. Computational modeling has also been applied to membraneless fuel cells. Chang et al. (2005) used numerical methods to investigate the performance of a colaminar fuel cell under varying operating conditions. Bazylak et al. (2005) compared fuel utilization use for different channel geometries and electrode placements, although their optimal architecture has yet to be used in an actual device.

In this chapter, design parameters for microfluidic membraneless fuel cell

architecture are discussed. Fabrication techniques are developed to facilitate the optimization of channel structure and electrode geometry, as pertains to enzymatic and colaminar fuel cells. The fabrication of PDMS stencils with two open surfaces is investigated. Standard fabrication techniques of microfluidic channels in SU-8 photoresist are adapted for use in microfluidic membraneless fuel cells. Finally, three-dimensional fuel cell architectures are briefly discussed.

3.2 Microfluidic Membraneless Fuel Cell Design

Optimization of microfluidic membraneless fuel cells primarily focuses on the goal of creating a high energy density power source for portable electronics. In order to maximize performance, several key aspects of fuel cell operation must be considered.

3.2.1 Electrode Surface Area Maximization

As the oxidation and reduction reactions occurring in a fuel cell are surface-based, electrode area must be maximized to achieve optimal power and energy density. One of the major motivations behind microfluidic fuel cells is the exploitation of the increase in surface area to volume ratio inherent to miniaturization. Microfabrication techniques are generally limited to rectangular channel geometries. By replication molding, the width and length of the channel are determined by the exposure pattern, while the channel height is determined by photoresist thickness on the template. Optimization of surface area for a rectangular cross-section results in an infinitely wide channel of infinitesimal height. Such a design is of course infeasible as pumping power would become a dominating parasitic load and operational characteristics of the device would suffer. Fabrication of such a structure would also pose difficulties, and the resulting device

would lack structural integrity. However, the surface area to volume ratio benefit associated with wide, squat channel structures is evident.

3.2.2 Charge Transport

Electron flow in a fuel cell occurs externally to the device, passing electrons from the anode to the cathode and delivering power to a load. In order to maintain electrical charge equilibrium with the movement of negatively-charged electrons, an equal and opposite transport of charge must occur within the device. Charge transport occurs by diffusion of ions in the bulk electrolyte. Acidic electrolyte H^+ ions are transported from the anode to cathode, or basic electrolyte OH^- ions are transported from cathode to anode to compensate for the electron charge transfer. As an example consider reactions occurring in an acidic electrolyte methanol-based fuel cell:

Anode: $$CH_3OH + H_2O \rightarrow CO_2 + 6H^+ + 6e^- \qquad (3.1)$$

Cathode: $$\frac{3}{2}O_2 + 6H^+ + 6e^- \rightarrow 3H_2O \qquad (3.2)$$

The oxidation of methanol at the anode releases 6 electrons to the external circuit and produces 6 H^+ ions. The reduction of oxygen at the cathode acquires 6 electrons from the external circuit and consumes 6 H^+ ions. As such, a deficiency of H^+ ions occurs at the cathode, while an excess is produced at the anode. In a weak supporting electrolyte solution, the timely transport of ions to the electrodes by diffusion and electromigration is essential to maintain the supply of necessary reactants. A strong supporting electrolyte solution, however, supplies an overabundance of ions throughout the device. The delivery of ions to the reaction sites is therefore not a rate-determining process

Ionic charge transport does greatly impact fuel cell operational characteristics, as

ohmic losses are incurred. The resistance of an ionic solution is proportional to the distance across which the current passes and its inherent resistivity, and inversely proportional to the cross-sectional area. As the separation between the anode and cathode increases, or the cross-sectional area available to conduction decreases, resistance losses in the cell increase. This negatively affects fuel cell performance by reducing the operating potential.

3.2.3 Fuel and Oxidant Transport

Rapid transport of fuel and oxidant to the electrodes is essential to provide high power densities. In a diffusion-limited scenario, the reaction rate at the electrode is limited by the flux of reactants to its surface. As shown in Figure 3.1, depletion regions are created near the surface of the electrodes. Minimizing the distance between the depletion region and bulk concentration region increases the rate of reactant transport, thus increasing the overall reaction rate in a diffusion-limited scenario. However, in a situation where the process is reaction rate limited, the rate of transport of reactants is secondary to the operation of the device as reactants are supplied at a much higher rate than they can be acted upon. In this case, fuel and oxidant concentrations are nearly constant throughout the cell [Kjeang et al. (2005 – in press)].

3.2.4 Enzymatic Fuel Cell Design

Enzymatic fuel cells are unique in that their electrodes are specific to a certain substrate. By coating the electrode surface with electrically-tethered enzymes, the reaction favoured by that enzyme becomes dominant, while the presence of other

substrates causes a negligible effect [Kjeang et al. (2005 – in press)]. As such, fuel and oxidant streams can be combined into a single, homogenous stream. While enzymes catalyze the conversion of fuel and oxidant, this has been found to occur more slowly than species transport, resulting in a reaction rate limited scenario [Kjeang et al (2005 – in press)]. Mass transport issues are therefore insignificant. In order to maximize electrode surface area, a wide and squat channel cross-section should be employed. As mixing of fuel and oxidant is of no concern, electrodes can be placed in a top-and-bottom configuration, as shown in Figure 3.2a. Extending the length of electrodes does not incur any performance penalties from charge or species transfer, allowing for simple device scale-up that must consider only fabrication and integration issues. Optimally, the distance between the anode and cathode is minimized to reduce electrical resistance, to the limits of fabrication feasibility and parasitic pumping losses.

3.2.5 Colaminar Fuel Cell Design

The performance of colaminar fuel cells depends greatly on limiting mixing between fuel and oxidant streams. Species that enter the mixing region by diffusion cannot be reacted in the cell and are not recoverable. Minimizing the amount of fuel that enters the mixing region has been shown to greatly improve fuel utilization [Bazylak et al. (2005)]. Within a rectangular channel, the side-by-side electrode configuration shown in Figure 3.2b minimizes the diffusion area between the colaminar fuel and oxidant streams, thus limiting the amount of each lost to the mixing region. Minimizing the height of the channel further reduces the diffusion area between the streams. However, charge transport also occurs by diffusion and so this attempt to limit the mixing of fuel

and oxidant also limits the transport of charge-carrying species, increasing the cell resistance. Optimizing channel width is a balancing act between increased surface area and increased ohmic resistance losses. As the electrodes become longer, the rate of ion transport slows due to the increased diffusion distance between anode and cathode. This increases the cell resistance at the further reaches of the electrodes and provides diminishing returns due to the higher cost and larger footprint of the increased electrode area for minimally increased power output.

3.3 Channel Fabrication

While the operational characteristics of enzymatic and colaminar fuel cells are distinct, optimal channel geometries for both fuel cell types are quite similar. An elongated rectangular channel cross-section serves to increase electrode surface area per unit volume. In order to allow for optimization of electrode geometry, the channel fabrication must facilitate flexible electrode patterning. Two methods of creating a channel structure with two open walls for electrode patterning are investigated: the fabrication of PDMS channel stencils and SU-8 channel structures.

3.3.1 Materials and Methods

Microchannel designs were drafted using AutoCAD (Autodesk, San Rafael, CA) and printed to film on a high-resolution imagesetter (Island Graphics, Victoria, BC). PDMS stencil templates were fabricated in SU-8 50 Photoresist (MicroChem, Newton, MA), following the precision volume ultra-thick SU-8 layer patterning methodology discussed in Chapter 2. Polydimethylsiloxane (PDMS) prepolymer and curing agent (Sylgard 184, Dow-Corning) were mixed at a 10:1 (wt/wt) ratio. PDMS was cured at

80°C and ambient pressure.

SU-8 25 Photoresist (MicroChem, Newton, MA) was used to fabricate SU-8 channel structures and adhesive layers. To create channel structures, photoresist was spun to the desired thickness, soft baked, exposed, and developed as per the methodology detailed in Chapter 2. To create adhesive layers, photoresist was spun to the desired thickness and soft baked to harden.

3.3.2 PDMS Stencil Fabrication

The fabrication of PDMS stencils creates a two-walled channel structure. This method has been employed as a template to micropattern substrates [Folch et al. (2000); Jackman et al. (1999)] and to create multilevel structures by stacking patterned PDMS stencils [Jo et al. (2000)]. The process of fabricating PDMS stencils is depicted in Figure 3.3. Initially, a molding template is created in photoresist, as is common to the rapid prototyping soft lithography method. PDMS pre-polymer is poured on top of the mold and degassed. A transparency film is then carefully applied on top of the PDMS, ensuring that no bubbles are entrapped. Rubber sheet and aluminum plates are placed on both sides of the assembly. The multilayer stack is then compressed using a clamp, with the rubber sheet serving to equally distribute the compressive force. PDMS remains only within the template pattern and is excluded from the top surface of the template structures. After curing, PDMS replicas are manually peeled from the template.

Figure 3.4 shows a 500 μm thick PDMS channel stencil, sealed reversibly to a microscope slide. The nominal width of the channel is 1 mm, however, the when sealed to a substrate the channel width varied up to 30% from the nominal size. This variation is

due to distortion of the thin, elastomeric PDMS layer during application on a solid substrate. Targeted channel lengths are typically on the order of centimeters, while channel heights are on the order of tens of micrometers [Bazylak et al (2005)]. This large aspect ratio results in a PDMS stencil of inadequate mechanical strength to resist deformation and maintain fidelity to the original design. PDMS stencils as thin as 50 μm have been fabricated, although no information on the aspect ratio of the stencil or geometrical accuracy of the sealed structure was presented [Folch et al. (2000)]. In order to utilize PDMS stencil channel structures in microfluidic membraneless fuel cells, electrode patterning methods would have to compensate for irregularities in the assembled channel width, which would be difficult to predict beforehand.

The solvent compatibility of PDMS could also pose problems for its incorporation into a microfluidic membraneless fuel cell. Methanol and ethanol are typical fuels for these devices. PDMS is known to absorb these and other solvents, causing swelling. Ethanol absorption, for instance, causes swelling of 4% [Lee et al. (2003)]. Before integration in a device, the effect of solvent absorption on channel geometry and sealing fidelity would require further investigation. Although the stencil fabrication capability presented here facilitates access to top and bottom electrode substrates, the mechanical and chemical characteristics of such stencils make them less desirable for the microfluidic membraneless fuel cells of interest.

3.3.3 SU-8 Channel Fabrication

SU-8 photoresist has been employed as a channel structure material due to its

structural strength, minimal reactivity, chemical stability with acids and bases, and high transparency to near-UV and visible light [Sikanen et al. (2005); Zhang et al., (2001); Bilenberg et al. (2004)]. Whereas PDMS stencils or polymeric gaskets must maintain a minimum feature height to avoid excessive deformation or structural failure during the assembly process, fabrication of channel structures in SU-8 allows for very short channel heights. SU-8 can easily be spin-coated to heights on the order of 1 um and patterned directly on the device's final base substrate [MicroChem (2002a)]. Therefore, the aspect ratio of the channel structure is of no significance to its fabrication. This greatly extends the geometrical capabilities available for channel structures, allowing for very small channel heights.

The concept of SU-8 channel fabrication is similar to template fabrication methods described in Chapter 2, except it is the channel side-walls that are patterned directly, instead of a negative relief of the fluid channel to be molded. Once the channel side-walls are fabricated, a uniform adhesive layer, typically an unexposed photoresist layer on a solid substrate, is applied as the top surface. Supplemental features must be incorporated into the channel design to ensure successful fabrication. Figure 3.5 shows a sample photomask for channel fabrication. Large area photoresist layers are prone to thermal gradient-induced cracking. To prevent this, stress lines (analogous to pre-form cracks in a sidewalk) are incorporated in the photomask design, thus controlling the location of breaks in the photoresist structure [Tuomikowski and Franssila (2005)]. Also, the fluid nature of the adhesive layer during the bonding process can cause blockage of the channels. Moats can be incorporated into the photomask design to prevent this. These supplemental channel structures are arranged around the required channel

structures and are preferentially filled by the flowing photoresist [Tuomikowski and Franssila (2005)].

Slightly differing processes for fabricating SU-8 channels have been developed by a number researchers [Jackman et al. (2001); Li et al. (2003); Mogensen et al. (2003); Sikanen et al. (2005); Tuomikowski and Franssila (2005)]. Figure 3.6 shows the process of fabricating SU-8 channels as detailed by Tuomikowski and Franssila (2005). First, the channel structure is patterned on a solid substrate, using the same process as template fabrication that was detailed in Chapter 2. On a second substrate, SU-8 is spin coated and completely soft baked. This unexposed SU-8 layer acts as an adhesive layer to seal the channel structure to the second substrate. The two layers are brought into contact and heated above 67°C, the glass transition temperature of unexposed SU-8. Pressure can be applied manually with tweezers to encourage bonding between the SU-8 layers. Once bonded, the adhesive layer is exposed without a mask. During the post-exposure bake, the two SU-8 layers fully bond, creating a solid channel structure.

For microfluidic fuel cell applications, the substrate surface underneath the initial photoresist structure can be patterned with electrodes before fabricating the channel pattern. This allows for one functional electrode surface. However, the second substrate surface remains coated in photoresist. In order to fabricate fuel cell channels with more than one functional surface, this method must be adapted. Figure 3.7 shows a schematic of the altered process developed here that allows for two-sided electrode patterning. Once bonding between the two photoresist layers is achieved, exposure of the adhesive photoresist layer is performed through a photomask. Exposure is prevented between the channel walls, while the rest of the photoresist is full exposed. After the post-exposure

bake, photoresist developer is flowed through the channel. This dissolves the unexposed photoresist, revealing the substrate surface within the channel structure. The resultant channel height is the sum of the two photoresist layer thicknesses. By this method, both top and bottom channel walls can be patterned with electrodes prior to channel fabrication, doubling the active electrode area. This method has the additional advantage over the PDMS stencil method in that high aspect ratio channels can be readily achieved.

Figure 3.8 shows an assembled SU-8 channel structure. As the photomask alignment is performed by hand, slight misalignment of channel walls between the two layers is unavoidable. To avoid misalignment in the future, a mask alignment module is soon to be available in the lab. Bubbles are visible within the channel walls; an unavoidable artifact of the sealing process, during which some air is entrapped in the adhesive layer. Channel wall thickness can be designed to ensure that bubbles cannot form leaks, but slight imperfections in the channel wall due to the presence of bubbles cannot be avoided. A more significant source of fabrication error is that electrode patterns on the substrate surfaces can interfere with SU-8 channel fabrication. While the electrodes themselves are placed within the flow channel, electrical contacts with outside of the cell act as opaque sections of a photomask and locally prevent exposure. This effect is shown schematically in Figure 3.9. During the development stage that cleans the upper substrate surface, photoresist masked by the electrode is slowly dissolved and the channel wall retreats. Full leakage is avoided by locally increasing the thickness of the channel wall at the electrode crossings and minimizing the time duration of the flow-through development process leaks. Minimizing the width of the adhesive layer and width of electrode crossings over the channel wall can also help to reduce the depth of

development [Cremers et al. (2003)]. After development, baking at 140°C polymerizes the unexposed photoresist.

3.3.4 Three-Dimensional Architectures

The expansion of power output from a single cell reaches practical limits, and in order to produce adequate power, multiple independent fuel cells are typically stacked. In the present context, the stacking of multiple microfluidic substrate-electrode-channel-electrode-substrate layers described is the most obvious three-dimensional integration method. When stacked, however, the thickness of substrates between individual cells introduces a significant amount of dead space, that is, volume of the final device that is not used for actual power production. Fully three-dimensional fuel cell architectures, however, offer significant benefits when considering scale-up from single fuel cell to operational device [Long et al. (2004)]. In Chapter 4, the design of a three-dimensional vanadium redox fuel cell architecture is presented, along with its potential for scale-up in geometry while maintaining the benefits of microscale fluid and species transport.

3.4 Summary

In this chapter, channel fabrication techniques towards the production of microfluidic membraneless fuel cells were discussed. Design parameters for microfluidic membraneless fuel cell architectures were detailed. Fabrication techniques were then developed to facilitate the optimization of channel structure and electrode geometry. First, the fabrication of PDMS stencils with two open surfaces was investigated. Due to the high aspect ratio of channel structures required for use in microfluidic fuel cells,

significant geometrical distortions occurred when sealing to a solid substrate. A novel adaptation of standard fabrication techniques for microfluidic channels in SU-8 photoresist was then presented, which allowed for the patterning of high aspect ratio channel structures with heights on the order of tens of micrometers and lengths on the order of centimeters, while incorporating two electrode-patterned surfaces. Finally, the extension to three-dimensional fuel cell architectures was briefly discussed.

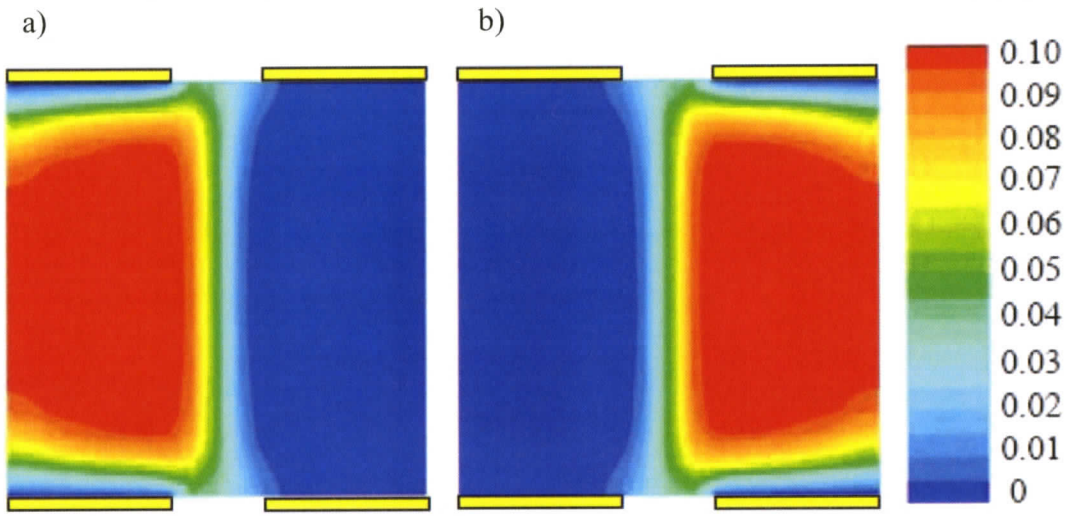

Figure 3.1 Fuel and oxidant mass fraction plots during fuel cell operation. Fuel (a) and oxidant (b) depletion zones are generated in the proximity of the electrodes as the reactants are consumed, while reactants diffuse into the mixing region at mid-channel. Adapted from Bazylak et al. (2004).

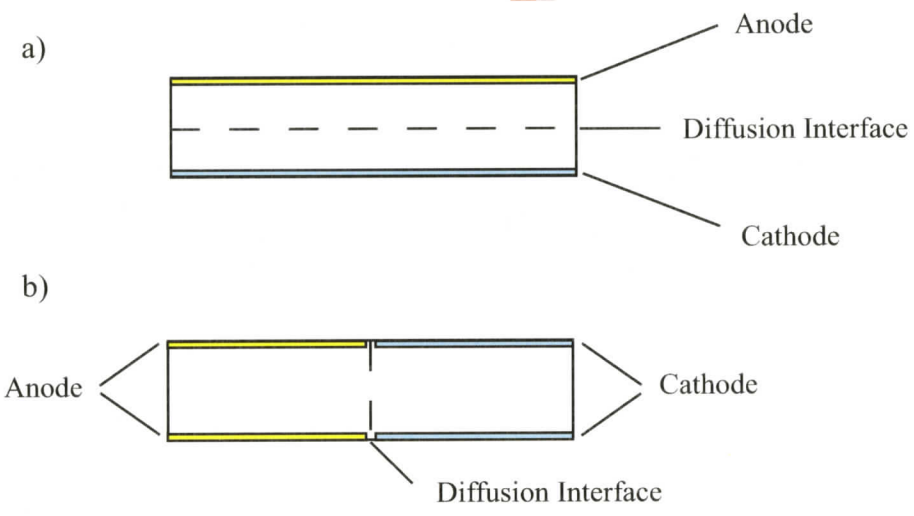

Figure 3.2 Optimized channel architectures for a) enzymatic fuel cell and b) colaminar fuel cell.

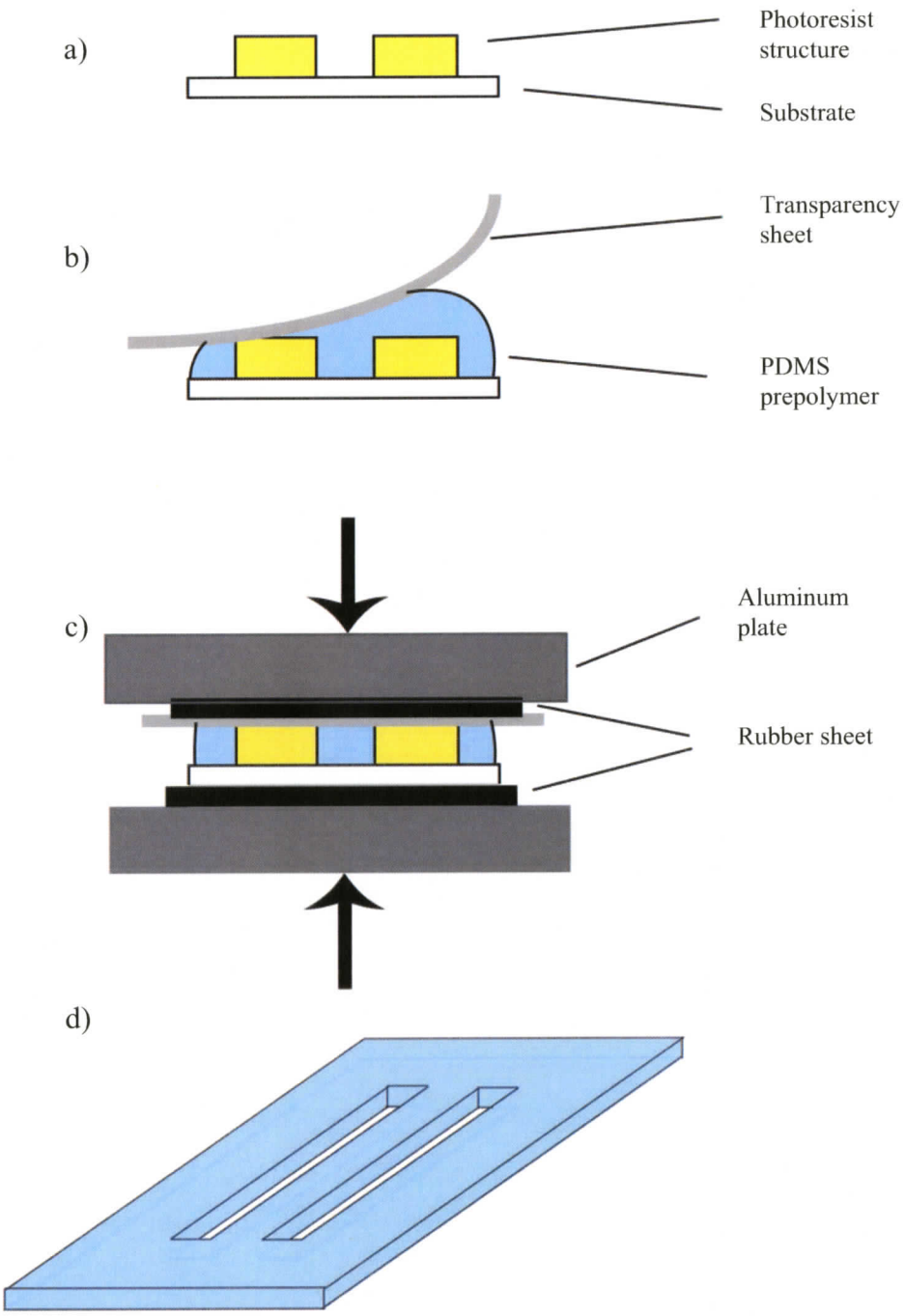

Figure 3.3 Schematic of PDMS stencil fabrication method: a) stencil template is fabricated in photoresist on a solid substrate, b) PDMS prepolymer is applied and degassed on the template, transparency sheet is applied carefully to avoid entrapping bubbles, c) compression stack with rubber sheet and aluminum plates is assembled, compressed in clamp, and PDMS is cured, d) compression stack is disassembled and PDMS stencil is manually removed from the template.

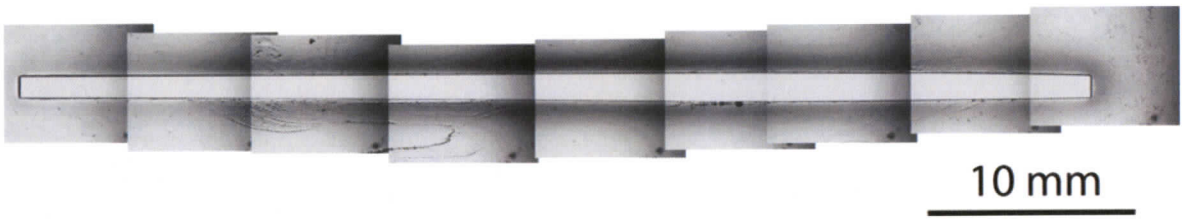

Fig 3.4 Composite image of PDMS channel stencil. Width variations up to 30% of nominal size occur when sealing to the substrate due to the flexible nature of the thin structure. The PDMS channel stencil was 350 μm thick.

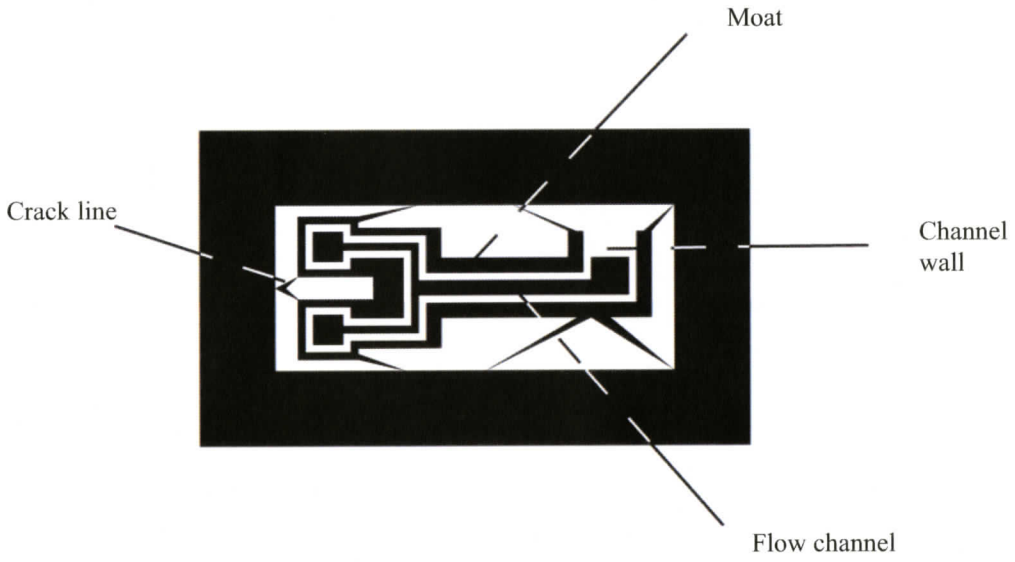

Fig 3.5 Image of an SU-8 channel structure photomask. To ensure high quality channel fabrication, photomask design incorporates crack lines to prevent uncontrolled cracking of photoresist layer and moats to preferentially fill with flowing photoresist and prevent channel blockages.

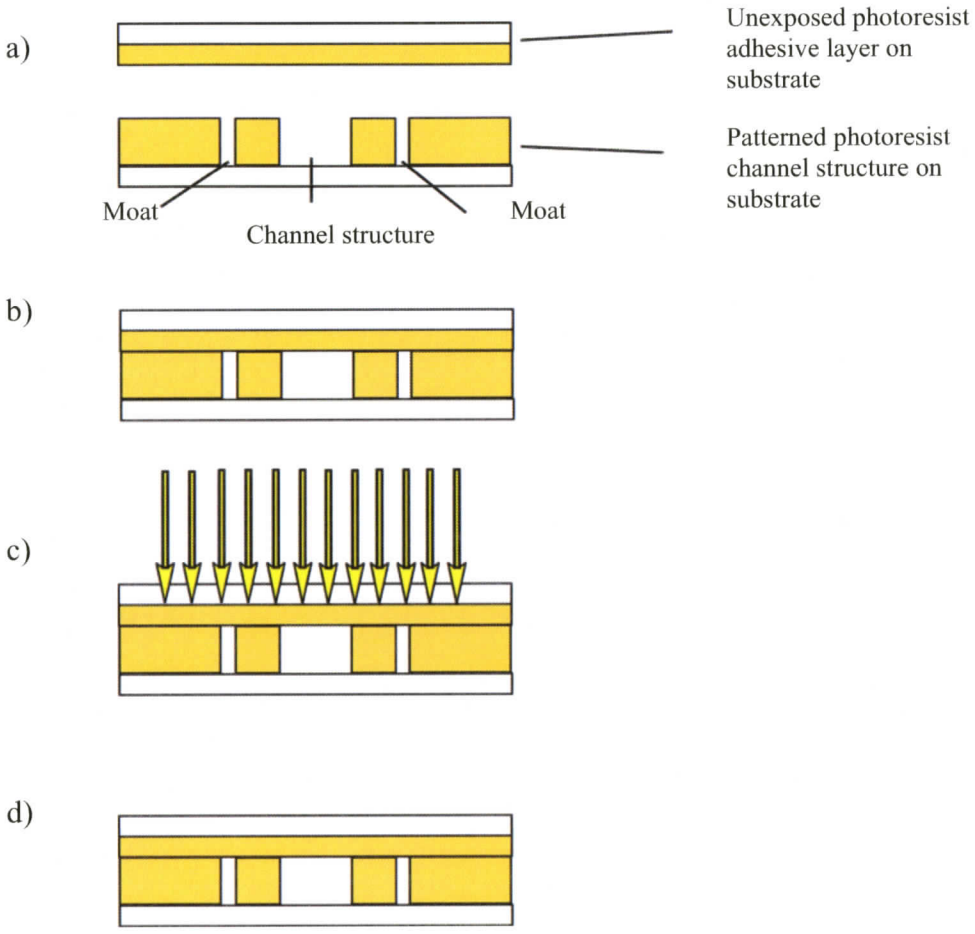

Fig 3.6 Schematic of standard SU-8 channel structure fabrication: a) channel structure is fabricated by standard photolithography techniques on a substrate, photoresist adhesive layer is created by soft baking photoresist on a second substrate, b) photoresist layers are brought into contact and heated above unexposed SU-8 glass transition temperature to bond, c) adhesive layer is polymerized by exposure and post-exposure bake, and d) enclosed channel structure is attained.

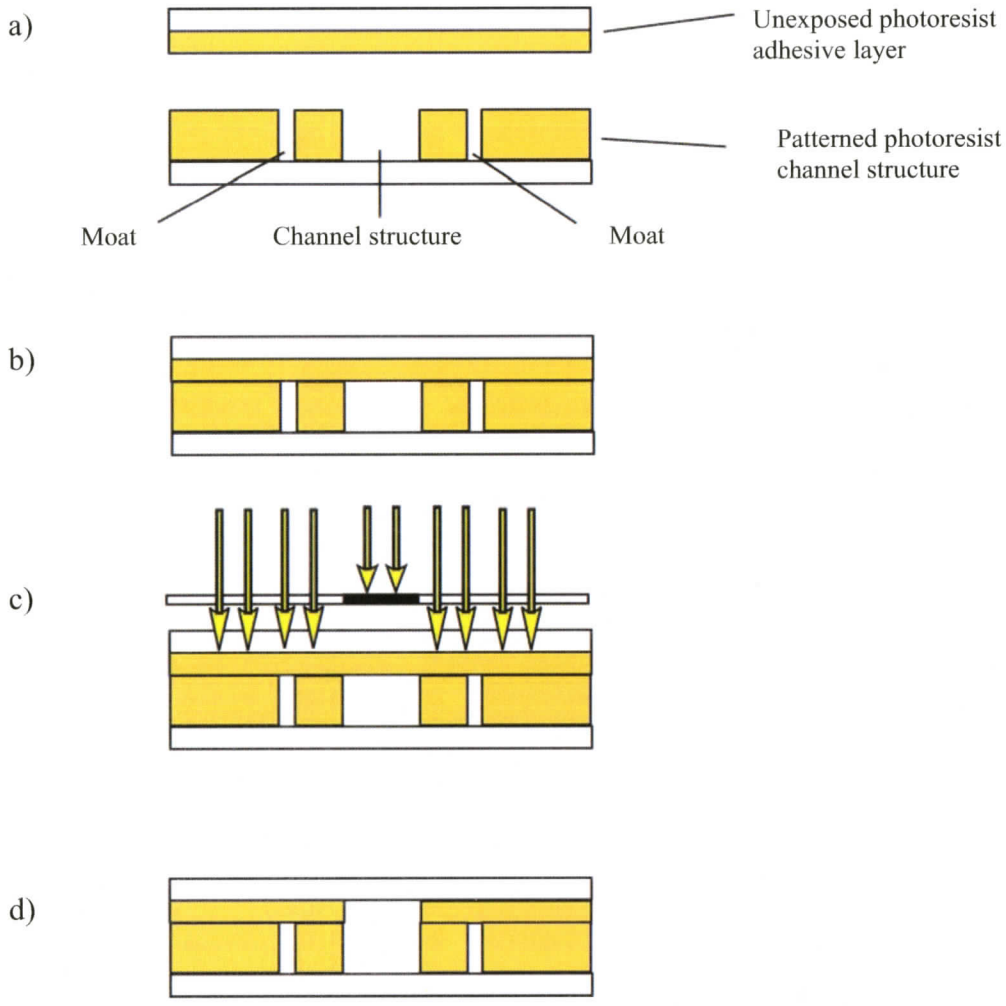

Fig 3.7 Schematic of SU-8 channel structure fabrication adapted for microfluidic membraneless fuel cells, a) channel structure is fabricated by standard photolithography techniques on a substrate, photoresist adhesive layer is created by soft baking photoresist on a second substrate, b) photoresist layers are brought into contact and heated above unexposed SU-8 glass transition temperature to bond, c) adhesive layer is polymerized by selective exposure followed by post-exposure bake, and d) SU-8 developer is flowed in enclosed channel to dissolve unexposed photoresist, revealing second substrate surface

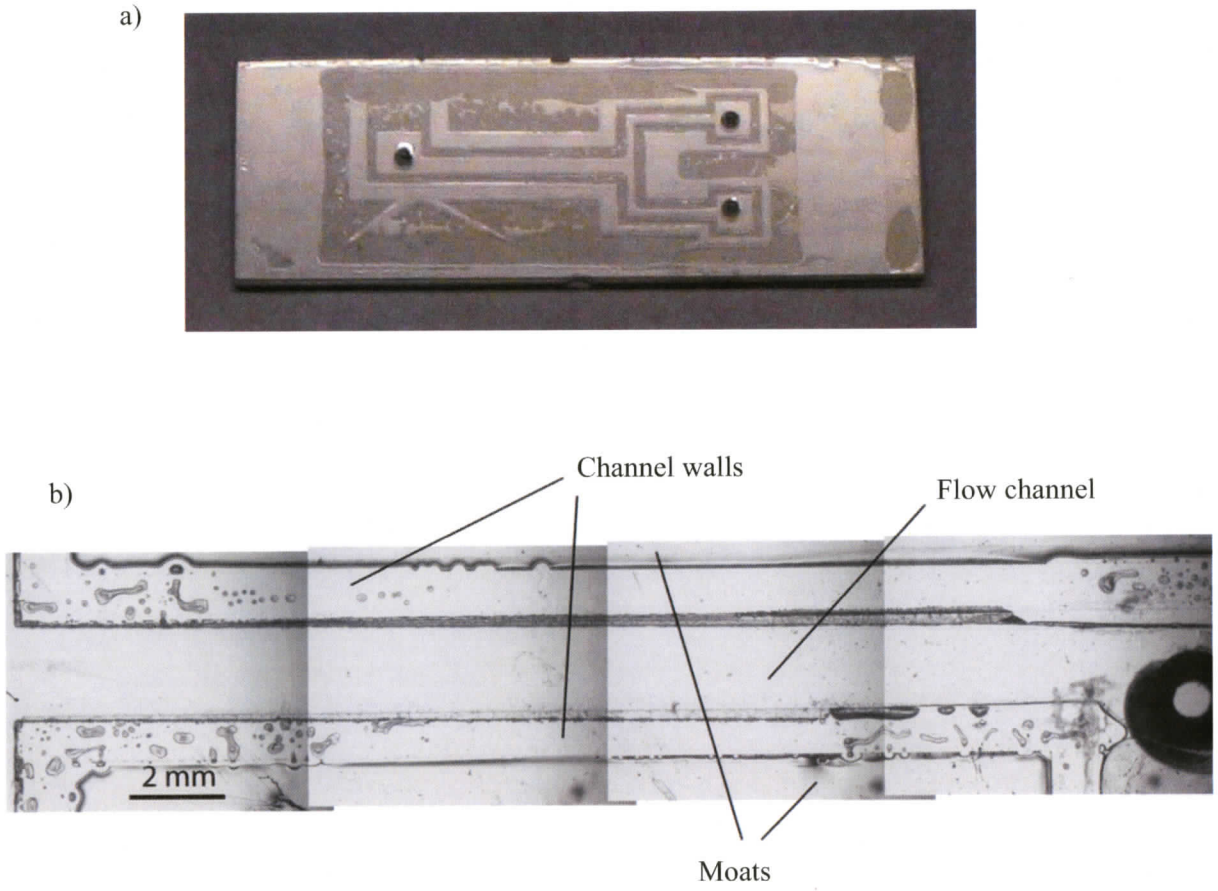

Fig 3.8 SU-8 channel structure fabricated by the adapted method, a) image of channel structure, b) magnified image. Misalignment due to manual photomask alignment is visible at the flow channel walls. Air bubbles are entrapped in the channel wall but do not breach the full width.

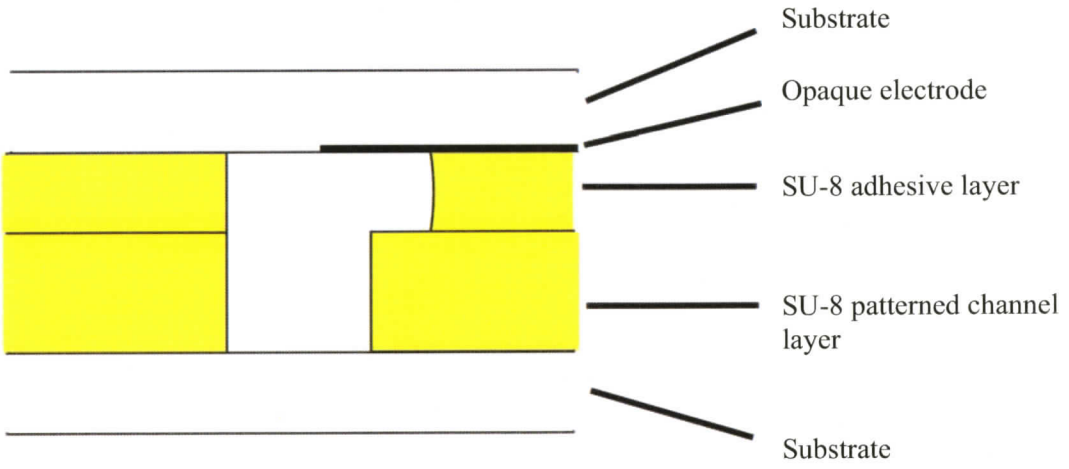

Fig 3.9 SU-8 channel cross-section showing affect of an electrode pattern interfering with the fabrication process by effectively masking the SU-8 adnesive layer. The adhesive layer below the electrodes is unexposed and retreats slightly during development process.

Chapter 4

ELECTRODE PATTERNING FOR MICROFLUIDIC MEMBRANELESS FUEL CELLS

In this chapter, electrode patterning methods are developed for utilization in microfluidic membraneless fuel cells. The deposition of thin-film gold layers is investigated using metallic and chemical adhesive layers. Lift-off and etching methods are developed for gold electrode patterning, as well as the in-situ patterning of gold electrodes using colaminar flow. Carbon electrode fabrication techniques are investigated. A variety of binders are investigated for use in carbon and polymer mixture electrodes and tested for appropriate stability. Patterning techniques for carbon and polymer mixture electrodes are also developed. Integration of devices with channel fabrication methods discussed previously in Chapter 3 is then discussed. Finally, a three-dimensional electrode and channel architecture using pencil leads is presented, facilitating scale-up in size within a single channel while maintaining the inherent benefits of microfluidics for fuel cell devices.

4.1 Electrode Patterning Background

All reactions taking place in a fuel cell occur at the anodic and cathodic electrode surfaces. The geometry and placement of electrodes, therefore, is vitally important to the operation of fuel cell devices. In order to optimize electrode geometry, methods of

efficiently patterning electrodes are required. Techniques to fabricate microelectrodes for use in microelectromechanical systems and microfluidic devices have borrowed greatly from methods used in the microelectronics industry [Ruska (1987); Madou (1997)]. Thin metallic films acting as current collectors or electrodes can be deposited on top of glass *via* vacuum deposition [Holland (1963)]. Thin films are comprised of a metallic adhesion layer and a conductive layer of gold or catalytic metal, typically on the order of 100 nm thick [Moore et al. (2004)]. Two methods exist to define electrode geometries. Both lift-off and etch patterning methods are common to the microelectronics industry and are well-developed [Widmann (1976); Ruska (1987)]. Both methods have been previously employed to fabricate electrodes for utilization in microfluidic and analytical devices [Van Gerwen et al. (1997); Koch et al. (1999); Studer et al. (2002); Cho et al. (2003); Liu and Cui (2005)].

A variety of additional methods of incorporating electrodes in microfluidic fuel cells have been attempted. These include the use of catalyst-coated graphite plates to act as electrodes, current collectors, and channel structures [Choban et al. (2005a)], integration of molded electrodes [Mitrovski et al. (2004)], and use of a palladium-catalyzed gas diffusion layer as a channel wall, oxygen exchange membrane, and electrode [Jayashree et al. (2005)]. Carbon microelectrodes have been fabricated by filling microfluidic channels with a carbon ink solution and hardening [Moore et al. (2005)] as well as by soft lithography molding techniques [Schueller et al. (1999)].

In this chapter, electrode patterning methods are developed for the fabrication of microfluidic membraneless fuel cells. Gold electrode patterning methods are developed for the fabrication of enzymatic fuel cell electrode bases and conductive underlayers.

Metallic and chemical adhesive layers are investigated for the deposition of thin-film gold layers on glass substrates. Gold patterning by lift-off and etching methods for the patterning of gold electrodes are presented. Carbon and polymeric binder mixtures are developed for use as electrodes in vanadium redox fuel cells. Methods of patterning carbon electrodes are investigated. Carbon pencil leads are also investigated for use in vanadium redox devices. The integration of patterned electrodes with channel structure fabrication methods described previously in Chapter 3 is detailed. Finally, a three-dimensionally structured vanadium redox fuel cell is presented, demonstrating the benefits of scaling up the power output of three-dimensional architectures compared to planar designs.

4.2 Materials and Methods

PDMS channel structures were fabricated from polydimethylsiloxane prepolymer (Sylgard 184, Dow Corning). SU-8 25 photoresist, SU-8 developer, SPR 220-7 positive tone photoresist, MF CD 26 positive photoresist developer, OmniCoat, and Remover PG were purchased from MicroChem (Newton, MA). Photoresist structures were patterned as described in Chapter 2. OmniCoat layers were patterned on glass by spin-coating at 3000 rpm and baking at 200°C for one minute. Transene TFA gold etch was purchased from Transene (Danvers, MA). A highly basic ferricyanide solution produced in-house was employed as the chromium etchant. Smooth-On PMC-790 polyurethane was purchased from Fairey and Co (Delta, BC). Graphite powder was purchased from Sigma-Aldrich (Oakville, Ont). Staedtler Mars micro carbon HB pencil leads were employed as electrodes. Carbon paint was purchased from SPI Supplies (Structure Probe

Inc, West Chester, PA).

4.3 Gold Electrode Patterning

Gold electrodes find many applications in microscale devices. Thin-film gold layers are commonly used as electrodes and as current collectors. Enzymatic fuel cells employ gold structures as an electrode base, with enzymes tethered to the surface by a conductive linker [Xiao et al. (2003)]. Gold electrodes have also been used to create an in-situ redox-based velocimetry device [Kjeang et al. (2006 – submitted)]. Gold under layers can also be used as current collectors for carbon electrodes due to the inherent low conductivity of most carbon mixtures. A variety of methods for the deposition and patterning of gold layers are now presented.

4.3.1 Thin-Film Gold Layer Deposition

Thin-film gold layers are created on a substrate by vacuum deposition [Holland (1963)]. As gold does not adhere well to glass, an intermediate adhesive layer is required. Metallic adhesive layers commonly used include chromium and titanium. Here, chromium was employed. Using a dual-source deposition chamber, a thin layer of chromium (~5nm) was initially deposited on the substrate, followed by a thick, conductive gold layer (~150nm). A dual-source deposition machine is necessary so that vacuum does not have to be broken to switch sources. If the vacuum is broken, the chromium layer becomes contaminated and the adhesion of gold is compromised.

Alternatively, a chemical adhesive layer can be applied to the substrate to improve the adhesion of gold. A linker, 3-mercaptopropyltrimethoxysilane (MPTMS),

was employed here as an adhesive monolayer. The substrate was initially cleaned with piranha solution to remove trace organic contaminants and create alcohol functions on the glass surface. Subsequently, the substrate was soaked in a 5% by volume solution of MPTMS in ethanol for 12 hours. After rinsing with water and drying the slides, gold was applied by vacuum deposition. While the chemical linker method creates a well-adhered gold surface, it was found to be unsuitable for electrochemical devices. When electrochemical reactions were performed at the surface of the gold electrode, the adhesion of the MPTMS linker degraded and the gold layer detached from the surface.

4.3.2 Gold Electrode Patterning Methods

Standard gold patterning techniques, by lift-off and wet etching, were developed. Patterning by lift-off is depicted in Figure 4.1. Initially, the glass substrate was patterned in photoresist such that the desired electrode areas were developed away, revealing the glass surface. The thin-film layer was then deposited on top of the photoresist substructure. Subsequent lift off of the photoresist layer by submersion in acetone removed the photoresist structure and the thin-film deposited on top of it. The gold layer remained only where it was deposited directly on to the glass surface.

Gold patterning by etching is depicted in Figure 4.2. In this process, the entire substrate surface was initially coated with the thin-film gold layer. The substrate was then coated in OmniCoat to prevent damage to the gold layer during the subsequent photoresist removal. Photoresist was patterned on top of the surface to cover the desired electrode areas. Where the gold layer was exposed, the OmniCoat layer was also developed to allow access to the surface. The substrate was then submerged in gold etch,

removing all gold not covered by photoresist, and subsequently in a basic ferricyanide chromium etch to remove the exposed chromium layer. Finally, the photoresist structure was removed by soaking in Remover PG, which selectively dissolved the OmniCoat layer and detached the photoresist structure from the surface.

Figure 4.3 shows an image of pre- and post-pattering gold surfaces. Both the etch and lift-off methods were capable of creating such patterned gold electrodes with high geometrical accuracy. The lift-off method was more susceptible to surface contamination, as a photoresist-coated surface is difficult to clean without damaging the photoresist structure. Contamination can break electrical contact through thin electrodes by locally preventing the deposition of the thin film. Substrates used with the etch method can be rigorously cleaned prior to coating of the entire surface to prevent contamination, or defects can be accommodated during the photoresist patterning stage. The etch method, however, requires optimization and control during the etching process. Excessive exposure to the etchant products dissolves the thin film below the protective photoresist layer, as shown in Figure 4.4. However, the rate of etching is on the order of nanometers per second and as such, extreme overexposure would be required to have a noticeable effect on the micron-scale electrode geometry.

4.3.3 In-Situ Gold Etching For Colaminar Microfluidic Fuel Cells

Exploiting the laminar nature of microfluidic flow, colaminar streaming of water and etchant is attainable. A schematic of this process is shown in Figure 4.5. By varying the inlet flow rates of the three streams, the width and cross-stream location of the etchant stream can be specified. Such a method is particularly appealing for the patterning of

colaminar fuel cell electrodes. As shown in Figure 4.6, irregularities in channel geometry cause local distortions of the nominal colaminar stream positions. Such irregularities are not uncommon, due to the small feature size of microfluidic channels and the correspondingly large effect of small inaccuracies. In a colaminar fuel cell, slight shifting of the streams causes fuel crossover if the mixing region comes into contact with one of the working electrodes. By employing gold etching to define the gap between electrodes after assembly, channel irregularities are automatically accounted for during the etching process. Also, the necessity of precision alignment of the channel structure on top of the electrodes is eliminated, as the electrode structure is precisely defined following channel placement. This would benefit scaled-up production of microfluidic membraneless fuel cells by greatly simplifying the assembly process.

Figure 4.7 shows a 2 mm wide gold layer selectively etched in a microfluidic channel by colaminar flow. Inlet flow rates are controlled by using a single syringe pump and syringes of differing diameters to set the relative stream flow rates. A 1 mL syringe with 4.7 mm diameter was used for the gold etch stream, while two 60 mL syringes with 26.7 mm diameter were used for the two water streams. For a 2 mm wide channel, this corresponds to an approximate nominal gold etch stream width of 160 μm and water stream widths of 920 μm each. By using independent syringe pumps, the width and cross-stream location of the etchant stream could be more finely controlled. As the flow traveled downstream, etchant diffused gradually into the water streams and the etched width correspondingly increased, from a minimum of 130 μm at the inlet to a maximum of 340 um at a downstream distance of 26 mm. As Figure 4.7 shows, the cross-stream location of the etched area oscillates slightly down the channel due to irregularities in the

channel geometry. For these experiments, a PDMS channel structure was pressure-sealed onto a gold-coated substrate by clamping. The unequal distribution of compressive force on the assembled device was the likely cause of the flow oscillations, as this would cause local variations in channel height. A chemical linker, MPTMS, was employed as the adhesive layer to eliminate the need for a chromium etching step. However, since gold is compatible with chromium etch, a blanket exposure to chromium etch could be employed after the precise gold etching step.

The broadening of the etch stream can be exploited to create tapered electrodes. Bazylak et al. (2005) employed tapered electrodes in their numerical model to improve fuel utilization of a colaminar fuel cell to a maximum of 52 %. As the mixing region width grew, the distance between the electrodes in their design was similarly widened to avoid fuel crossover. The broadening of the mixing region at the electrode surface occurs by diffusion, quantified in colaminar, pressure driven flow by Ismagilov et al. (2000) as:

$$\Delta x \approx \left(\frac{Dhy}{U}\right)^{1/3} \tag{4.1}$$

where D is the species diffusivity, h is the channel height, y is the downstream distance, and U is the maximum flow velocity. The broadening of the gold etchant stream can be matched to that of the reactants in a colaminar fuel cell by altering the flow velocity to compensate for differences in the diffusivity of the two species. By this method, tailored electrode patterns that allow for improved fuel utilization may be formed in-situ, eliminating the necessity of precision alignment during assembly of the device while accommodating channel irregularities.

4.4 Carbon Electrode Patterning Methods for Vanadium-Based Fuel Cells

Vanadium fuel cells operate similarly to conventional fuel cells, controlling oxidation and reduction reactions to produce useful electrical current. However, conventional fuels and oxidants are replaced with different vanadium species. The anodic reaction oxidizes V^{2+} to V^{3+} while the cathodic reaction reduces V^{5+} to V^{4+}. Conventional systems have achieved wire-to-wire efficiencies over 70 % [Tokuda et al. (2000)]. Using these vanadium species in a microfluidic device affords the opportunity of operating in a colaminar membraneless architecture.

The operating potentials of the vanadium device are close to that of the electrolysis of water, and thus traditional catalysts such as platinum cannot be employed [Ferrigno et al. (2002)]. Carbon electrodes serve to catalyze the oxidation and reduction reactions of the vanadium species while suppressing the electrolysis of water. Methods of constructing and patterning carbon electrodes are now presented.

4.4.1 Carbon and Polymer Mixture Electrodes

One carbon electrode patterning approach pursued here involves mixing graphite microparticles and polymeric binder, diluted with an appropriate solvent to attain the desired viscosity. Such a method could be similarly applied to the fabrication of electrodes with other catalyst particles. Due to the inherently low conductivity of the carbon mixture, electrodes must be patterned on top of a current collector, in this case, a thin gold film. The binder holds the carbon particles together and adheres the mixture to the current collector. The carbon particles serve two functions: to act as the catalyst for the vanadium species oxidation and reduction reactions and to conduct electrons from the

electrode surface to the current collector. Increasing the carbon content of the mixture is beneficial as it creates more reaction sites on the electrode surface and increases the conductivity of the mixture. Optimization of the carbon content of the electrode mixture would balance the need for many reaction sites to achieve high reaction rates and high conductivity with the resulting decrease in structural strength and adhesion of the electrode material.

In order to operate effectively in a fuel cell environment, the carbon and polymer mixture must be compatible with chemicals and processes encountered during device assembly and operation. Chemical exposure during assembly varies with the assembly method. Fabricating a fuel cell device with a PDMS channel stencil, as detailed in Section 3.3.2, does not subject the electrodes to any chemicals. However, an SU-8 photoresist channel structure, as described in Section 3.3.3, requires the flowing of photoresist developer, an acetate-based organic solvent. Developing time during this process was short, typically only a couple of minutes but varying based on the adhesive layer thickness. As such, long-term solvent compatibility is not required, but electrode material degradation in SU-8 developer must be minimal. Additionally, during the operation of a vanadium redox device the electrodes will be subjected to electrochemical reaction in the presence of an acidic electrolyte.

A variety of potential binders were investigated, including SPR 220-7 positive tone photoresist, SU-8 negative-tone photoresist, and polyurethane. Commercially-available carbon paint was also tested for compatibility. Chemical compatibility was determined by soaking patterned electrodes in SU-8 developer for approximately half an hour. Acid stability was investigated by soaking in 1 M sulfuric acid and 1 M phosphoric

acid for prolonged periods of over 2 hours. Electrochemical stability was determined by oxidizing and reducing vanadium species in solution and visually monitoring the carbon electrode surface. Long-term electrochemical stability could be determined by monitoring the current of an operating electrode over a longer period of time.

Positive photoresist mixtures were created using acetone as the solvent and were baked to harden. The mixture was incompatible with SU-8 developer and many other solvents as the binder readily dissolved in their presence. However, the electrodes were found to be stable in the presence of acids and during electrochemical reactions. As such, it could be employed in a microfluidic fuel cell using a PDMS stencil channel structure. The long-term stability of this electrode material is questionable, however, since exposure to light degrades positive-tone photoresist.

SU-8 negative photoresist mixtures were diluted using SU-8 developer. Using UV-light exposure to polymerize the photoresist is not possible in this case, as the carbon particles block the interrogating light. However, polymerization of SU-8 does occur at elevated temperatures greater than 135 °C [Lin et al. (2002)]. As such, polymerization was accomplished by baking the mixture at 140 °C. The resulting electrode was found to be compatible with SU-8 developer, acids, and was electrochemically stable.

Commercially-available carbon paint was also investigated. When soaked in SU-8 developer, the bulk of the paint detached from the surface, but a thin, transparent carbon layer remained. The remaining layer was stable during a second soak in SU-8 developer. However, the thin layer detached from the surface when exposed to acid. Carbon paint was therefore found to be unsuitable as an electrode material.

With the polyurethane mixture, acetone was used as a solvent. The resulting

mixture was cured at room temperature for 24 hours. The mixture was found to be stable in the presence of SU-8 developer and acids for moderate periods of time. Electrochemical stability has not yet been investigated, but is expected based on previous publications [Lin et al. (2001)].

4.4.2 Patterning Carbon and Polymer Mixture Electrodes

Two methods of patterning carbon and polymer mixture electrodes were investigated. The casting method developed here is depicted in Figure 4.8. Initially, a substrate is patterned with the thin-film gold layer to act as a current collector, as described in Section 4.3. Photoresist is then patterned on top of this layer such that the desired electrode areas are developed away to create a cavity and reveal the gold underlayer. A carbon mixture of SU-8 photoresist or polyurethane, graphite particles, and appropriate solvent is then made with a paste-like consistency. The photoresist cavity is filled with the carbon paste and excess is removed by scraping with a razor blade. A similar method was employed by Engel et al. (2005). Depending on the solvent content, the carbon mixture was found to shrink significantly during curing, requiring multiple fills to create a planar surface. Once filled, the channel structure may be assembled on top of the photoresist layer. Figure 4.9 is an image of a cast carbon mixture electrode.

Alternatively, a lift-off method was developed for the patterning of carbon electrodes. Figure 4.10 is a schematic of this method. First, a substrate is patterned with a conductive gold underlayer as described in Section 4.3. Photoresist is then patterned such that the desired electrode areas are developed away. A heavily diluted carbon

mixture is then created. A thin film of the carbon mixture is deposited on the substrate, either by spin-coating or dip-coating. Other coating alternatives exist, including airbrushing. The resulting thickness of the carbon layer can be tailored by the solvent content of the mixture. After curing, the photoresist layer is lifted-off.

Figure 4.11 shows images of electrodes fabricated by carbon mixture lift-off. As cured polyurethane is acceptably stable in the presence of acetone, this solvent can be used to directly strip the photoresist layer. Positive tone photoresist is not stable in the presence of these solvents, and as such is not amenable to the lift-off method. SU-8 mixtures require the use of an auxiliary OmniCoat layer underneath the photoresist patterning structure. This layer must be developed off of the revealed gold surface to allow direct contact with the carbon layer. After carbon coating, submersion in Remover PG selectively dissolves the OmniCoat layer and lifts off the structured SU-8 layer, while the carbon and SU-8 electrode remains adhered to the surface. This method allows for the production of thin carbon electrodes with microscale features by a method that is amenable to scaled-up production, using either polyurethane or SU-8 photoresist as the polymeric binder.

4.4.3 Integration of Solid Carbon Electrodes

The fabrication of electrodes using a carbon particle and polymer mixture is a multi-step process. Photoresist patterning steps are needed to pattern both the conductive gold layer and the carbon layer. Elimination of the conductive gold layer would greatly simplify the fabrication of carbon electrode structures, but is not feasible due to the low conductivity of carbon and polymer mixtures. Solid carbon structures are investigated

here as an alternative to patterned carbon electrodes. Specifically, commercially available pencil leads are proposed to be used as carbon electrodes. The resistance of a 0.5 mm diameter pencil lead is minimal, approximately 0.7 Ω cm^{-1}, thus eliminating the need for a separate current collector. Pencil leads have also been found here to have adequate chemical and electrochemical stability for use as redox device electrodes. Their integration as electrodes is now investigated. The term pencil lead is a misnomer, as pencil leads are typically mixtures of graphite and clay and contain no lead whatsoever [Ritter (2001)]. Herein the more correct term "graphite rod" will be employed in place of "pencil lead".

Embossing

One method of incorporating graphite rods into a microfluidic structure is to embed them in the channel wall. Polyurethane was chosen as a base substrate due to its machinability by embossing, high chemical resistance, and expected electrochemical stability. The process developed here is depicted in Figure 4.12. Initially, polyurethane prepolymer is coated on a solid substrate and cured. Graphite rods are secured in recesses of an aluminum plate by friction fitting. The aluminum plate is pressed onto the polyurethane surface and the stack is heated to 140 deg C. A clamp exerts compressive force on the stack, embedding the graphite rods into the polyurethane. After one hour of compression, the stack is slowly cooled to room temperature while maintaining compression. The graphite rods are preferentially adhered to the polyurethane surface and remain embedded after the stack is disassembled. In order to attain a planar surface, the protruding graphite rod edges are sanded. Figure 4.13 is an image of a graphite rod –

polyurethane electrode structure.

4.5 Device Integration

The planar electrode-patterned substrates developed here can be incorporated into a fuel cell device by employing the channel fabrication methods detailed in Chapter 3. Not all channel structures are amenable to the variety of electrode patterning methods. A brief discussion of these compatibilities follows.

Single-sided fuel cells employing only one electrode-patterned surface can utilize PDMS channel structures created by standard microfabrication techniques. PDMS stencil channel structures allow the incorporation of two electrode-patterned substrates, resulting in a double-sided fuel cell. Both standard channels and stencil channel structures were shown here to be irreversibly sealable to the glass and polyurethane substrates by oxygen plasma exposure, which offers a simple and proven assembly procedure [Duffy et al. (1998)]. PDMS will not irreversibly bind to gold or SU-8 photoresist layers. For gold electrode devices, the electrical contacts through channel walls can cause leaks unless sealed by an alternative method, such as applying epoxy after assembly or clamping the structure. Sealing to an SU-8 layer similarly requires clamping or an additional sealant to prevent leaks around the channel structure. Figure 4.14 shows a single-sided vanadium redox device with electrodes patterned by carbon mixture casting.

SU-8 photoresist channel structures are able to create sealed channel structures, as described in Section 3.3.3, with two active electrode surfaces on a wider variety of electrode substrates. Coating of SU-8 photoresist-based electrodes, gold, and glass poses

no problems. However, SU-8 coating is incompatible with polyurethane electrodes and substrates. Images of SU-8 coatings on glass substrates coated with carbon electrode mixtures are shown in Figure 4.15. The SU-8 layer retreats from the polyurethane and carbon mixture, forming scattered pools. In comparison, the SU-8 and carbon mixture does not cause the retreat of the photoresist layer, making this material more compatible with the SU-8 channel structure fabrication method. It is conceivable that the retreat of SU-8 from polyurethane can be accommodated during electrode patterning by containing the carbon electrode within the channel walls.

An electrode patterning method that employs lift-off gold and carbon patterning can reduce the complexity of the fabrication process. Before lifting off the photoresist structure to reveal the gold electrodes, the carbon layer is coated. By this method, only one photoresist patterning and lift-off step is required. The resulting gold underlayer, including electrical contacts that cross channel walls, would be entirely covered in carbon mixture. The carbon electrode and photoresist channel structure would therefore have to be compatible.

4.6 Three-Dimensional Graphite Rod Bundle

For most applications, the power output of a single fuel cell is inadequate. Attempting to increase the power output from a single cell reaches practical limits, as detailed in Chapter 3. In order to produce adequate power, multiple independent fuel cells are commonly stacked. In the context here, multiple microfluidic substrate-electrode-channel-electrode-substrate layers are incorporated in a single device. The thickness of the substrate layers introduces a significant amount of dead space that is not

used for actual power production. This unutilized volume serves to decrease the power and energy density of the device. A potential solution to this scenario is the use of three-dimensional channel structures.

Instead of creating planar electrodes, as described in Section 4.4.3, an arrangement of graphite rods in a three-dimensional electrode structure is proposed here. A schematic of a three-dimensional colaminar fuel cell device is shown in Figure 4.16. The design features anodic and cathodic electrode regions comprised of several independent tubular electrodes. Fluid flow occurs in the spaces between adjacent graphite rods, while reactions occur on the surfaces of the electrodes. The inherent benefits of microfluidics for fuel cell devices are maintained by the microscale spacing of the electrodes. However, the actual channel cross-section can have geometries on the order of millimeters or centimeters. In order to maintain the benefits of microfluidic behaviour, non-reactive tubes with similar spacing are positioned between the electrode regions. To accommodate the mixing region at the interface of the fuel and oxidant streams, the central carbon electrodes can be replaced with non-reactive insulators to prevent reactions from occurring while maintaining microfluidic mixing behaviour.

Due to the bulk of the graphite rod geometry, the active electrode area to total channel volume fraction for the design shown in Figure 4.16 is 0.022 cm^{-1}, less than that of the planar electrode geometry of Bazylak et al (2005), featuring a ratio of 0.077 cm^{-1}. Similar observations have been made for tubular three-dimensional lithium ion battery architectures [Long et al. (2004)]. The benefit of three-dimensional architecture, however, is that the scale-up of size and power output is greatly simplified, as depicted in Figure 4.17. The power output increase from this architecture cannot be realized by

increasing its width since mass transport limitations and ohmic losses become significant, as in the planar colaminar design. However, the expansion in height does not negatively impact the performance of the device, eliminating scale up issues and allowing geometries such as that shown in Figure 4.17. Therefore a single channel on the order millimeters or even centimeters in height could be employed to produce as much electrical power as a stack of several microscale channels. Individual electrical connections to each of the graphite rod electrodes are possible, and would facilitate a high degree of control over the output current and potential.

4.18 is an image of an assembled three-dimensional graphite rod device. This device was fabricated by CNC machining of Delran, a chemically resilient polymer. While this device is currently under experimental investigation, some improvements on this proof-of-concept design are already evident. For one, the fixed dimension of the graphite rod electrodes limits design variability. While Bazylak et al. (2005) found the mixing region between colaminar streams of their design to reach a maximum width of 150 μm in a 24 mm long channel, the minimum separation in the present case is one graphite rod diameter, or approximately 560 μm. The fabrication of custom electrodes with smaller feature sizes would greatly increase options for the optimization of this design and potentially decrease the amount of cross-sectional space wasted by the bulk electrode volume. One option for custom solid carbon electrode fabrication is the molding of carbon electrodes by soft lithography and their incorporation into microfluidic devices. This process has been successfully performed previously, creating electrodes with features as small as 2 μm utilizing common microfabrication processes [Schueller et al. (1999)]. Optimal electrode geometry would necessarily consider structural strength

and conductivity of the final carbon structure.

4.7 Summary

In this chapter, electrode patterning methods were developed for utilization in microfluidic membraneless fuel cells. The deposition of thin-film gold layers was investigated using metallic and chemical adhesive layers. Lift-off and etching methods were developed for gold electrode patterning, as well as the in-situ patterning of gold electrodes using colaminar flow. Carbon electrode fabrication techniques were investigated. A variety of binders were investigated for use in carbon and polymer mixture electrodes and tested for appropriate stability. Patterning techniques for carbon and polymer mixture electrodes were also developed. While a number of binders were viable for the fabrication of carbon electrodes, the lift-off patterning methodology favoured the more resilient binders, polyurethane and SU-8 photoresist. The incorporation of carbon graphite rods for vanadium redox fuel cells was investigated. A three-dimensional electrode and channel architecture using graphite rods was presented, facilitating scale-up in size within a single channel while maintaining the inherent benefits of microfluidics for fuel cell devices. The integration of devices was discussed, with particular attention focused on the compatibility of methods for constructing channel structures and electrode substrates. Through testing, SU-8 photoresist channel structures were found to be compatible with thin-film carbon and gold electrodes, while PDMS stencil channels were more compatible with polyurethane-based electrode substrates.

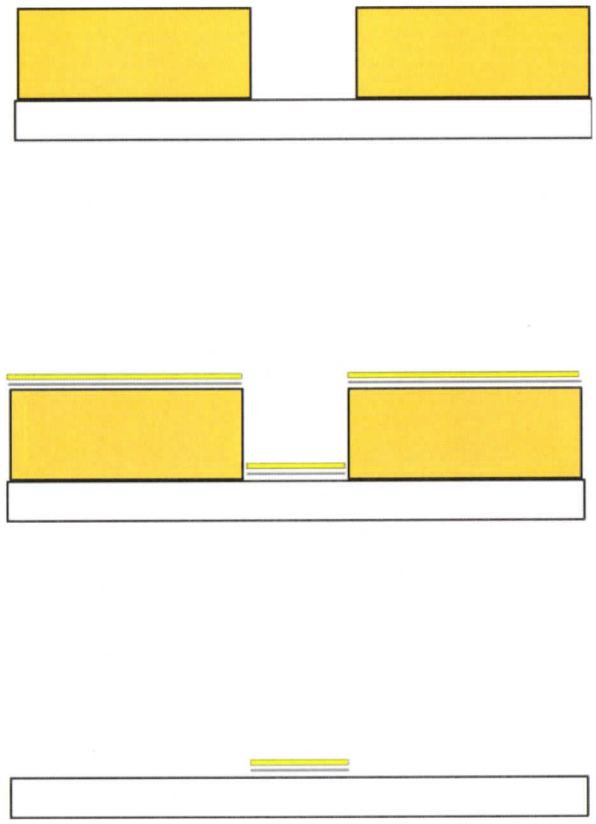

Figure 4.1 Schematic of the gold lift-off process.

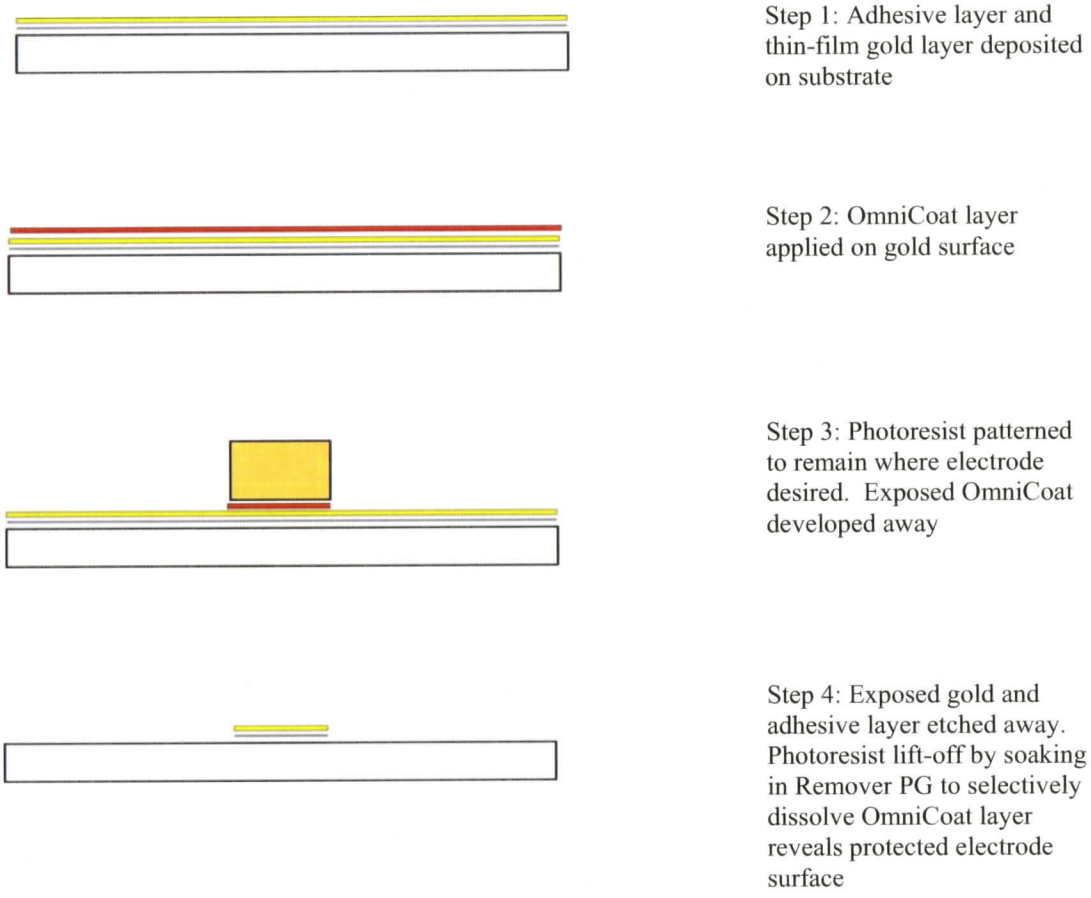

Figure 4.2 Schematic of the gold etch process.

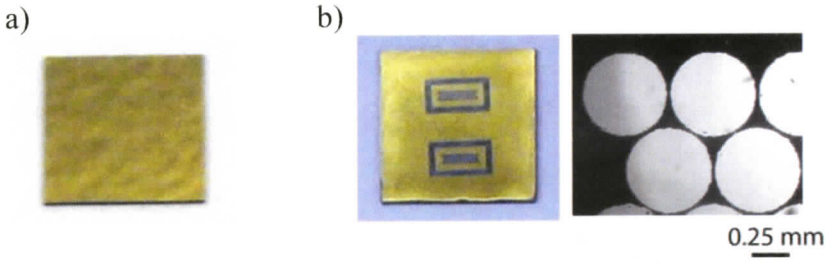

Figure 4.3 Images of gold surface (a) before patterning and (b) after patterning

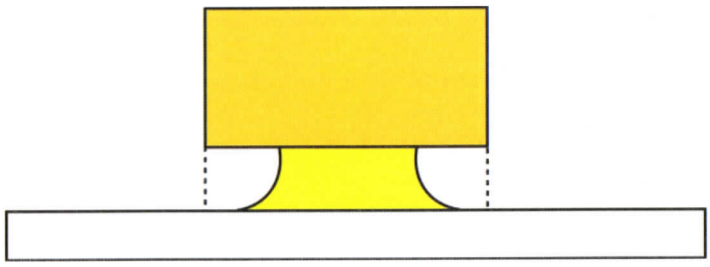

Figure 4.4 Effect of over-exposure to metal etchant. Nominally protected metal layer is etched away underneath the protective photoresist layer. Dashed lines indicate extents of nominal electrode pattern.

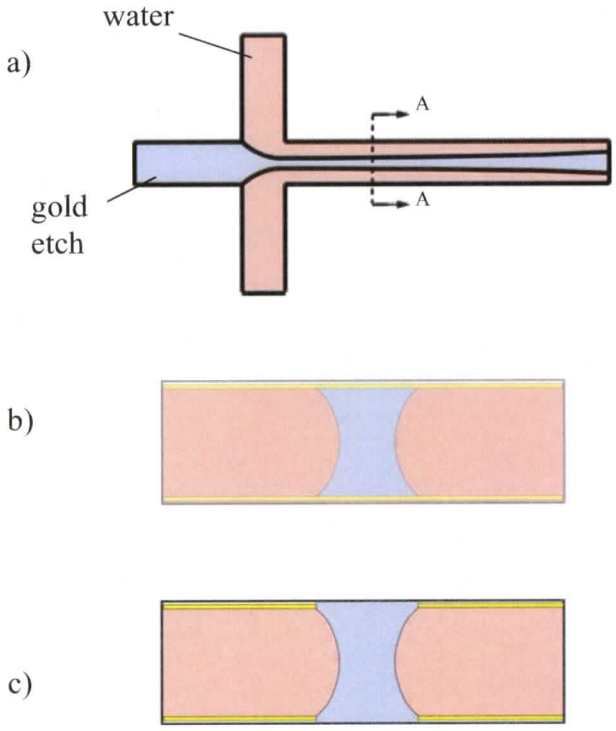

Figure 4.5 In-situ etching of gold electrodes, a) colaminar streaming of water (red) and etchant (blue), b) channel cross-section A-A at onset of etching, c) channel cross-section A-A after etching removes metal film.

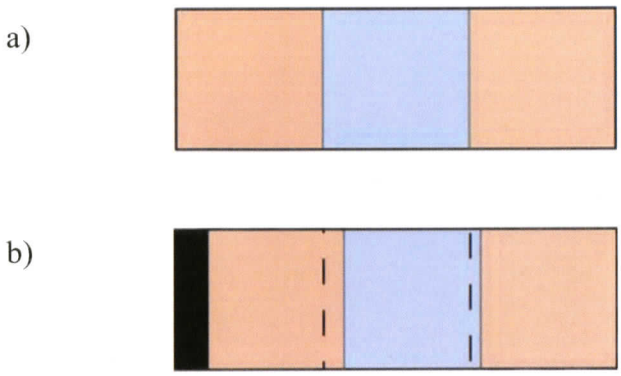

Figure 4.6 Effect of channel geometry irregularities on location of distinct colaminar streams, a) defect-free cross-section and b) width defect in channel. Black block is the channel obstruction, dashed lines represent the nominal locations of streams.

Figure 4.7 Composite image of in situ gold etching. Colaminar flow of gold etch solution sheathed by two water streams enters on the left and travels downstream. Broadening of the stream by diffusion is visible, as are slight distortions in the cross-stream location of the independent streams.

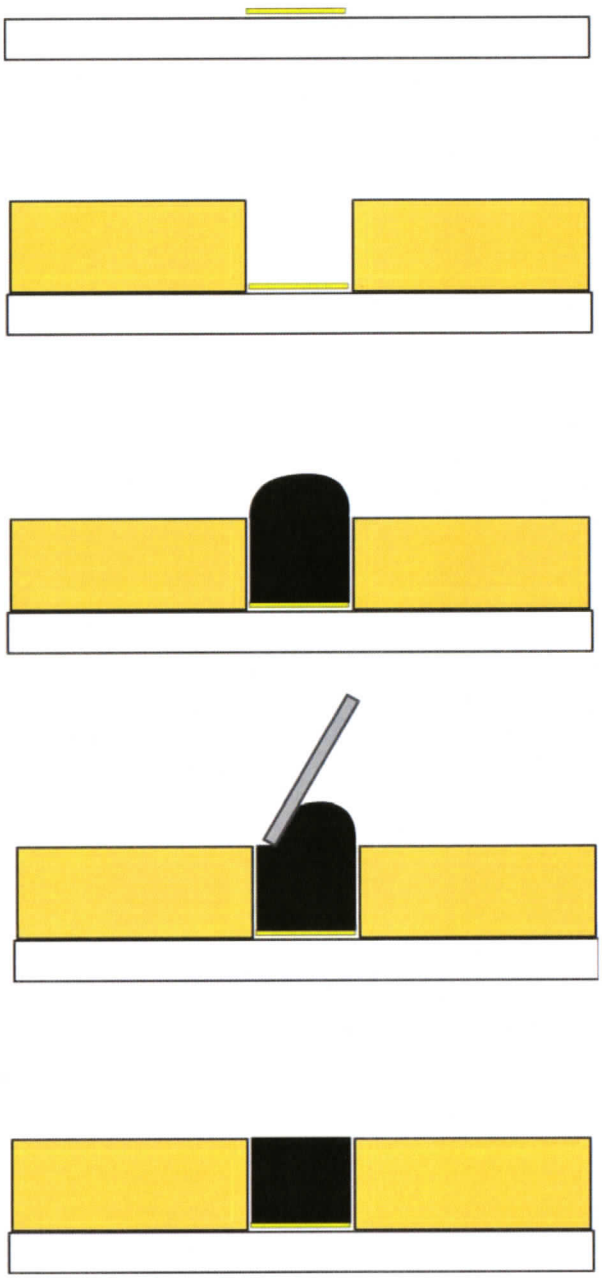

Step 1: Substrate patterned with gold current collector layer, as described in Section 4.3

Step 2: Substrate patterned with photoresist, cavity created in desired electrode location

Step 3: Cavity filled with carbon paste

Step 4: Excess carbon paste removed with razor blade

Step 5: Polymer binder is cured, creating carbon electrode. Channel structure is assembled on photoresist layer

Figure 4.8 Schematic of carbon mixture casting method.

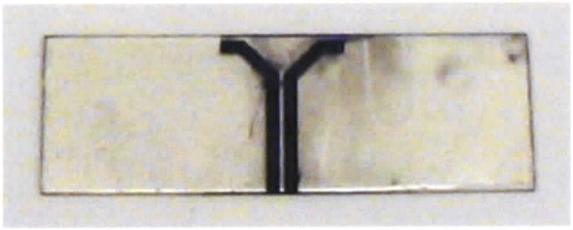

Figure 4.9 Image of carbon electrodes patterned by the casting method. Complete removal of the carbon electrode mixture from the surrounding areas is elusive, although electrical contact between the electrodes is avoided.

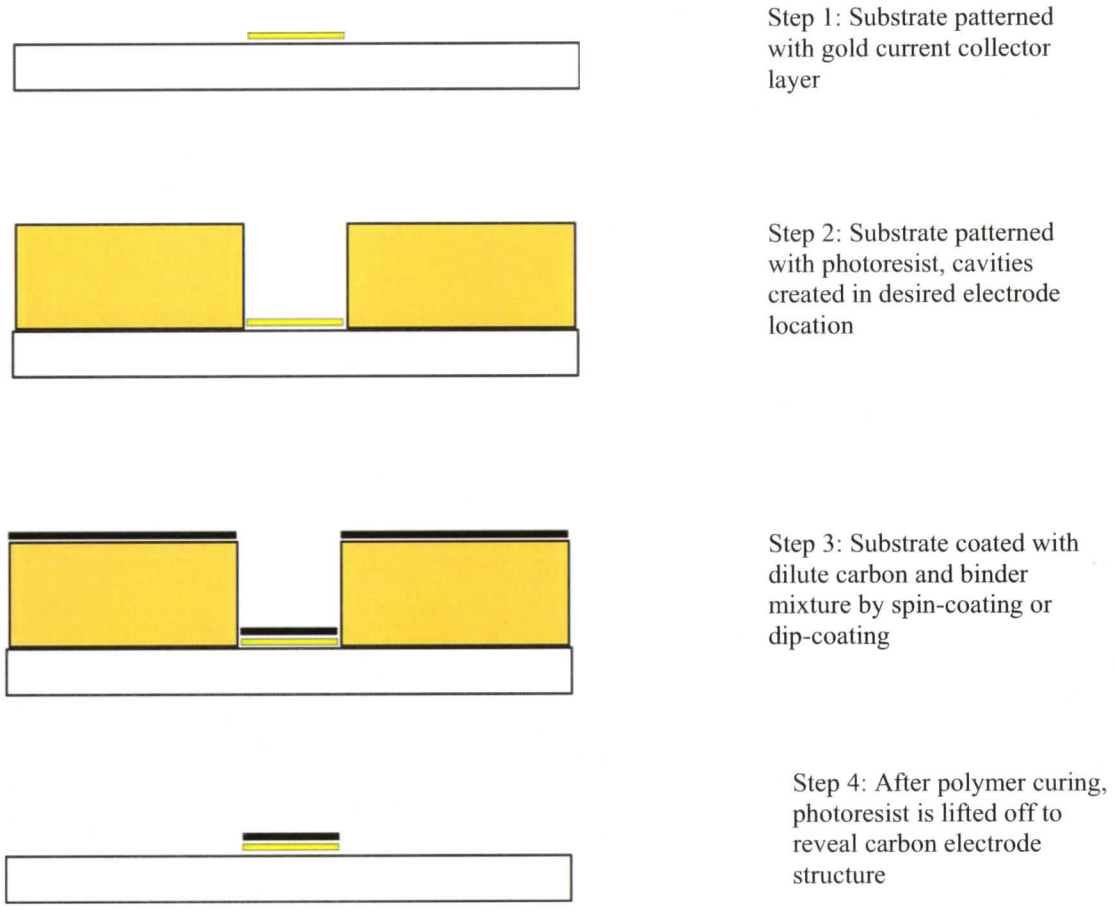

Figure 4.10 Schematic of carbon mixture lift-off patterning method.

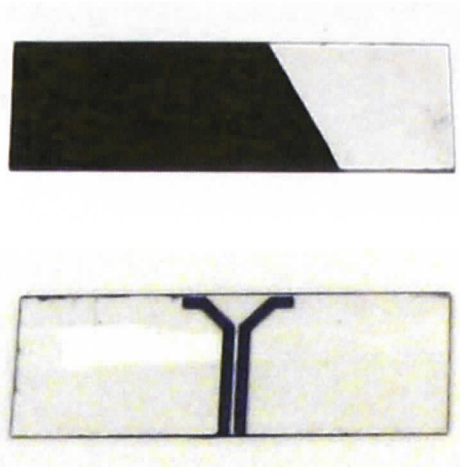

Figure 4.11 Image of electrodes fabricated by carbon mixture lift-off patterning.

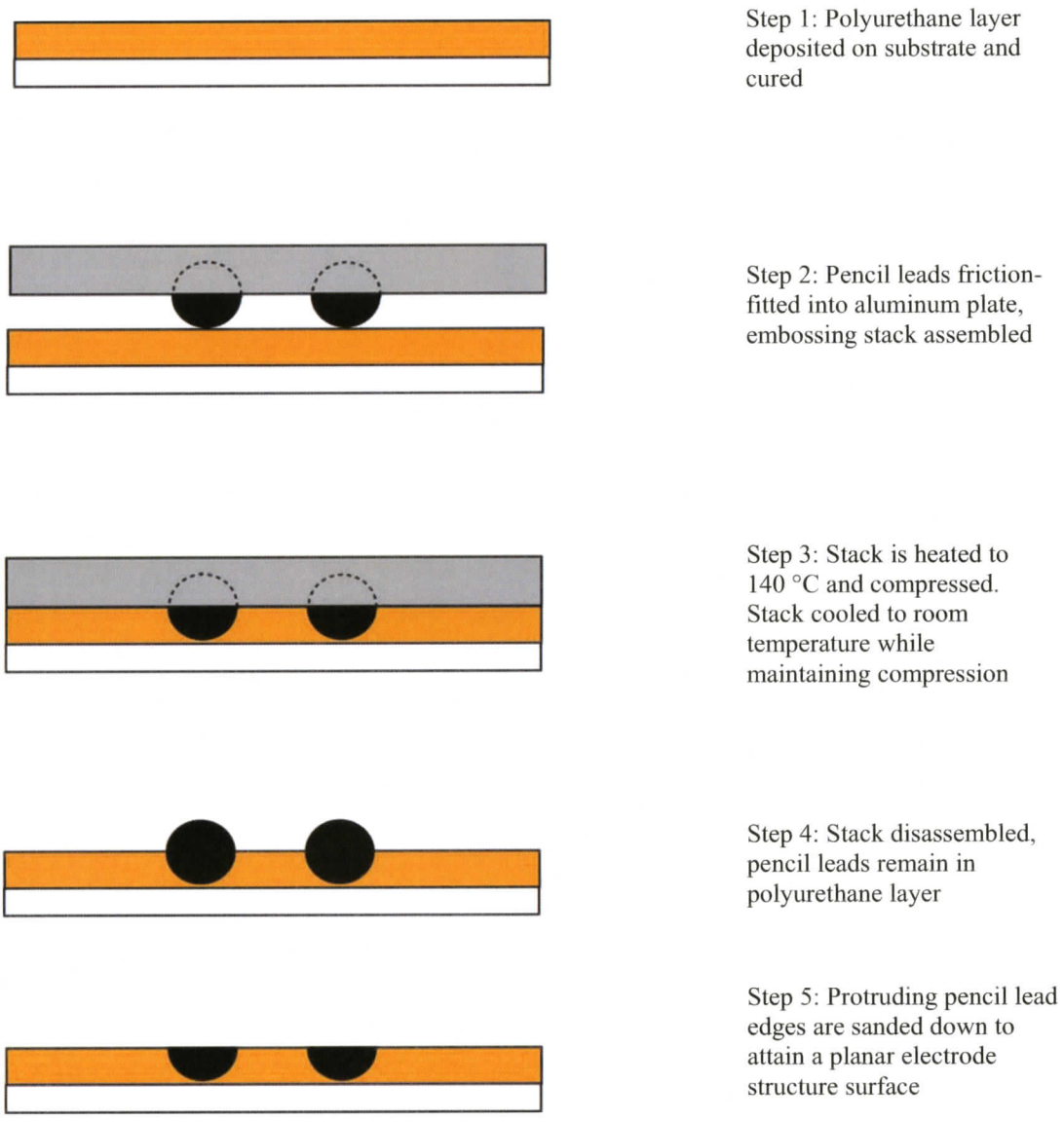

Figure 4.12 Schematic of graphite rod embossing method.

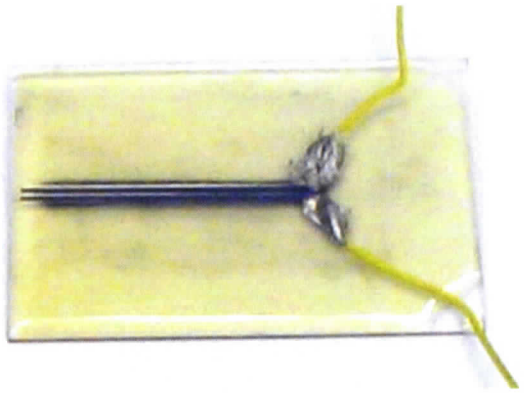

Figure 4.13 Image of graphite rod electrodes integrated in a polyurethane substrate by hot embossing

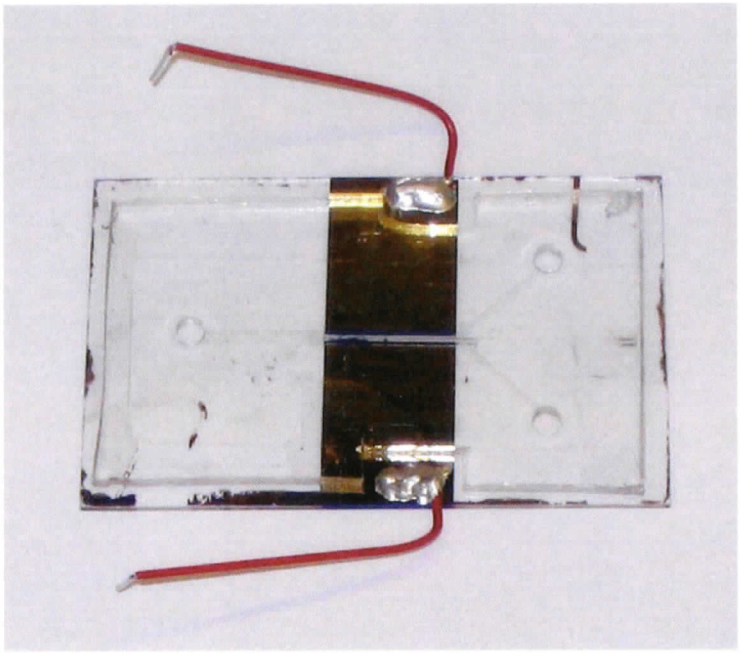

Figure 4.14 Single-sided vanadium redox fuel cell. Gold electrodes act as current collectors, transferring electrons from carbon electrodes within the channel. PDMS channel structure would be clamped to the base substrate during operation to prevent leakage.

Figure 4.15 SU-8 layer on carbon electrode coated substrates, a) polyurethane and carbon mix, b) SU-8 photoresist and carbon mix. SU-8 layer retreats from polyurethane mixture, but is amenable to coating SU-8 and carbon mixture

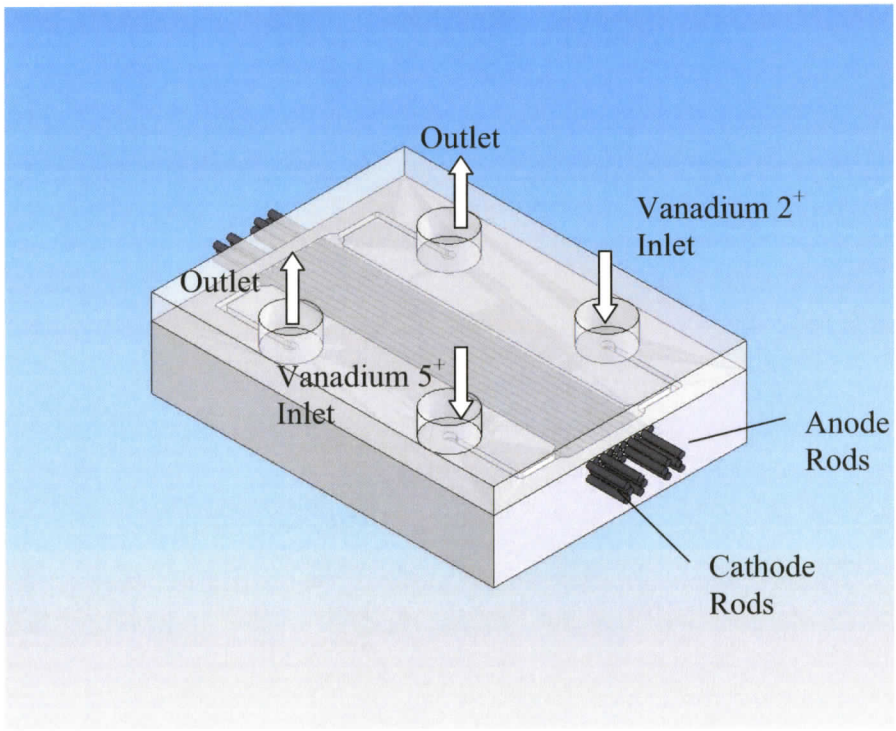

Figure 4.16 Schematic of three-dimensional graphite rod device. Dual inlets and outlets allow for the delivery and removal of the distinct vanadium species streams

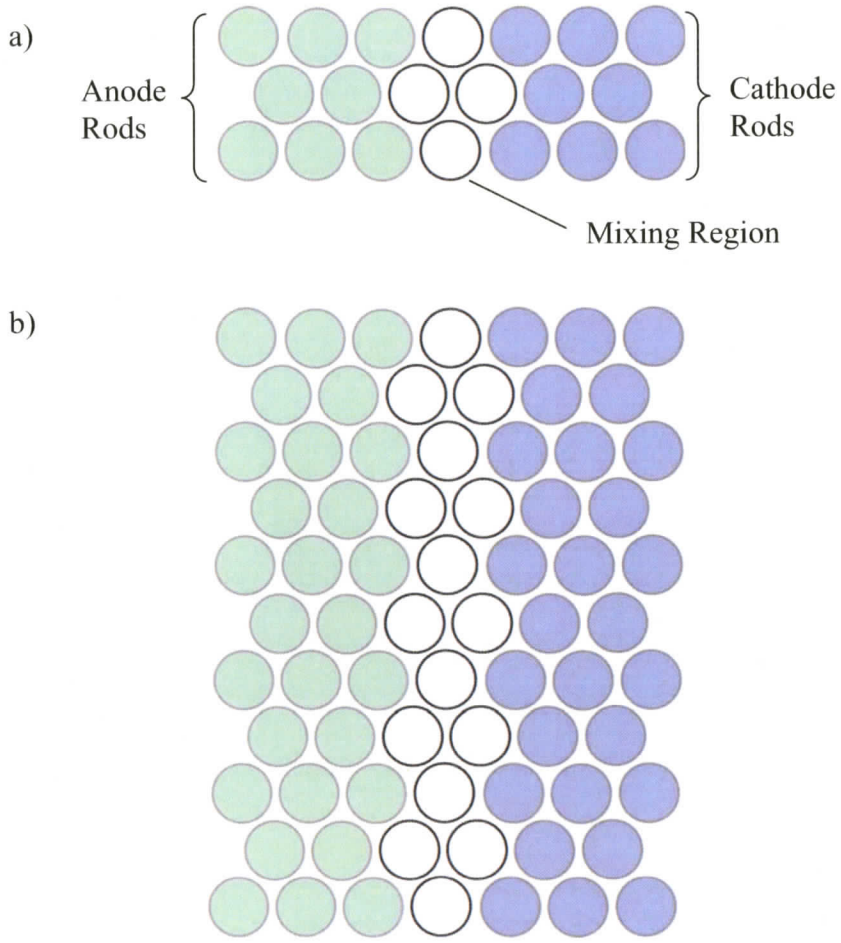

Figure 4.17 Schematic of the scale-up of the proposed three-dimensional fuel cell geometry featuring anodic and cathodic electrodes separated by neutral mixing region rods. A short channel cross-section (a) can be directly expanded in height (b) while microfluidic flow and transport characteristics remain similar throughout.

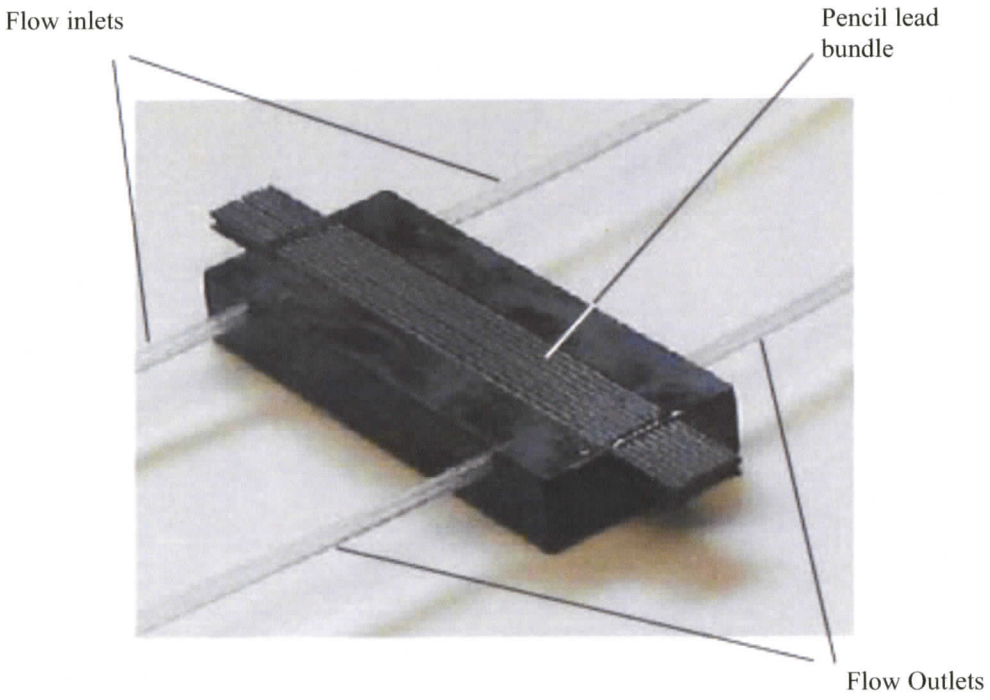

Figure 4.18 Image of three-dimensional graphite rod electrode vanadium redox fuel cell.

Chapter 5

DYNAMIC MICROFLUIDIC PHOTOMASKING

This chapter presents a novel microfluidic photomasking strategy. Laminar microfluidic streaming is exploited to achieve photomasking with dynamic spatial control. Two light absorbing streams hydrodynamically focus a transparent stream to define a line of light transmission. A device incorporating two such microfluidic layers, aligned orthogonally, enables light transmission only where the transparent streams overlap. Control of fluid flow in the microfluidic layers enables dynamic spatial control of the exposed region. Application to microarray patterning is investigated, and application to microfabrication is demonstrated via photoresist patterning. When applied to microfabrication in a frontal photopolymerization mode, this method affords both planar and depth-wise control of feature geometry.

5.1 Introduction

Photomasking is central to common microfabrication and micropatterning methods. Photolithographic methods of microfabrication exploit the selective exposure of a photosensitive material to define structure geometry. Originally adopted for use in microelectronics fabrication, similar techniques have subsequently been applied to microelectromechanical systems (MEMS) and microfluidics [Madou (1997); Duffy et al. (1998); Becker and Locascio (2002); Ng et al. (2002)]. In this process, a thin layer of photoresist is selectively exposed through a photomask with opaque and transparent

designs. Fabrication quality in this process is entirely dependent on the photomask resolution and its fidelity to the original design. Inexpensive high-resolution transparency photomasks created by image setting can attain minimum features of ~25um, with a turnaround time from design to printed mask to fabricated structure of less than a day [Duffy et al. (1998)]. Resolution can be improved by using a photo plotter, with minimum features of ~8um and similar cost and time expenditures [Linder et al. (1998)]. Higher resolution masks are also available. Metal on glass masks, for example, can achieve a minimum feature size of ~ 500 nm [McDonald et al. (2000)], but are significantly more costly and require more time to produce. In all cases, photomask designs are permanent. Altering the design requires the fabrication of new photomasks, with the associated cost and time investment.

In addition to structural fabrication, photomasking methods are commonly applied to both DNA and protein microarray patterning [Pellois et al. (2000); Gao et al. (2004)]. DNA microarrays allow high-throughput, parallel processing of DNA samples while consuming small amounts of reagents. Surface-bound probes of specific nucleic acid sequences specifically bind to their complimentary sequence, if present in the test DNA, emitting a fluorescent signal [Tyagi and Kramer (1996)]. Oligonucleotide probes can be synthesized by sequential addition of nucleic acids in the desired sequence, following direct or indirect photo-initiated cleavage of chain-terminating molecules [Gao et al. (2001)]. One such method, as commercialized by Affymetrix (Santa Clara, CA), uses metal on glass photomasks to create the exposure pattern to tailor specific oligonucleotide sequences at each array location. Four unique masks are necessary for each base acid length of the oligonucleotide probes. In general, masks cannot be reused and thus

changing the design of a single probe requires the fabrication of an entire new set of masks. While this is less of an issue for large fabrication runs, smaller-scale applications require more flexible probe construction methods. In this context, dynamic exposure methods are attractive as the time and cost involved in producing a new mask set for each probe design change are eliminated.

One challenge associated with photolithographic microstructure fabrication is creating structures of multiple heights. A number of techniques have been developed using conventional photomasks. Anderson et al. (2000) fabricated three-dimensional microfluidic systems in PDMS through two-level photolithography. In this process, an initial photoresist layer is exposed with a structure but not developed. A second layer is applied and subsequently exposed with the aid of an aligner to create a second level. Cabral et al. (2004) created multilevel fluidic devices with controlled height through frontal photopolymerization, wherein the photoresist is exposed through a transparent substrate and the 'front' of polymerized resist grows out from the substrate with increasing exposure dose. By controlling the exposure dose, the resulting structure height can be manipulated through selective, multiple exposures. Other methods involved grayscale photomasks to allow for three-dimensional patterning in a single exposure. O'Shea et al. (1995) used halftone chrome masks, where different densities of the opaque chrome create varying exposure levels. Wu et al. (2002) employed reduction lithography through an array of microlenses to pattern low resolution gray-scale masks. Microfluidic photomasks for gray-scale photolithography were developed by Chen et al. (2003). Channels were filled with UV-absorbing dye of varying concentrations, thus allowing for different levels of light exposure onto a layer of positive photoresist. Interrogation with

10% of the nominal exposure light was found to not alter the positive-tone photoresist, while increased exposure created correspondingly deeper cavities. The emphasis of the method of Chen et al. (2003) was on altering photoresist structure height through varying dye concentration within the photomask channels. Exposure features were spatially fixed by the dye channel configuration.

In this work, a dynamic photomasking methodology is developed. Laminar microfluidic streaming is applied to achieve photomasking with dynamic spatial control. The method exploits the light transmission contrast between light-absorbing streams and a hydrodynamically-focused transparent stream in a multilayer microfluidic chip. Visible light microscopy is employed to characterize the flow, dispersion, light transmission, and resulting photomask performance. Application to microarray patterning is investigated and application to microfabrication is demonstrated via photoresist patterning.

5.2 Materials and Methods

5.2.1 Device Fabrication

Microchannel designs were drafted using AutoCAD (Autodesk, San Rafael, CA) and printed to film on a high-resolution imagesetter (Island Graphics, Victoria, BC). SU-8 50 Photoresist (MicroChem, Newton, MA) was spun to the desired thickness, baked, exposed, and developed as detailed in Chapter 2 to pattern both layers of the microfluidic chip. For a desired channel height of 50 μm, photoresist was spun at 2000 rpm for 30 seconds following an initial ramping stage. Polydimethylsiloxane (PDMS) prepolymer and curing agent (Sylgard 184, Dow-Corning) were mixed at a 10:1 (wt/wt) ratio. PDMS was then cast on the master. Following degassing, PDMS was cured at 80°C at ambient

pressure. A thin featureless layer of PDMS was similarly fabricated, using the flat bottom of a 3" petri dish to create a smooth surface. PDMS containing the channel structure was sealed permanently to the thin PDMS flat after exposure to oxygen plasma, as detailed elsewhere [McDonald et al. (2000)]. A second PDMS channel structure was then permanently sealed to the opposite side of the PDMS flat, creating a single chip with two independent microfluidic layers. Test slides for the application of the photomasking method to photoresist patterning were coated with a 25 μm photoresist layer using SU-8 25 (MicroChem, Newton, MA) using a similar coating procedure as outlined above.

5.2.2 Solutions

Naphthalene green B (Sigma-Aldrich, Oakville, Ont) was dissolved in Millipore water (Millipore, Billerica, MA) to make an 8% solution by weight. Millipore water was used as the transparent stream. All solutions were filtered with a 0.45 μm syringe filter immediately prior to use.

5.2.3 Experimental Setup

Pressure driven flow to each inlet was supplied by a straightforward gravity-feed system. Flexible tubing was used to deliver water from independent reservoirs to the respective chip inlets. The inlet pressure at each reservoir was independently controlled by adjusting the height of the connected free surface along a graduated stand. A syringe pump was connected to the outlet of each microfluidic layer to regulate total flow rate through each layer. Alternatively, independently controlled syringe pumps could be employed at each inlet.

The light transmission characteristics of the photomasking system were analyzed using a Leica DMLM fluorescence microscope with a Retiga 8-bit cooled CCD camera. The chip was illuminated from below using a standard halogen microscope bulb. Before reaching the camera, the light passed through the low-pass filter of the microscope, blocking light of wavelengths smaller than 590 nm. Images were scaled such that peak transmission was set to full scale (T=1.0).

Exposure patterns were generated in a 25 μm thick layer of negative photoresist by exposure with collimated light through the microfluidic photomask. A frontal exposure methodology was employed [Cabral et al. (2004)]. Frontal exposure facilitates three-dimensional photoresist patterning through control of the exposure dose at desired locations. In contrast to the common direct exposure mode, incompletely exposed areas are reproduced and adhere to the substrate. The photomasking system presented here is especially amenable to this method, as a complete exposure consists of the independent exposure of any number of sub-regions, all of which could receive different exposure levels and resultant structure heights.

5.3 Results and Discussion

A schematic of the microfluidic photomasking strategy and an image of the system in operation are shown in Figure 5.1. The basic component of the exposure system is a three-inlet microfluidic layer. A transparent stream enters the middle of the exposure region and is sheathed by two light-absorbing dye streams. The three streams pass through the exposure region in co-laminar flow. During exposure, light is transmitted exclusively through the transparent stream. Orienting a second independent

microfluidic layer orthogonal to the first limits light transmission to the small area where the two clear streams cross out-of-plane.

The proportion of light transmitted through an absorbing medium is described by Beer's law [Mauro (1966)]:

$$T = 10^{-Ch\varepsilon} \tag{5.1}$$

where ε is the specific absorbance of the medium for the wavelength of interrogating light, C is the concentration of absorbing material, and h is the distance traveled through the medium. To achieve low light transmission through an absorbing medium, the thickness and concentration of the absorbing medium must be maximized. Dye concentration is limited by its solubility in the working fluid, in this case distilled water. It is also noteworthy that light transmission has been found to deviate from this relation at high dye concentrations [Dorland's (2003)]. The height of dye containing channels is practically limited by fluid control, which becomes more difficult for larger channels, and transport characteristics as dictated by the aspect ratio of the focused stream.

The wavelength or wavelength band of the exposure light source employed determines the required spectral absorbance characteristics of the dye. An extensive library of dyes exists with absorption maxima throughout the UV and visible spectrum [Gurr (1971)]. Dye absorbance is typically limited to a finite wavelength range. If a broad band source is employed, a filter to remove undesired wavelengths may be required. Alternatively, a mixture of dyes with varying absorbance maxima can be prepared to achieve a broader absorbance range, to the limit of solubility.

The dye used here, Naphthol green B, was selected due to its high light absorption in convenient wavelength ranges. This dye is particularly absorbent in the near-UV

range. It is thus well-suited to photoresist applications, as SU-8 is optimally exposed using wavelengths between $\lambda = 350$ nm and $\lambda = 400$ nm [MicroChem (2002a)]. A second region of high light absorbance occurs at wavelengths greater than $\lambda = 625$ nm, making it a suitable dye for visible-light analysis. Naphthalene green B molecules are relatively large, with a molecular weight of 878 g/mol, which limits diffusion of the dye in co-laminar flow.

Relatively thick and thin transparent streams at five sample cross-stream positions are shown in Figure 5.2. The thin stream was approximately 50 μm wide, while the thick stream was approximately 100 μm wide, and both exhibit laminar hydrodynamic focusing. The overall flow rate through each microfluidic layer was approximately 2.5 mm/s for both the 50μm and 100μm cases. Control over stream location and thickness was achieved by varying flow rates of the inlet channels independently. The cross-stream location of the transparent stream was controlled by varying the relative flow rates of the sheathing streams. The thickness of the clear stream can be altered by increasing its flow rate or by decreasing the flow rates of the dye streams. This dynamic spatial control is achieved by exploiting the inherent flexibility of laminar microfluidic flow. Transmission contours for both cases where each transparent stream is aligned with the centerline are plotted in Figure 5.3a. The reduction in peak height due to diffusion is more pronounced in the case of the thinner stream due to higher concentration gradients. Thus at downstream distances, a thicker stream is able to achieve much higher contrast ratios. The consequence, however, is increased stream width which limits the attainable exposure pattern resolution. Transport of the dye into the transparent streams is limited due to the laminar nature of flow and occurs only by cross-stream diffusion. However,

stream mixing still has a significant effect on the transmission ratio. Ismagilov et al. (2000) theoretically and experimentally investigated the broadening of pressure driven laminar flow by diffusion, as described in Chapter 4. A one-third power relationship applies to stream broadening at the channel walls, while a one-half power relationship applies to stream broadening at the centre of the channel where the diffusion region grows more slowly [Ismagilov et al. (2000)]. In contrast, electroosmotic flow in microstructures is characterized by an effectively flat velocity profile, and results in reduced species transport between streams as compared to the pressure driven case. Indirect UV detection has been employed in capillary electrophoresis where non-UV-absorbing ions are differentiated from an absorbent dye phase based on light transmission, with dye concentrations ranging from 1.5 mM to 100 mM [Shamsi and Danielson (1994); Macka et al. (2001a); Macka et al. (2001b)]. The application of electrokinetic flow to microfluidic photomasking was investigated here, however, the high dye concentration required to achieve adequate light absorbance was not amenable to electrokinetic flow. Specifically, pressure driven flow was preferred due to the high ionic strength of the solution.

Composite transmission images from single stream transmission data (as shown in Figure 5.2) are shown in Figure 5.3b. Transmission through intersections of two such microfluidic layers, oriented orthogonally, is predicted by the composite array transmission image, plotted for each case in Figure 5.3c. The resulting arrays have 169 elements with mean spacing of 115μm and 55 μm corresponding to the 50μm and 100μm stream thickness cases, respectively. Flow enters the exposure region from left to right for the first layer, and from top to bottom for the second layer. The effect of diffusion on

transmission through the exposure areas is particularly apparent in the 50μm stream case, resulting in a much reduced contrast ratio. Dot patterns closer to the inlets of the two layers transmit significantly more light than those closer to the outlet of the exposure region, where dye has had more time to diffuse into the clear stream. The array pattern for the 100μm case exhibits much improved uniformity and a contrast ratio over 10:1. The optical system here was not optimized; most notably much of the light passing through the dye stream would be eliminated if a more properly matched filter was used. The optical filter employed here passed light of wavelengths greater than 590 nm, whereas the optimal dye absorbance begins at wavelengths greater than 625 nm, with a maximum at 690 nm. Thus it is expected that aligning the spectral characteristics of each of the dye, filters, and light source to the patterning application of interest would result in further improved contrast ratios.

The multilayer microfluidic photomask is shown in operation in Figure 5.4. These images were highly overexposed such that both transparent streams could be visualized. As shown, selected areas throughout the exposure region (6.25 mm2) may be independently interrogated by varying the flow rates of the inlet streams. Thus dynamic microfluidic control of both layers results in a photomask drawing capability akin to the common 'Etch-a-Sketch' toy (Ohio Art Company). Coordinated control with the exposure shutter results in full drawing capability. Different exposure shapes are also possible by varying the relative flow rates of the transparent streams. Line segments, squares, and rectangles are readily patterned by this method.

Applying the dynamic microfluidic photomasking method to photoresist patterning resulted in the exposure patterns shown in Figure 5.5. The low magnification

view (Figure 5.5a) shows the patterned dot as well as the component streams surrounding the exposure region. The photoresist is exposed everywhere not covered by a dye stream, and clear streams leading to and from the exposure region are clearly visible. The absorbing dye in each fluidic layer provided sufficient masking to inhibit photoresist polymerization, and the feature formed at the intersection of the transparent streams is well defined. Enlarged views of the exposed dot show a substantial fully exposed region surrounded by a ring of minimally exposed photoresist corresponding to reduced transmission in the dye diffusion boundary layers. This building-by-exposure effect is enabled by frontal photopolymerization where photoresist is exposed through the base substrate, the exposed front occurring initially at the interface and moving outward with increasing light exposure [Cabral et al. (2004)]. Thus, combining the in-plane flexibility of the dynamic microfluidic photomasking technique with depth-wise control offered by frontal photopolymerization, results in fully dynamic three-dimensional photolithography capabilities. As with all photomasking operations, the number of features patterned on a given substrate is limited by stray light accumulation during the exposure of photoresist. A maximum exposure time threshold will always limit the number of exposures possible, depending on the absorbance of the dye streams. For the setup and operating conditions described here, slight exposure began to occur throughout the exposure region after 90 s cumulative exposure, corresponding to three or more full exposures of the 25 μm thick photoresist layer. The maximum exposure time limit can be increased by increasing the effective absorbance of the dye streams and reducing species transfer between the colaminar streams.

5.4 Summary

This chapter presents a novel microfluidic photomasking strategy. Hydrodynamic focusing of light absorbing and transparent microfluidic streams is exploited to achieve photomasking with dynamic spatial control. Whereas traditional photomasks are permanently patterned with a certain design, the concept presented here affords the user dynamic control over the exposure pattern. The method shows promise for array-based patterning applications, and microfabrication based on photolithography. Application to photoresist patterning resulted in well defined feature shape and spatial control. Combining the in-plane flexibility of the dynamic microfluidic photomasking technique with depth-wise control offered by frontal photopolymerization, results in fully dynamic three-dimensional photolithography capabilities. Ultimately, the effectiveness of the presented photomasking system is governed by both the diffusion between the colaminar streams and the correlation between the bandwidth of interrogating light, the dye's bandwidth of high absorbance, and the bandwidth required by the application.

a.)

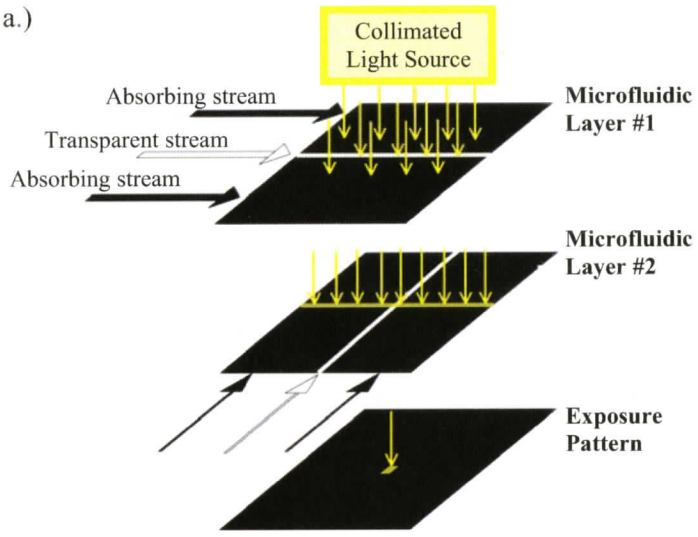

b.)

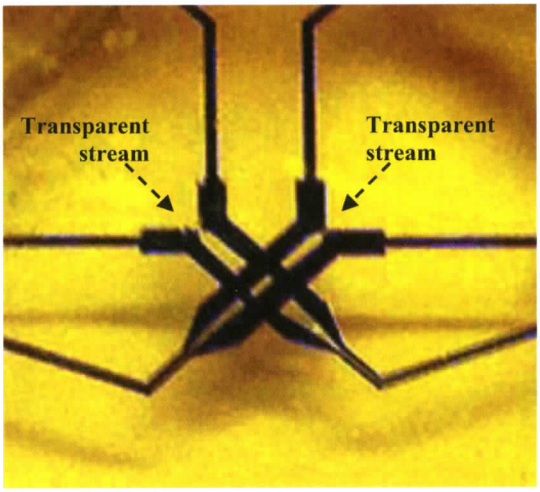

Figure 5.1 The dynamic microfluidic photomasking method. a) Schematic illustrating the light transmission through the transparent streams flanked by light absorbing streams in each orthogonally-aligned microfluidic layer; b) image of the operational bifold microfluidic photomasking device.

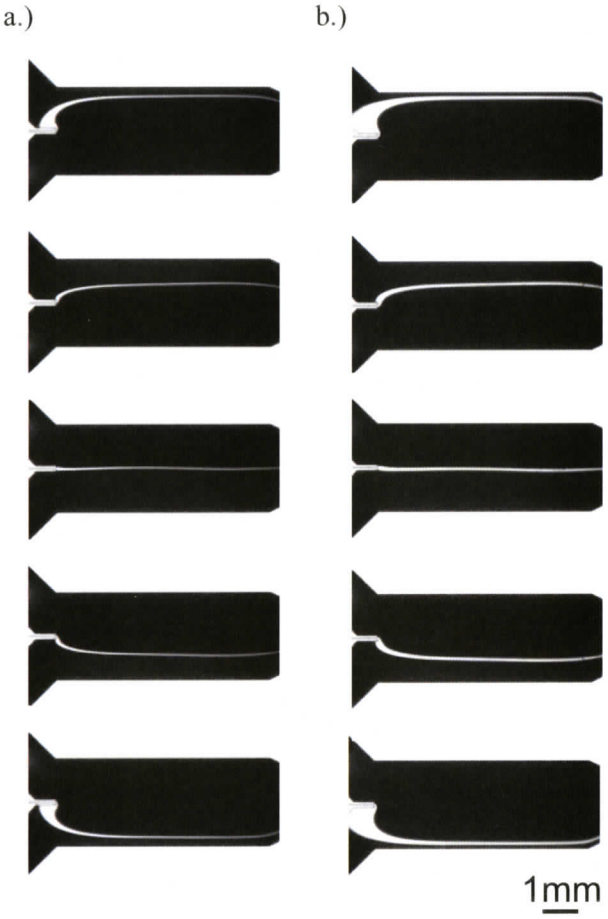

Figure 5.2 Transmission images showing sample cross stream locations of transparent stream, a) 50 μm thick stream, b) 100 μm thick stream.

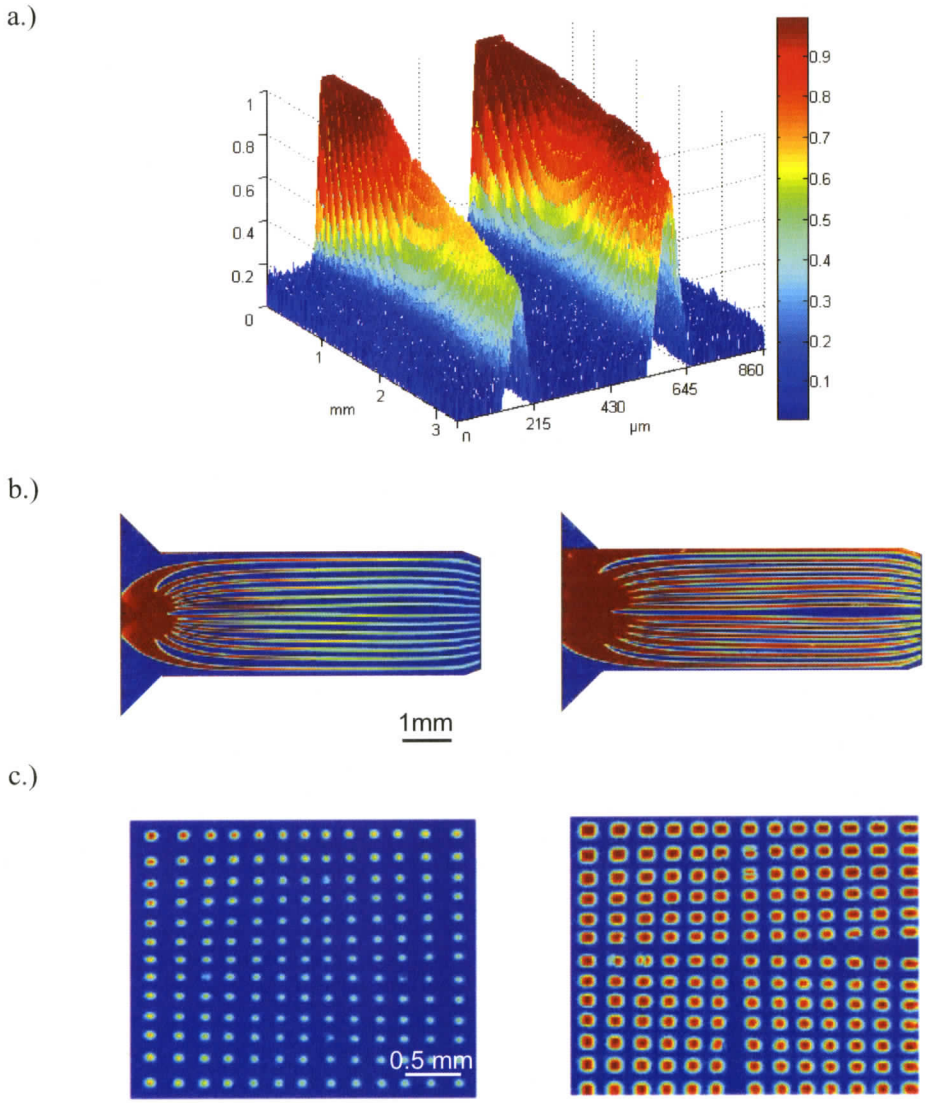

Figure 5.3 a) Downstream transmission contours for a centered 50 µm thick stream (left) and 100 µm thick stream (right); b) Composite transmission image of cross stream locations for 50 µm streams (left) and 100 µm streams (right); and c) Corresponding composite array transmission images. Colour bar corresponds to relative transmission.

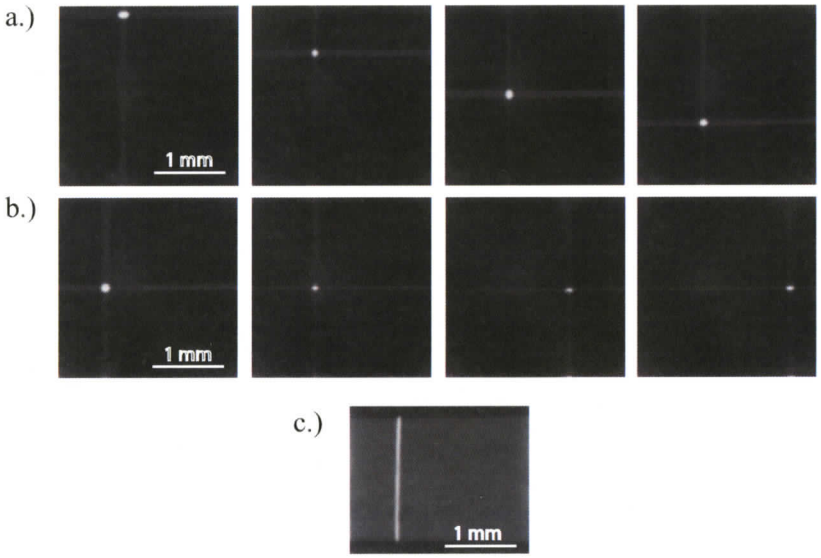

Figure 5.4 Visible light transmission images of dynamic microfluidic photomask in operation showing: a) vertical translation of exposure area; b) horizontal translation of exposure area; and c) line exposure pattern. Images were overexposed to reveal stream paths in each case.

Chapter 6

SUMMARY AND FUTURE WORK

6.1 Summary and Contributions of this Thesis

This thesis is part of an ongoing collaborative research project focused on the development of microstructured enzymatic fuel cells. The primary goal is the development of microfabrication techniques to advance this technology. Work toward this goal includes the development of basic microfabrication capabilities, the adaptation of traditional channel fabrication strategies to facilitate optimization of the fuel cell device, the development of gold and carbon electrode patterning techniques, and the design and development of a novel dynamic microfluidic photomasking device. The key contributions are summarized below.

6.1.1 Fabrication of Polymeric Microfluidic Devices

Microfabrication techniques were developed for microfluidic devices, specifically for microfluidic membraneless fuel cells. Processing parameters for the in-house fabrication of microchannels by rapid prototyping soft lithography were investigated and optimized. These techniques were then adapted for the fabrication of ultra-thick photoresist structures. Channel structure fabrication methods for microfluidic membraneless fuel cells were developed, using PDMS stencil and photoresist-based channel structures. Both methods were capable of facilitating the optimization of

electrode geometry and placement.

6.1.2 Electrode Patterning for Microfluidic Devices

Electrode patterning methods were developed for integration in microfluidic devices. This work was performed with a particular focus on microfluidic membraneless fuel cells, although similar techniques could be employed to incorporate electrodes in other microfluidic devices. Thin-film metallic layer patterning strategies were investigated for the patterning of gold electrodes and high conductivity current collectors. Carbon electrode fabrication techniques were investigated using two distinct methodologies. A carbon and polymeric binder mixture was employed to fabricate thin-film carbon electrodes and investigated to ensure chemical and electrochemical stability during assembly and operation. Graphite rods were also integrated into microfluidic devices by embossing in a polyurethane substrate and incorporation in a three-dimensional fuel cell architecture. The integration of electrode-patterned substrates and channel structures was investigated.

6.1.3 Dynamic Microfluidic Photomasking

A dynamic microfluidic photomasking device was developed and tested experimentally. Laminar microfluidic streaming was exploited to achieve photomasking with dynamic spatial control. Two light absorbing streams hydrodynamically focused a transparent stream to define a line of light transmission. A device incorporating two such microfluidic layers, aligned orthogonally, enabled light transmission only where the transparent streams overlap. Control of fluid flow in the microfluidic layers enables

dynamic spatial control of the exposed region. Application to microarray patterning was investigated and application to microfabrication was demonstrated via photoresist patterning. When applied to microfabrication in a frontal photopolymerization mode, this method affords both planar and depth-wise control of feature geometry.

6.2 Proposed Expansions of this Work

Many aspects of this work have uncovered opportunities for future research projects. Some of these opportunities are discussed below.

6.2.1 Experimental Investigation of Carbon Electrode Performance

Methods of fabricating and patterning carbon and gold electrodes have been developed in this thesis. An experimental investigation into the performance of the electrodes in an actual device is required for design optimization. The performance of carbon electrodes will be dependent on their reactivity and long term stability. Reactions occur on carbon surfaces and as such, maximization of the carbon content at the electrode – liquid interface is necessary to achieve optimal current density. However, the stability of high-carbon content electrodes is expected to diminish due to the lower polymeric binder content. A balance between electrode stability and performance must be reached to determine the optimal ratio of binder and carbon particles.

6.2.2 Carbon Structure Fabrication and Integration in Fuel Cell Devices

A higher degree of control over three-dimensional fuel cell architecture can be realized with the development of carbon structure fabrication techniques. Glassy carbon

microstructures have previously been fabricated by soft lithography, a process well-adapted to standard microfluidic laboratory infrastructure [Schueller et al. (1999)]. Fabrication of custom carbon structures may eliminate the design limitations of incorporating relatively large pencil leads as electrodes. Electrode size, shape, and spacing could be more accurately addressed and optimized for three-dimensional fuel cell performance. The development of carbon structure fabrication methods could lead to the development of electrode geometries very different from the tubular graphite rods investigated in this thesis. Porous carbon electrodes offer very high surface area, and as such could greatly improve the power density of planar fuel cell devices. A similar structure is commonly employed as the gas diffusion layer in polymer electrolyte membrane fuel cells.

6.2.3 Catalyst Coating of Electrode Structures

Traditional fuel cells utilize precious metals as catalysts to improve current density. While carbon electrodes are a viable alternative for vanadium redox devices, traditional fuel-consuming fuel cells require the development of catalyst deposition techniques. Work towards this goal is currently underway. Enzymes can be tethered to gold surfaces through an intermediary linker monolayer that facilitates electron conduction. To avoid the harsh environment of device assembly, monolayer formation and subsequent enzyme attachment can be performed in situ after assembly. Coating of the anode and cathode with different enzymes could be achieved in a multi-step method. Prior to the introduction of the enzyme, the linker monolayer can be selectively removed from one of the electrodes by applying an appropriate electric potential. The bare

electrode would subsequently be coated with a linker monolayer and its enzyme, resulting in selectively patterned anode and cathode electrodes. Alternatively, traditional precious metal catalysts can be employed to accelerate reactions within fuel cell devices. The in-situ electrodeposition of platinum and palladium catalyst on a gold underlayer offers many advantages to deposition before assembly. Ideally, a smaller amount of reactants is required, improving the efficiency of the deposition procedure. Most importantly, however, is the combination of in-situ deposition and colaminar gold electrode etching. Colaminar gold etching divides the base anodic and cathodic electrode structures in-situ, thus accommodating any channel imperfections that could otherwise cause fuel cross-over. The subsequent deposition of catalyst serves to functionalize the electrode structures. Pre-patterned and catalyzed electrodes would require precision alignment during assembly, which is not amenable to scaled-up production.

Similarly, carbon structures could be coated with catalyst and used with traditional fuels. The deposition of traditional catalysts on carbon structures and their incorporation in microfluidic fuel cells can be investigated. Alternatively, strategies for enzyme attachment to carbon structures would allow for the adaptation of the presented three-dimensional architecture to enzymatic fuel cells. The tethering of enzymes to gold surfaces is well developed. As such, a preliminary approach may involve an intermediate step to deposit a thin-film gold layer on the carbon structure surface. Finally, methods of directly tethering enzymes to a carbon surface could be investigated to eliminate the intermediate gold coating step.

References

Agarwal, M., Gunasekaran, R. A., Coane, P., and Varahramyan, K., (2005). "Scum-free patterning of SU-8 resist for electroforming applications" *Journal of Micromechanics and Microengineering*, **15**, 130-135.

Anderson, J., Chiu, D., Jackman, R.J., Cherniavskaya, O., McDonald J.C., Wu, H., Whitesides, S.H., and Whitesides, G.M., (2000) "Fabrication of topologically complex three-dimensional microfluidic systems in PDMS by rapid prototyping" *Analytical Chemistry*, **72**, 3158-3164

Atencia, J., and Beebe, D. J., (2005). "Controlled Microfluidic Interfaces" *Nature,* **437**, 648-655.

Auroux, P.-A., Koc, Y., de Mello, A., Manz, A., and Day, P. J. R., (2004). "Miniaturised nucleic acid analysis" *Lab on a Chip*, **4**, 534-546.

Barton, S. C., Gallaway, J., and Atanassov, P., (2004). "Enzymatic biofuel dells for implantable and microscale devices" *Chemical Reviews*, **104**, 4867-4886.

Bazylak, A., Sinton, D., and Djilali, N., (2005). "Improved fuel utilization in microfluidic fuel cells: a computational study" *Journal of Power Sources*, **143**, 57-66.

Becker, H., and Gartner, C., (2000). "Polymer micro fabrication methods for microfluidic analytical applications" *Electrophoresis*, **21**, 12-26.

Becker, H., and Locascio, L., (2002). "Polymer microfluidic devices" *Talanta*, **56**, 267-287.

Bennetto, H. P. (1990). "Electricity generation by microorganisms" *Biotechnology Education*, **1**, 163-168.

Bilenberg, B., Nielsen, T., Clausen, B., and Kristensen, A., (2004). "PMMA to SU-8 bonding for polymer based lab-on-a-chip systems with integrated optics" *Journal of Micromechanics and Microengineering,* **14**, 814-818.

Bogdanov, A. L., and Peredkov, S. S., (2000). "Use of SU-8 photoresist for very high aspect ratio x-ray lithography" *Microelectronic Engineering*, **53**, 493-496.

Bohl, B., Steger, R., Zengerle, R., and Koltay, P., (2005). "Multi-layer SU-8 lift-off technology for microfluidic devices", *Journal of Micromechanics and Microengineering*, **15**, 1125-1130.

Cabral, J. T., Hudson, S. D., Harrison, C., and Douglas, J. F., (2004). "Frontal photopolymerization for microfluidic applications" *Langmuir*, **20**, 10020-10029.

Carlier, J., Arscott, S., Thomy, V., Fourrier, J. C., Caron, F., Camart, J. C., Druon, C., and Tabourier, P., (2004). "Integrated microfluidics based on multi-layered SU-8 for mass spectrometry analysis" *Journal of Micromechanics and Microengineering*, **14**, 619-624.

Chang, M. H., Chen, F., and Fang, N. S., (2005 – in press). "Analysis of membraneless fuel cell using laminar flow in a Y-shaped microchannel" *Journal of Power Sources*.

Chen, Y.-H. and Chen, S.-H., (2000). "Analysis of DNA fragments by microchip electrophoresis fabricated on poly(methylmethacrylate) substrates using a wire-imprinting method" *Electrophoresis*, **21**, 165-170.

Chen, Y. and Pepin, A., (2001). "Nanofabrication: Conventional and nonconventional methods" *Electrophoresis,* **22**, 187-207.

Chen, C., Hirdes, D., and Folch, A., (2003). "Gray-scale photolithography using microfluidic photomasks" *Proceedings of the National Academy of Sciences,* **100,** *4,* 1499-1504.

Cho, S. K., Moon, H., and Kim, C. J., (2003). "Creating, transporting, cutting, and merging liquid droplets by electrowetting-based actuation for digital microfluidic circuits" *Journal of Microelectromechanical Systems,* **12**, 70-80.

Choban, E. R., Markoski, L. J., Wieckowski, A., and Kenis, P. J. A., (2004). "Microfluidic fuel cell based on laminar flow" *Journal of Power Sources*, **128**, 54-60.

Choban, E. R., Spendelow, J. S., Gancs, L., Wieckowski, A., and Kenis, P. J. A., (2005a). "Membraneless laminar flow-based micro fuel cells operating in alkaline, acidic, and acidic/alkaline media" *Electrochimica Acta,* **50**, 5390-5398.

Choban, E. R., Waszczuk, P., and Kenis, P. J. A., (2005b). "Characterization of limiting factors in laminar flow-based membraneless microfuel cells" *Electrochemical and Solid-State Letters,* **8**, A348-A352.

Chou, H. P., Spence, C., Schere, A., Quake, S., (1999). "A microfabricated device for sizing and sorting DNA molecules" *Proceedings of the National Academy of Science*, **96**, 11-13.

Coleman, J. T., McKechnie, J., and Sinton, D., (2006 – in press). "High-efficiency electrokinetic micromixing through symmetric sequential injection " *Lab on Chip,* in press.

Conradie, E. H., and Moore, D. F., (2002). "SU-8 thick photoresist processing as a functional material for MEMS applications" *Journal of Micromechanics and Microengineering,* **12,** 368-374.

Cremers, C., Bouamrane, F., Singleton, L., and Schenk, R., (2001). "SU-8 as resist material for deep x-ray lithography" *Microsystems Technologies*, **7,** 11-16.

Degani, Y., and Heller, A., (1988). "Direct electrical communication between chemically modified enzymes and metal electrodes. 2. Methods for bonding electron-transfer relays to glucose oxidase and D-amino-acid oxidase" *Journal of the American Chemical Society*, **110,** 2615-2620.

De Leebeeck, A., Kumar, K., Brolo, A. G., Gordon, R., and Sinton, D., (2006). "On-chip detection with nanohole arrays", *Proceedings of IEEE/LEOS Summer Topicals 2006 Optofluidics Meeting*, Quebec, QC, July 2006.

de Mello, A., (2002). "Plastic fantastic?" *Lab on Chip*, **2**, 31N-36N.

Dorland's Illustrated Medical Dictionary (2003). Saunders: Philadelphia, PA

Duffy, C., McDonald, J. C., Schueller, O. J. A., and Whitesides, G.M., (1998). "Rapid prototyping of microfluidic systems in poly(dimethylsiloxane)" *Analytical Chemistry*, **70**, 4974-4984.

Duffy, D. C., Schueller, O. J. A., Brittain, S. T., and Whitesides, G. M., (1999). "Rapid prototyping of microfluidic switches in poly(dimethyl siloxane) and their actuation by electro-osmotic flow" *Journal of Micromechanics and Microengineering*, **9**, 211-217.

Dyer, C. K., (2002). "Fuel cells for portable applications" *Journal of Power Sources,* **106**, 31-34.

Engel, J. M., Chen, J., Bullen, D., and Liu, C., (2005). "Polyurethane rubber as a MEMS material: characterization and demonstration of an all-polymer two-axis artificial hair cell flow sensor" *18th IEEE International Conference on Microelectromechanical Systems*, Miami Beach FL, January 2005.

Ferrigno, R., Stroock, A. D., Clark, T. D., Mayer, M., and Whitesides, G. M., (2002). "Membraneless vanadium redox fuel cell using laminar flow" *Journal of the American Chemical Society*, **124,** 12930-12931.

Fiorini, G., Lorenz, R. M., Kuo, J. S., and Chiu, D. T., (2004). "Rapid prototyping of thermoset polyester microfluidic devices" *Analytical Chemistry,* **76**, 4697-4704.

Folch, A., Ayon, A., Hurtado, O., Schmidt, M. A., and Toner, M., (1999). "Molding of deep polydimethylsiloxane microstructures for microfluidics and biological applications" *Journal of Biomechanical Engineering*, **121**, 28-34.

Folch, A., Jo, B. H., Hurtado, O., Beebe, D. J., and Toner, M., (2000). "Microfabricated elastomeric stencils for micropatterning cell cultures" *Journal of Biomedical Materials Research*, **52**, 346-353.

Gao, X., LeProust, E., Zhang, H., Srivannavit, O., Gulari, E., Yu, P., Nishiguchi, C., Xiang, Q., and Zhou, X., (2001). "A flexible light-directed DNA chip synthesis gated by deprotection using solution photogenerated acids" *Nucleic Acids Research,* **29,** *22,* 4744-4750.

Gao, X ., Gulari, E., and Zhou, X., (2004). "In situ synthesis of oligonucleotide microarrays" *Biopolymers,* **73,** 579-596.

Garland, P. and Serafinowski, P., (2002). "Effects of stray light on the fidelity of photodirected oligonucleotide array synthesis" *Nucleic Acids Research,* **30**.

Gray, B., and Jaffer, S., (2005). "Microfluidic interconnects in SU-8 photopolymer" *Proceedings of the ASME 3rd International Conference on Microchannels and Minichannels*, Toronto, July 2005.

Gregg, B. A., and Heller, A., (1990). "Cross-linked redox gels containing glucose oxidase for amperometric biosensor applications" *Analytical Chemistry*, **62**, 258-263.

Guo, L., Cheng, X., and Chou, C. F., (2004). "Fabrication of size-controllable nanofluidic channels by nanoimprinting and its application for DNA stretching" *Nano Letters*, **4**, 69-73

Gurr, E., (1971). *Synthetic dyes in biology, medicine, and chemistry,* Academic Press, New York.

Heller, A., (2003). "Plugging metal connectors into enzymes" *Nature Biotechnology*, **21**, 631-632.

Heller, A., (2004). "Miniature biofuel cells" *Physical Chemistry Chemical Physics* **6**, 209-216.

Holland, L., (1963). *Vacuum Deposition of Thin Films*. Aberdeen University Press, Aberdeen, Scotland.

Hosokawa, K., Hanada, K., and Maeda, R., (2002). "A polydimethylsiloxane (PDMS) deformable diffraction grating for monitoring of local pressure in microfluidic devices" *Journal of Micromechanics and Microengineering,* **12**, 1-6.

Hruby, J., (2001). "LIGA technologies and applications" *MRS Bulletin*, April, 337-340.

Ismagilov, R. F., Stroock, A. D., Kenis, P. J. A., and Whitesides, G. M., (2000). "Experimental and theoretical scaling laws for transverse diffusive broadening in two-phase laminar flows in microchannels" *Applied Physics Letters*, **76** (17) 2376-2378.

Jackman, R. J., Duffy, D. C., Cherniavskaya, O., and Whitesides, G. M., (1999). "Using elastomeric membranes as dry resists and for dry lift-off" *Langmuir,* **15**, 2973-2984.

Jackman, R. J., Floyd, T. M., Ghodssi, R., Schmidt, M. A., and Jensen, K. F., (2001). "Microfluidic systems with on-line UV detection fabricated in photodefinable epoxy", *Journal of Micromechanics and Microengineering,* **11**, 263-269.

Jayashree, R. S., Gancs, L., Choban, E. R., Primak, A., Natarajan, D., Markoski, L. J., and Kenis, P. J. A., (2005). "Air-breathing laminar flow-based microfluidic fuel cell" *Journal of the American Chemical Society*, **127**, 16758-16759.

Jo, B. H., Van Lerberghe, L. M., Motsegood, K. M., and Beebe, D. J., (2000). "Three-dimensional micro-channel fabrication in polydimethylsiloxane (PDMS) elastomer," *Journal of Microelectromechanical Systems,* **9**, 76-81.

Joshi, P. P., Merchant, S. A., Wang, Y., and Schmidtke, D. W., (2005). "Amperometric biosensors based on redox polymer-carbon nanotube-enzyme composites" *Analytical Chemistry*, **77**, 3183-3188.

Juang, Y.-J., Lee, L. J., and Koelling, K. W., (2002). "Hot embossing in microfabrication. Part 1: Experimental" *Polymer Engineering and Science*, **42**, 539-550.

Kamholz, A. E., (2004). "Proliferation of microfluidics in literature and intellectual property" *Lab on a Chip*, **4**, 16N-20N.

Katz, E., Willner, I., and Kotlyar, A. B., (1999). "A non-compartmentalized glucose-O_2 biofuel cell by bioengineered electrode surfaces" *Journal of Electroanalytical Chemistry*, **479**, 64-68.

Kenis, P. J. A., Ismagilov, R. F., and Whitesides, G. M., (1999). "Microfabrication inside capillaries using multiphase laminar flow patterning" *Science*, **285**, 83-85.

Kenis, P. J. A., Ismagilov, R. F., Takayama, S., and Whitesides, G. M., (2000). "Fabrication inside microchannels using fluid flow" *Accounts of Chemical Research,* **33**, 841-847.

Kim, B. H., Ryu, S. H., Choi, D. K., and Chu, C. N., (2005). "Micro electrochemical milling" *Journal of Micromechanics and Microengineering*, **15**, 124-129.

Kjeang, E., Sinton, D., and Harrington, D. A., (2005 – in press) "Strategic enzyme patterning for microfluidic biofuel cells" *Journal of Power Sources*.

Kjeang, E., Roesch, B., McKechnie, J., Harrington, D. A., Sinton, D., and Djilali, N., (2006 – submitted). "Integrated electrochemical velocimetry for microfluidic devices" *Lab on a Chip*, submitted.

Koch, M., Evans, A. G. R., and Brunnschweiler, A., (1999). "Design and fabrication of a micromachined Coulter counter" *Journal of Micromechanics and Microengineering*, **9**, 159-161.

Lagally, E. T., Simpson, P. C., and Mathies, R. A., (2000). "Monolithic integrated microfluidic DNA amplification and capillary electrophoresis analysis system" *Sensors and Actuators B*, **63**, 138-146.

Lee, J. Park, C., and Whitesides, G. M., (2003) "Solvent compatibility of poly(dimethylsiloxane)-based microfluidic devices," *Analytical Chemistry*, **75**, 6544-6554.

Li, S., Freidhoff, C., Young, R., and Ghodssi, R., (2003). "Fabrication of micronozzles using low-temperature wafer-level bonding with SU-8" *Journal of Micromechanics and Microengineering*, **13**, 732-738.

Lin, C. L., Kao, H.-M., Wu, R.-R., and Kuo, P.-L., (2001). "Multinuclear solid-state NMR, DSC, and conductivity studies on solid polymer electrolytes based on polyurethane/polydimethylsiloxane segmented copolymers" *Macromolecules*, **35**, 3083-3096.

Lin, C. H., Lee, G. B., Chang, B. W., and Chang, G. L., (2002). "A new fabrication process for ultra-thick microfluidic microstructures utilizing SU-8 photoresist" *Journal of Micromechanics and Microengineering*, **12**, 590-597.

Linder, V., Wu, H., Jiang, X., and Whitesides, G. M., (2003). "Rapid prototyping of 2D structures with feature sizes larger than 8 μm" *Analytical Chemistry*, **75**, 2522-2527.

Liu, J., Cai, B., Zhu, J., Ding, G., Zhao, X., Yang, C., and Chen, D., (2004). "Process research of high aspect ratio microstructure using SU-8 resist" *Microsystem Technologies*, **10**, 265-268.

Liu, C. C., and Cui, D. F., (2005). "Design and fabrication of poly(dimethylsiloxane) electrophoresis microchip with integrated electrodes" *Microsytem Technologies*, **11**, 1262-1266.

Lorenz, H., Despont, M., Fahrni, N., LaBianca, N., Renaud, P., and Vettiger, P., (1997). "SU-8: a low-cost negative resist for MEMS" *Journal of Micromechanics and Microengineering*, 1997, **7**, 121-124.

Lorenz, H., Despont, M., Fahrni, N., Brugger, J., Vettiger, P., and Renaud, P., (1998). "High-aspect-ratio, ultra thick, negative-tone near-UV photoresist and its applications for MEMS" *Sensors and Actuators A,* **64**, 33-39.

Lorenz, H., Despont, M., Vettiger, P., and Renaud, P., (1998b). "Fabrication of photoplastic high-aspect ratio microparts and micromolds using SU-8 UV resist" *Microsystem Technologies*, **4**, 143-146.

Ma, M., Qu, L., and Shi, G., (2005). "Glucose oxidase electrodes based on microstructured polypyrrole films" *Journal of Applied Polymer Science*, **98**, 2550-2554.

Macka, M., Johns, C., Doble, P., and Haddad, P.R., (2001a). "Indirect Photometric Detection in CE Using Buffered Electrolytes – Part I, Principles" *Liquid Chromatography Gas Chromatography*, **19**, 1, 38-47.

Macka, M., Johns, C., Doble, P., and Haddad, P.R., (2001b). "Indirect Photometric Detection in CE Using Buffered Electrolytes – Part 2, Practical Rules" *Liquid Chromatography Gas Chromatography*, **19**, 2, 178-188.

Madou, M.J., (1997). *Fundamentals of Microfabrication*, Boca Raton, FL: CRC Press.

Mano, N., Mao, F., and Heller, A., (2002). "A miniature biofuel cell operating in a physiological buffer" *Journal of the American Chemical Society*, **124**, 12962-12963.

Mano, N., Mao, F., and Heller, A., (2003). "Characteristics of a miniature compartment-less glucose-O_2 biofuel cell and its operation in a living plant" *Journal of the American Chemical Society*, **125**, 6588-6594.

Mauro, J. A., (1966). *Optical Engineering Handbook.* Syracuse, NY: General Electric.

McDonald, J. C., Duffy, D. C., Anderson, J. R., Chiu, D. T., Wu, H., Schueller, O. J. A., and Whitesides, G. M., (2000). "Fabrication of microfluidic systems in poly(dimethylsiloxane)" Electrophoresis, **21**, 27-40.

McKechnie, J. and Sinton, D. (2005). "Two-dimensional microfluidic photomasking for microarray patterning" *Proceedings of the 2005 ASME International Mechanical Engineering Congress and Exposition,* Orlando, November, 2005.

McKechnie, J. and Sinton, D. (2006). "Dynamic Microfluidic Photomasking" *Proceedings of the IEEE/LEOS Summer Topicals 2006 – Optofluidics Meeting,* Quebec, QC, July, 2006.

McKechnie, J. and Sinton, D. (2006 – submitted). "Dynamic Microfluidic Photomasking" *Journal of Microelectromechanical Systems*, submitted.

MicroChem, *Nano SU-8: Negative tone photoresist, formulations 2-25*. Newton, MA, 2002a.

MicroChem, *Nano SU-8: Negative tone photoresist, formulations 50-100*, Newton, MA, 2002b.

Mitrovski, S. M., Elliott, S. C. C., and Nuzzo, R. G., (2004). "Microfluidic devices for energy conversion: Planar integration and performance of a passive, fully immersed, H_2-O_2 fuel cell" *Langmuir*, **20**, 6974-6976.

Mitrovski, S. M., and Nuzzo, R. G., (2006). "A passive microfluidic hydrogen-air fuel cell with exceptional stability and high performance" *Lab on a Chip*, **6**, 353-361.

Mogensen, K., El-Ali, J., Wolf, A., and Kutter, J., (2003). "Integration of polymer waveguides for optical detection in microfabricated chemical analysis systems" *Applied Optics*, **42**, 4072-4079.

Moore, C. M., Minteer, S. D., and Martin, R. S., (2004). "Microchip-based ethanol/oxygen biofuel cell" *Lab on a Chip*, **5**, 218-225.

Ng, J, Gitlin, I., Stroock, A. D., and Whitesides, G. M., (2002). "Components for integrated poly(dimethylsiloxane) microfluidic systems" *Electrophoresis*, **23**, 3461-3473.

O'Shea, D. C. and Rockward, W. S., (1995). "Gray-scale masks for diffractive-optics fabrication: II. Spatially filtered half tone screens", *Applied Optics*, **34**, 7518.

Pellois, J. P., Wang, W., and Gao, X., (2000). "Peptide synthesis based on t-Boc Chemistry and Solution Photogenerated Acids", *Journal of Combinatorial Chemistry*, **2**, 355-360.

Priestnall, M. A., Kotzeva, V. P., Fish, D. J., and Nilsson, E. M., (2002). "Compact mixed-reactant fuel cells" *Journal of Power Sources,* **106**, 21-30.

Qin, D., Xia, Y., Rogers, J. A., Jackman, R. J., Zhao, X.-M., and Whitesides, G. M., (1998). "Microfabrication, microstructures and Microsystems" *Topics in Current Chemistry*, **194**, 1-20.

Quake, S., and Scherer, A. (2000). "From micro- to nanofabrication with soft materials" *Science*, **290**, 1536-1540.

Reyes, D. R., Iossifidis, D., Auroux, P.-A., and Manz, A., (2002). "Micro total analysis systems. 1. Introduction, theory, and technology" *Analytical Chemistry*, **74**, 2623-2636.

Ritter, S., (2001). "Pencils and pencil lead" *Chemical and Engineering News*, **79**, 35.

Rolland, J. P., Van Dam, R. M., Schorzman, D. A., Quake, S. R., and DeSimone, J. M., (2004). "Solvent-resistant photo curable 'liquid teflon' for microfluidic device fabrication" *Journal of the American Chemical Society,* **126**, 2322-2323.

Ruska, W. S., *Microelectronic Processing: An Introduction to the Manufacture of Integrated Circuits*. McGraw-Hill, New York, 1987.

Schueller, O. J. A., Duffy, D. C., Rogers, J. A., Brittain, S. T., and Whitesides, G. M., (1998). "Reconfigurable diffraction gratings based on elastomeric microfluidic devices" *Sensors and Actuators A*, **78**, 149-159.

Schueller, O. J. A., Brittain, S. T., and Whitesides, G. M., (1999). "Fabrication of glassy carbon microstructures by soft lithography" *Sensors and Actuators A,* **72**, 125-139.

Shamsi, S. A., and Danielson, N. D., (1994). "Napthalenesulfonates as Electrolytes for Capillary Electrophoresis of Inorganic Anions, Organic Acids, and Surfactants with Indirect Photometric Detection" *Analytical Chemistry*, **66**, 3757-3764.

Sikanen, T., Tuomikoski, S., Ketola, R. A., Kostiainen, R., Franssila, S., and Kotiaho, T., (2005). "Characterization of SU-8 for electrokinetic microfluidic applications" *Lab on a Chip*, **5**, 888-896.

Stone, H. A., Stroock, A. D., and Ajdari, A., (2004)"Engineering flows in small devices: Microfluidics toward a lab-on-a-chip" *Annual Review of Fluid Mechanics*, **36**, 381-411.

Studer, S., Pepin, A., Chen, Y., and Ajdari, A., (2002). "Fabrication of microfluidic devices for AC electrokinetic fluid pumping" *Microelectronic Engineering,* **61-62**, 915-920.

Takayama, S., McDonald, J. C., Ostuni, E., Liang, M. N., Kenis, P. J. A., Ismagilov, R. F., Whitesides, G. M., (1999). "Patterning cells and their environments using multiple laminar fluid flows in capillary networks" *Proceedings of the National Academy of Science*, **96**, 5545-5548.

Thorsen, T., Maerkl, S. J., and Quake, S. R., (2002). "Microfluidic large-scale integration" *Science*, **298,** 580-584.

Tokuda, N., Kanno, T., Hara, T., Shigematsu, T., Tsutsui, Y., Ikeuchi, A., Itou, T., Kumamoto, T., (2000). "Development of a redox flow battery system" *SEI Technical Review*. Osaka, Japan: Sumitomo Electric Industries, June, 2000.

Tulock, J., Shannon, M., Bohn, P., and Sweedler, J., (2004). "Microfluidic separation and gateable fraction collection for mass-limited samples" *Analytical Chemistry,* **76**, 6419-6425

Tuomikowski, S., and Franssila, S., (2005). "Free-standing SU-8 microfluidic chips by adhesive bonding and release etching" *Sensors and Actuators A*, **120**, 408-415.

Tyagi, S. and Kramer, F. R., (1996). "Molecular beacons: Probes that fluoresce upon hybridization" *Nature Biotechnology,* **14**, 303-308.

Van Gerwen, P., Laureys, W., Huyberechts, G., De Beeck, M. O., Baert, K., Suls, J., Varlan, A., Sansen, W., Hrmans, L., and Mertens, R., (1997). "Nanoscaled interdigitated electrode arrays for biochemical sensors" *1997 International Conference on Solid-State Sensors and Actuators, Chicago, June 1997.*

Widmann, D. W., (1976). "Metallization for integrated circuits using a lift-off technique" *IEEE Journal of Solid-State Circuits*, **SC-11**, 466-471.

Willner, I., and Willner, B., (2001). "Biomaterials integrated with electronic elements: en route to bioelectronics" *TRENDS in Biotechnology*, **19**, 222-230.

Wu, H., Odom, T.W., and Whitesides, G.M., (2002). "Reduction photolithography using microlens arrays: Applications in gray scale photolithography" *Analytical Chemistry*, **74**, 3267-3273.

Xiao, Y., Patolsky, F., Katz, E., Hainfeld, J. F., and Willner, I., (2003). " 'Plugging into enzymes': Nanowiring of redox enzymes by a gold nanoparticle" *Science*, **299**, 1877-1881.

Zhang, J., Tan, K. L., Hong, G. D., Yang, L. J., and Gong, H. Q., (2001a). "Polymerization optimization of SU-8 photoresist and its applications in microfluidics and MEMS" *Journal of Micromechanics and Microengineering,* **11**, 20-26.

Zhang, J., Tan, K. L., and Gong, H. Q., (2001b). "Characterization of the polymerization of SU-8 photoresist and its applications in micro-electro-mechanical systems (MEMS)" *Polymer Testing*, **20**, 693-701.

Zhang, J., Chan-Park, M. B., and Conner, S. R., (2004). "Effect of exposure dose on the replication fidelity and profile of very high aspect ratio microchannels in SU-8" *Lab on a Chip,* **4,** 646-653.

Zhu, J., Zhu, Z., Lai, Z., Wang, R., Guo, X., Wu, X., Zhang, G., Zhang, Z., Wang, Y., and Chen, Z., (2002). "Planar amperometric glucose sensor based on glucose oxidase immobilized by chitosan film on prussian blue layer" *Sensors*, **2**, 127-136.